NOTE TO USERS

BIOMECHANICS OF THE FOOT AND ANKLE DURING ICE HOCKEY SKATING

by

©CURT DEWAN

A Thesis

Submitted to the Faculty

of

Graduate Studies and Research

In partial fulfillment of the requirements for the degree of:

Masters of Science

Department of Kinesiology and Physical Education

McGill University

Montreal, Quebec

June, 2004

Your file Votre référence
ISBN: 0-494-06389-0
Our file Notre référence
ISBN: 0-494-06389-0

Abstract

This study describes the biomechanics of the foot and ankle during the transitional and steady state skating strides using kinematic, kinetic, and myoelectric measures. A data set for five collegiate hockey players was completed (mean ± SD: age = 21.8 ± 1.9 years, height = 1.81 ± 0.05 m, mass = 83.3 ± 8.0 kg). Three acceleration strides and a constant velocity stride were examined on ice. An electrogoniometer at the ankle was used to measure angular displacement and velocity values. Myoelectric activation patterns were measured at the vastus medialis, tibialis anterior, peroneus longus, and medial gastrocnemius of the right lower limb. Kinetic pressure profiles were measured using piezo resistive fabric sensors providing accurate pressure measurement within the narrow confines of the skate boot-to-foot/ankle interface. Sixteen flexible piezo-resistive sensors (1.2 cm x 1.8 cm x 0.2 cm thick) were taped to discrete anatomical surfaces of the plantar, dorsal, medial and lateral surface of the foot, as well as to the posterior aspect of heel and leg. Repeated measures ANOVAs and Tukey post hoc tests found few significant differences among stride variables; however insights into the mechanics of ice hockey skating at the foot and ankle are given.

Résumé

Le but de cette étude était de décrire la biomécanique du pied et de la cheville pendant le patinage de hockey sur glace en phase d'acceleration et en phase de vitesse constante avec des mesures cinématiques, cinétiques, et myoelectric traditionnelles. Un echantillon de trois pas d'acceleration et un pas a vitesse constante ont ete etudie sur la glace. Cinq joueurs collégiaux d'hockey ont complete ces etudes (écart-type moyen de ±: âge = ± 21,8 1,9 ans, taille = ± 1,81 0,05 m, poids = ± 83,3 8,0 kilogrammes). Un electrogoniometre pose sur la cheville a été employé pour obtenir des profils d'écart angulaire du pied et de la cheville. Une examination des modèles d'activation de muscles en se servant du signal EMG a ete complete après que la peau ait été rasée, rodée et nettoyée au site du placement d'électrodes au-dessus des vastus medialis, tibialis antérieurs, peroneus longus , et gastrocnemius médial du membre inférieur droit. Des profils cinétiques de pression ont été mesurés à l'aide des fournissant la mesure précise de pression dans l'interieur du patin a l'interface entre le patin et la cheville ou le pied. Les « piezo resistive fabric sensors » flexibles de seize (1,2 centimètres X 1,8 centimètres X 0,2 centimètres d'épaisseur) ont été places sur les surfaces anatomiques discrètes du pied plantaire, du pied dorsal, de l'aspect postérieur du talon et de la jambe, de l'aspect médial du pied, et de l'aspect latéral du pied. Des mesures répétées ANOVAs ont été exécutées, suivi du test Tukey. Ces analyses ont trouvé peu de différences significatives entre les variables mesurees. Cependant une appreciation plus approffondi de la biomécaniques du patinage sur glace patinant sont suggeres par ces données.

Acknowledgements

I would like to thank the Hockey Research team at McGill University, especially my supervisor, and friend, Dr. David Pearsall. His experience, direction, and encouragement were immeasurable. Special thanks also deservingly go to Dr. Rene Turcotte for his experience and perspective. Of the many strong peers associated with the Hockey Research team I would like to thank JJ Loh for the time necessary for the development of the data processing modules, Ryan Chang, and Robyn Goudreault for sharing their experience and Allejandro Vilasenor for his technical assistance and for teaching me to speak Spanish.

TABLE OF CONTENTS

LIST OF TABLES

LIST OF FIGURES

Chapter 1

Introduction

Ice hockey is a fundamental part of Canadian culture; for example, images of hockey players can be found on the monetary units and some of the most prominent Canadian icons are hockey players. Toronto historian and author William Kilbourn (1959) once said "If I were asked by some stranger to North American culture to show him the most important religious building in Canada, I would take him to Toronto's Maple Leaf Gardens." This perspective on ice hockey is pervasive across Canada and in many nations located in the northern hemisphere. Despite the popularity of hockey there is a relatively small quantitative understanding of the physics of the game. For instance, surprisingly little about the mechanics of skating, and in particular the interface between skater and ice that allows for efficient locomotion the skate. The earliest known forms of skates circa (9th century), were made of bone, (found in Sweden). Wooden skates with iron facings appeared in the 14th century. Skates made entirely of iron were introduced in the 17th century. Steel skates, with straps and clamps to fasten them to the shoes, were sold in the 1850s, and later came the skate permanently attached to the shoe (Vaughan 2001). Since the invention of the rudimentary STARR "Spring Skates" in 1863 by John Forbes and Thomas Bateman at The Starr Manufacturing Company Ltd, the design of skates has evolved drastically into the multi million dollar industry of today.

In a limited sense it seems that the cart has been put in front of the horse in the design of hockey skates. Changes in skate design affect comfort and efficiency, which in turn ultimately affects skating performance. Hancock et al. discussed the influence of skate design on performance 'The design and construction of a hockey skate boot has a definite influence on the functioning of the ankle joint complex, and skate manufacturers

should consider these factors when designing for optimal skate performance.' In particular the relevance of fatigue and muscle activity at the foot and ankle was shown by Forestier (2001) in an experiment conducted

> 'to investigate how an isometric exhaustion test allowing to fatigue specifically the tibialis anterior of young male adults affects the positioning accuracy of the ankle using an active matching task. The results highlighted the potentially deleterious effects of fatigue on the functionality of the proprioceptive system.'

This conclusion is quite pertinent to performance because under normal circumstances, it is believed that ankle proprioception is critical to the establishment of an internal reference, allowing stabilization of the body with respect to an external gravitational reference.' (Di Fabio et al. 1990.) The idea that during movement and dynamic balance humans sometimes behave as an inverted pendulum (Ishida et al.1999) and that ankle response is sufficient to counteract minor perturbations occurring during normal stance has been proposed. Predisposition to injury risk is associated with proprioceptive awareness and compensatory muscle firing pattern alterations was outlined by Rozzi (1999), and represents another consequence of design modifications. Relevant to design issues for footwear Reinschmidt and Nigg (2000) report that recently a new concept concerning movement control through footwear has emerged:

- The skeleton has a preferred path for a given movement task (e.g. running, skating)
- If an intervention (e.g. orthotic) supports the preferred movement path, muscle activity can be reduced. If an intervention counteracts the preferred movement path, muscle activity must be increased.
- Optimal footwear reduces muscle activity.

- Optimal footwear feels comfortable because muscle activity and the resulting fatigue are minimized.
- Performance should increase with optimal footwear since they minimize muscle activity and thus energy expenditure.

These concepts indicate the importance of quantifying the skeletal kinematics of the skater in addition to the myoelectric activity. Pressure distribution about the foot and ankle are also insightful to propose what features of the footwear are imposing constraints that counteract the preferred movement path; and to how the skater is generating the steering and propulsive forces necessary to meet the objectives of the skater and arrive at an intended location.

An important component in skate design is the rigidity or stiffness of the skate boot (Turcotte et al., 2001a). The rigidity has its usefulness in terms of protective value and facilitates medial lateral ankle stability but frequently it is the cause of much discomfort for some skaters. It is noted that from a podiatric point of view, hockey players have a reputation for "pathological" feet i.e. foot deformations, bunions, callosities etc... Injury prevention, performance and comfort are not independent of each other. Perhaps skate design can continue to evolve with an empirical understanding of foot and ankle parameters to increase performance and reduce the occurrence of foot pathologies for skaters and hockey players.

1.1 Nature and Scope of the Problem

There is an uncertainty of the pressure magnitudes and distribution between the foot and ankle in the skate boot. Previous works measuring pressures in locomotion have

focussed principally on the plantar aspect of the foot. In fact few human locomotive studies in general have measured pressure on a surface other than the plantar foot (Hillmann, 2000). Due to the lack of analysis of discrete pressure measurements from the dorsal, medial, lateral and posterior surfaces of the foot and ankle there has been no describing the "levering" of the foot and ankle inside the skate boot in an effort to transmit forces from skate boot to blade to ice through

1.2 Significance of the Problem

Despite the abundance of literature collected in other sports (i.e. soccer, basketball) or of other skills (i.e. running, jumping) much remains to be examined to understand the complexities of tasks involved in the sport of ice hockey (Pearsall et al., 2000; Lafontaine et al., 1998; Montgomery, 1999, 2001) let alone the effect of equipment design and construction on task performance. In general, research into the mechanics of the sport of ice hockey has been limited (Pearsall et al. 1999, 2000). For instance, some rudimentary aspects of the forward stride (Chang et al., 2002; Goudreault et al., 2002; Turcotte et al., 2001a, 2002; Pearsall et al., 2001, Purvis et al., 2001; Marino, 1977, 1979, 1983, 1984; Marino et al., 1978, 1979; Nobes et al., 2002; Hoshizaki et al., 1989), and starts and stops (Naud et al., 1979, 1980, Lamontagne et al., 1983) have been described but little has been written regarding specific issues of skate design and construction (Turcotte et al., 2001). The scarcity of quantitative biomechanical analyses of hockey skating is at least in part a result of the difficulties experienced undertaking biomechanical investigations in the hockey environment. Further complicating the

experimental requirements the movements are three-dimensional in nature and generally take place over fairly large spaces.

Consequently literature discussing quantitatively foot and ankle kinematics during ice hockey skating is quite scarce. Of those studies many used cinematographic techniques which have critical limitations described by (Chang et al. 2002). The inaccuracies of measuring ankle frontal plane kinematics, in a relatively small spatial volume using cinematographic techniques were summarized by Milani & Hennig (2000). Few investigations have measured movements of the foot and ankle inside the skate; the importance of studying the foot and ankle inside the skate was stressed by Al Hadi & Lamontagne (2000). They addressed the accuracy of marker placement on the exterior boot as a representation of bone and skin landmarks. They concluded that there was a significant movement of the foot within the boot when the foot was placed in controlled positions. (Chang et al. 2002) was the first study employing electrogoniometry in the skate boot and record skin based kinematic data of the ankle.

In terms of athletic footwear the running shoe is the most studied foot wear product. Given the large number of active runners (e.g. 15 – 30% of North America's population) the frequent running injuries, the substantial market associated with running movement may have accounted for this "research boom" (Reinschmidt and Nigg 2000). The "research boom" in running shoes has created an ample source for kinetic and pressure data in running that provides some baseline measures to compare with skating. Due to the aforementioned paucity of literature surrounding ice hockey skating in general the amount of kinetic and pressure studies previously recorded in hockey skating mirrors that of the kinematic studies, it is quite rare.

The insole characteristics of the skate boot modify the blade to ice interaction considerably, and as such in shoe pressure measurement are of special interest. Hennig & Milani (2000) stated that "the design of footwear for running should depend on a sound knowledge of the force and pressure environment during ground contact". In running, measurements of plantar forces have contributed to orthotic device evaluation and comparisons. Pressure measurements in running and walking allow researchers and clinicians the ability to see how many abnormalities may manifest themselves as plantar pressure distributions. Thus the link from running and walking to skating is inferred. This study provides insights into the contact pressure of the plantar aspect of the foot and in addition to other key foot and ankle surfaces. The relevance of surface pressures on other regions of the foot is revealed by Hosein and Lord (2000) in their study in shoe plantar shear measurements. The results of their study suggested that plantar shear does not sustain the majority of the anterior acceleration force acting on the body, in late stance phase, or the lateral force acting in early stance phase. This finding led the authors to deduce that the anterior acceleration forces 'must be reacted by pressure against the upper shoe.' They further went on to speculate that 'shoe design and fit may be critical factors in shod shear measurement.' Therefore by collecting pressure measurements about the global surface of the foot and ankle an indication of footwear "fit" is given. This issue of fit has implications for knowing the amount and temporal loading patterns between the foot – footwear interface and thus by extension some performance and health implications.

In general, a complete description of locomotion accounts for at least the kinetic, kinematic and myoelectric components. Hence the purpose of this study is to provide

such a profile of the foot and ankle during the skating stride. The above mentioned descriptions will provide the basis for an account of the loading and levering of the foot and ankle inside the skate boot to transmit forces from skate boot to blade and to ice.

1.3 Objectives of the study

The purpose of this study is to present a profile the foot and ankle kinetics and kinematics during on ice forward hockey skating at a high velocity (between 25, and 30 km/hr), as well as to identify concurrent muscle activation profiles of some of the prime movers of the foot and ankle to better understand the mechanics of the foot and ankle inside the hockey skate during this forward skating condition. In addition an objective comparison of foot and ankle parameters between the initial acceleration strides versus constant velocity strides will be performed, in an attempt to measure the changing mechanics of the transitional phases from rest to top forward locomotion speed.

1.4 Hypotheses

The following hypotheses are stated:

(1) There will be significant differences in the stride duration between respective acceleration strides and significant differences in the stride duration between acceleration strides and constant velocity strides.

(2) There will be significant differences in minimum and maximum kinetic, kinematic and myolectric measurements between respective acceleration strides and constant velocity strides.

1.5 Operational Definitions

Skating stride: Movement pattern from blade contact to blade contact of the right foot.

Stride rate: The number of strides per minute

Stride Phases and/or Events:

1) Initial Contact (IC): blade-to-surface contact begins
2) Glide (G) Phase: following initial contact; blade orientation steers body movement forward
3) Push-off (PO): at the end of glide phase, blade turns outward (external) to allow hip extension, abduction and external rotation, knee extension and ankle plantar flexion to propel body forward on contralateral limb.
4) Swing phase (SW): lower limb non-weight bearing; hip, knee flex and ankle dorsiflex to allow lower limb to swing forward to begin the next stride.

ASCII: American Standard Code for Information Interchange. A format of a file that can be read by the specialized software developed in this study.

Pressure Profile: A pressure versus percent of stride graph

Percent of Stride: The time of an event relative to the time for the entire stride. The range of this variable is from 0 to 100 percent.

Plantar surface: The surface of the sole of the foot.

Dorsal surface: The surface of the dorsum of the foot.

Posterior surface: The surface of the posterior foot and ankle.

Medial surface: The surface of the medial foot and ankle.

Lateral surface: The surface of the lateral foot and ankle.

Hysterisis: Is the energy lost when loading or unloading a sensor.

Creep: The tendency for readings to steadily increase under a constant load.

Kinetics: The area of biomechanics concerned with the forces producing motion or maintaining equilibrium.

Kinematics: The area of biomechanics concerned with describing motion without regard to the forces producing it.

Goniometry: The measurement of joint motion or joint position.

1.6 Limitations

1. The flexible electrogoniometers measured movements in only two planes. Movements along the longitudinal axis are not measured.
2. The goniometers provided local angles only, global angles were not available.
3. The piezo resistive sensors measured the pressure normal to the surface of the foot (i.e. shear forces were not measured).

1.7 Delimitations

1) Subjects included both forwards and defensemen
2) Only high intensity skating (i.e. 90 – 95% of peak velocity) was examined.

Chapter 2

Review of the Literature

Given the limited research specific to ice hockey, our best understanding of forward skating mechanics may be drawn from research focused on speed skating (de Boer et al, 1985, 1987; de Koning et al, 1991; van Ingen Schenau et al, 1989). Interpretation of speed skating mechanics can be useful for identifying the general movement patterns similar to ice hockey; however, caution was suggested by Marino (1979) before equivocating the two skills due to fundamental differences in equipment, skill, repertoire, and play context preclude suggesting a direct transfer of speed skating to ice hockey skating.

Athletes, coaches, athletic trainers, and equipment designers would benefit from having more information on the specific ice hockey stride biomechanics so as to improve skating technique development and maintenance, as well as, aiding in establishing rehabilitative regimes during recovery from lower limb injuries. The following text reviews the skating research completed in hockey.

2.1 Basic Patterns of the Skating Stride

The skating stride is a complex series of simultaneous joint movements. The locomotion in skating is fundamentally unique from other forms of human locomotion. The primary difference in skating lies in the method of propulsion. In most locomotion, the majority of the push-off force acts parallel to the direction of travel. While in skating, only a component of the push-off force acts parallel to the direction of travel, as the skate blade is oriented obliquely during push-off. The oblique orientation of the skate blade is

necessary for propulsion on the ice surface with a coefficient of friction 0.003 to 0.007 as reported by Jobse et al. (1990). Minkoff et al. (1994) describes that the primary differences are seen in during skating push-off when a lateral motion is generated by synchronous hip extension, hip abduction, and knee extension but with limited plantar flexion. The coordination pattern in skating is therefore a unique adaptation of the more natural movements of walking or running (van Ingen Schenau et al., 1989).

Marino (1977) stated that the forward stride is bi-phasic with alternating periods of single and double support. In speed skating, the periods of single support and double support were described as glide and propulsion phases, respectively. During the propulsion phase the center of mass of the body is accelerating horizontally; conversely a horizontal deceleration of the center of mass occurs during the glide phase.

Differences have been observed between forward skating at a constant velocity versus accelerating. In particular, there appears to be a substantial decrease in the double support phase when accelerating in the forward direction. Marino (1979) recorded the acceleration patterns of four moderately to highly skilled hockey players. It was noted that the skaters were able to maintain positive acceleration throughout both the single and double support phases of the stride. During the beginning of the acceleration phase the skaters had a tendency to use very short, choppy strides. The recovery leg came down in a position of lateral rotation combined with hip flexion, knee flexion, and ankle plantar flexion. This position contributed to the propulsion that began during the double support phase and lasted throughout the stride. Subjective evaluation suggested that the striding pattern while skating at a constant, fast speed consisted of a smooth stroking motion in which the skate did not complete its outward turn until the non-support foot approached

touchdown. No period of glide was detected in the initial strides of the acceleration phase.

2.2 Fundamentals of Surface Electromyography (EMG)

A comprehensive review of surface electromyography and of the muscles of interest in this study of ice skating is given by Goudreault (2002) below.

Muscle tissues are excitable tissues, meaning they have electric potential differences established across their cell membranes. These potentials are created by differences in ion concentrations between the intracellular and extracellular domains.

These electrical potentials are relatively constant while the muscle cell is at rest, however this potential changes as the muscle contracts. That is, muscle contraction is associated with a "muscle action potential" (MAP), which is an action potential that propagates bidirectionally along the muscle fiber. It is the summation of many muscle action potentials that gives rise to the electromyogram (EMG).

The MAP is a depolarization (more positive) of the cell membrane followed by a repolarization (more negative), created by a movement of ions through ion channels in the cell membrane. This changing of membrane potential can be measured by: (i) placing needle electrodes into the belly of a muscle (Intramuscular EMG), or (ii) placing Ag-AgCl electrodes on the surface of the body (surface EMG). The electrodes transduces the motor action potential (converting ionic currents into electrical currents), and the resultant EMG signal can be recorded following appropriate amplification and filtering.

- The frequency content of the surface EMG signal ranges from ~DC to 250 Hz. However, electrodes produce half cell potentials (i.e., noise) which make the

measurement of DC components of the EMG impossible. Motion artifact (produced by motion of the electrode relative to the skin) is also a problem, and occurs in the range of 0 to 10 Hz. For these reasons, the surface EMG is typically bandpass filtered over the range of 10 to 250 Hz to eliminate low frequency noise and increase the signal to noise ratio (Guyton & Hall 1996).

EMG is a common measurement tool used to estimate the activity of individual muscles in terms of their contribution to complex coordination patterns (Basmajian et al., 1985; Clarys, 1987; DeLuca, 1997; Stegeman et al., 2000). It is important to understand the factors that generate the signal, as well as precautions to eliminate as much signal interference as possible. De Luca's (1997) comprehensive review paper discusses the usefulness and limitations of the EMG in biomechanics. For instance, EMG can be used to indicate periods of muscle activation, and provide the timing sequence of one or more muscles performing a task. It can also be used qualitatively to estimate the relationship to the force produced by a muscle or a group of muscles. A third application of EMG is a general indicator of fatigue occurring within a muscle by displaying time-dependent changes prior to any force modification, thus predicting the onset of contractile fatigue. When EMG signals are rectified and smoothed, the amplitude may be qualitatively related to the amount of force measured (Deluca 1997), although the accuracy can be questionable due to a variety of factors that can influence an EMG signal.

Several external factors that can affect the signal are the electrode location and configuration, cross talk (electrical activity of other muscles), and the orientation of the electrodes with respect to the muscle fibres (DeLuca, 1997; Herzog and Nigg, 1999).

Internal factors that also have an effect on the signal are the number of active motor units, fibre type, blood flow, fibre diameter, depth and location of the active fibres, as well as the amount of tissue between the surface of the muscle and the electrode. Other factors affecting the signal can include band-pass filtering aspects of the electrode, detection volume of the electrode, superposition of action potentials in the detected EMG signal, conduction velocity of the action potential, and spatial filtering due to the position of the electrode compared to the active muscle fibres.

To ensure the EMG signal is detected and recorded with maximum fidelity, a differential electrode configuration (i.e. bipolar) should be used, and the electrodes located on the muscle belly between the myotendinous junction and the nearest innervation zone (DeLuca, 1997; Delagi et al., 1980). The resulting signal magnitude should be expressed as the Root Means Square (RMS) from the raw signal (DeLuca, 1997). This differential amplification arrangement will remove the majority of unwanted false electrical signal or noise. A standard spacing of one centimetre is appropriate with the anatomical arrangement (i.e. size and shape) of most muscles, and has other advantages, such as a lower impedance and elimination of the noise component, especially the noise generated at the electrode/tissue interface. To further improve electrical contact with the electrodes, superficial cutaneous cells should be removed by use of an abrasive paper and alcohol swabs.

In addition, all efforts must be made to eliminate cross talk (i.e. inter-muscle signal transmissions) so as to obtain a signal that represents the specific muscle being observed. Therefore, it is necessary to devise a procedure to determine electrode placement for each muscle. The Anatomic Guide for the Electromyographer by Delagi et al. (1980) maps out

a suggested electrode placement for each specific muscle. Attention to accurate and consistent electrode placement, as well as consistent electrode size, can in part reduce the potential for cross talk from adjacent muscles.

To permit comparisons between muscle stride patterns measured at different stride velocities, it is common to "normalize" the stride cycle duration. Winter (1990) explains a procedure of averaging the EMG signals of several strides (i.e. from contact to contact), by transforming the time values onto a normative time scale from 0 to 100. This allows for comparisons within and between subjects. This has become an accepted way to present data in literature.

2.3 Comparison of Muscle Activity of the Vastus Medialis

Table 2.3.1: Chart of muscle activity; determined from EMG results of forward skating in ice- hockey

At 24 km/hr	**Glide**	**Push-off**	**Swing**
	0 - 33% stride	33 – 63% stride	63 – 100 % stride
Vastus Medalis	Knee flexed Smaller peak at activity onset, then decreases. Eccentric to act as stabilizer	Peaks at mid push-off phase Knee extension Concentric work	Off
Tibialis Anterior	Ankle dorsiflexed Peaks, then decreases Isometric activity	Off Ankle extension	On, peaks Dorsiflex to reposition
Peroneus Longus	Ankle dorsiflexed Peaks then decreases Eccentric ankle flexion	Peaks as ankle pushes into plantar flexion Concentric ankle extension	Off Ankle flexion
Gastrocnemius (medial)	Off	Peaks Ankle extension Concentric activity	Activity decreases, then off

For this muscle the three studies had similar results (Figure 3b). De Koning et al. showeds that the muscle activity peaks at 0.6 s before the end of push-off, then remained constant during the glide phase of the stroke. There is very little activity in the muscle after push-off. During the wind-up and release phases, Minkoff et al. described the VM muscle activity as being eccentric due to knee extension, but it is concentric VM activity would then result in knee extension. Minkoff et al. also reported active concentric hip flexion during the recovery phase, this referred to the entire quadriceps muscle group;

which would include the rectus femoris activity. Since they did not report knee flexion or extension, it may be assumed that the vastus medialis is inactive (off). Hinrichs also showed that late in the stride the muscle is "off".

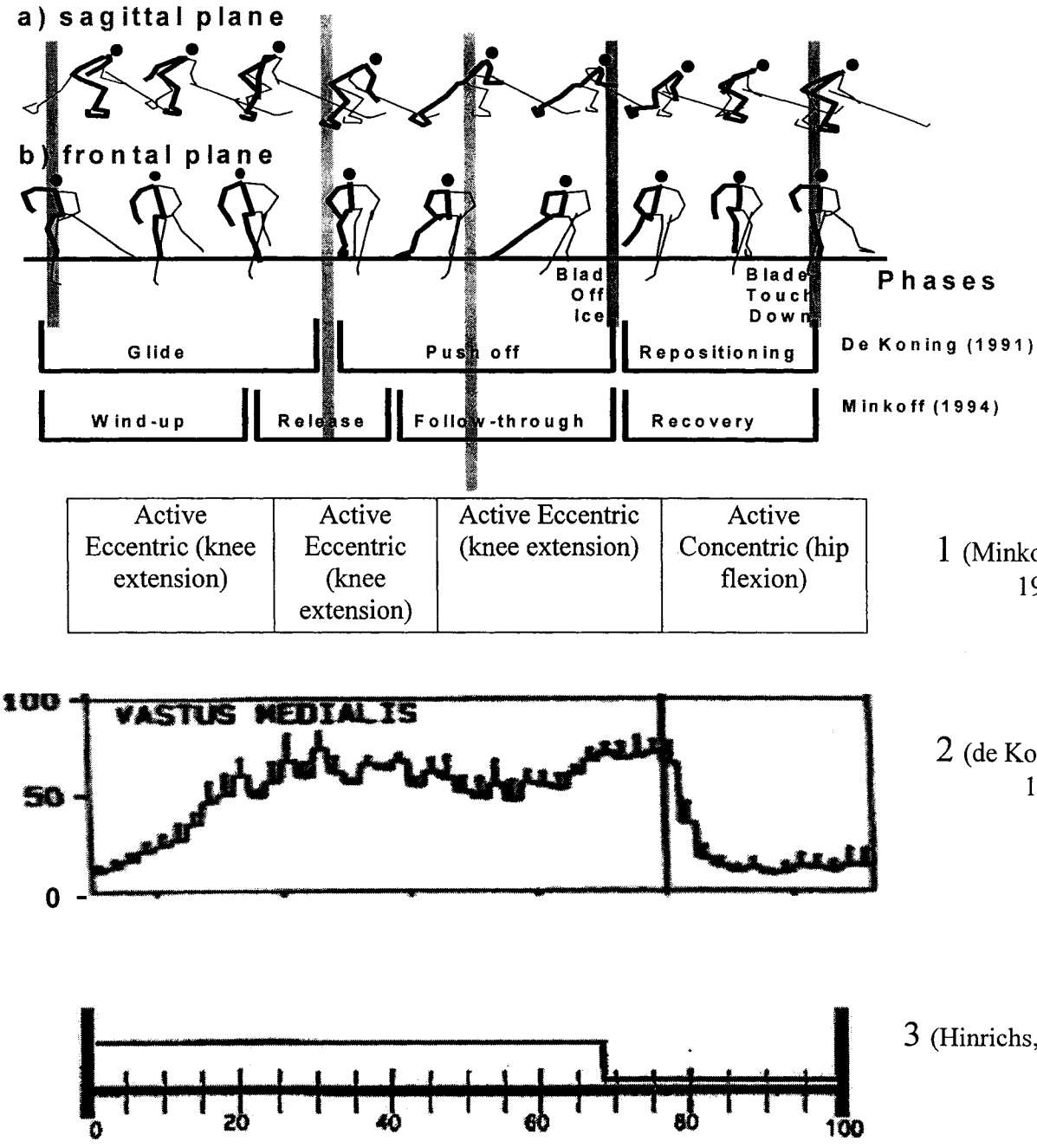

FIGURE 2.3.1: COMPARISON OF MUSCLE ACTIVITY OF THE VASTUS MEDIALIS

2.4 Comparison of Muscle Activity of the Gastrocnemius

From all three studies (Figure 3d), it can be determined that the gastrocnemius is primarily active throughout most the stride, until after push-off. De Koning et al. showed activity present from the beginning until peaking at push off. After "push-off" the activity declined. Minkoff et al. suggested that early in the stride the gastrocnemius worked eccentrically during knee flexion; however, it is possible that the activity seen in the muscle is generating concentric plantar flexion.

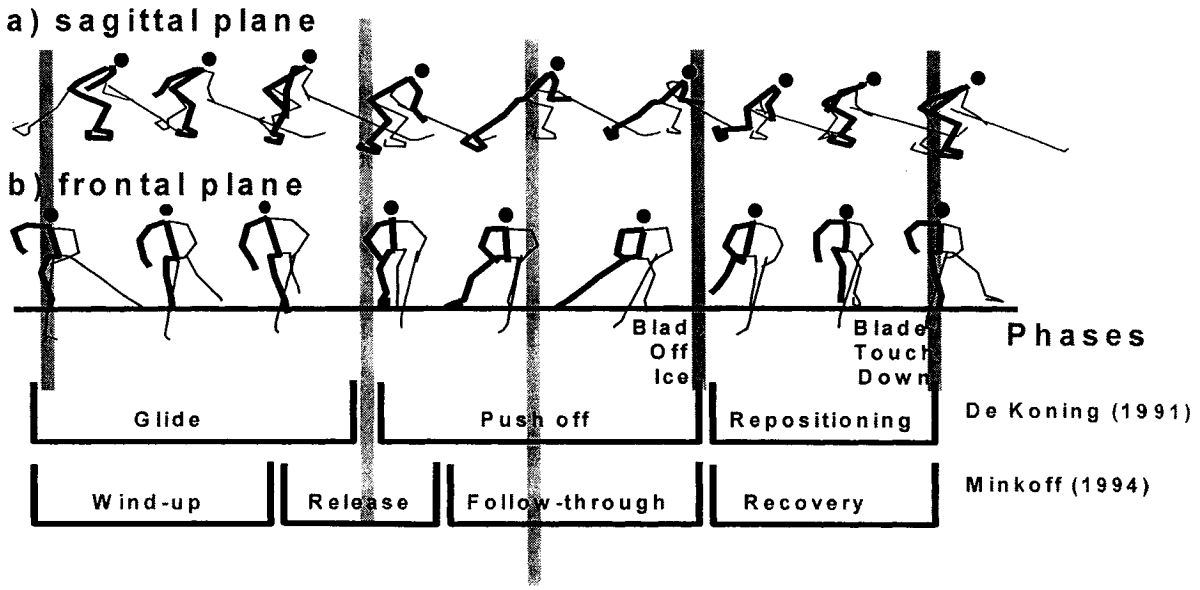

Active Eccentric (knee extension)	Active Eccentric (knee extension)	Active Concentric (ankle plantar flexion)	Inactive

1 (Minkoff et al., 1994)

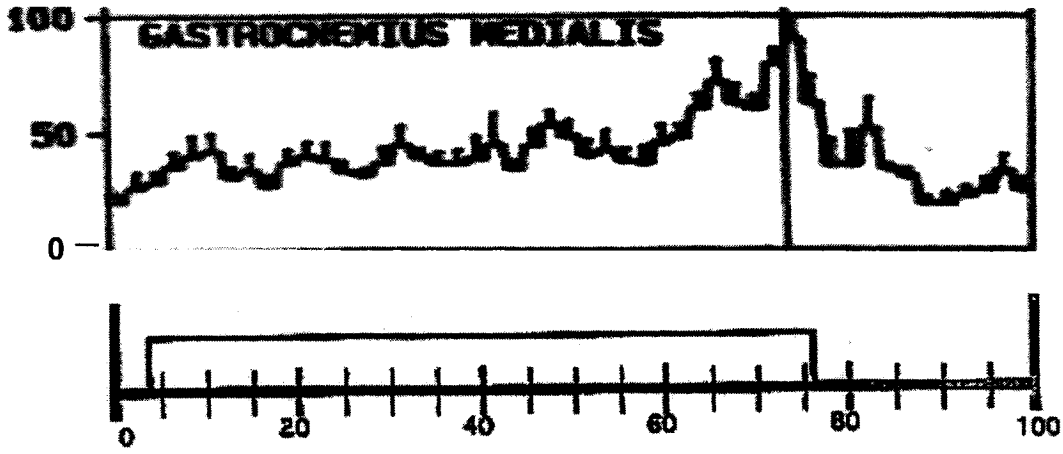

2 (de Koning et al., 1991)

3 (Hinrichs, 1994)

FIGURE 2.4.1: COMPARISON OF MUSCLE ACTIVITY OF THE GASTROCNEMIUS

2.5 Comparison of the Muscle Activity of the Tibialis Anterior

There is a large discrepancy between Minkoff's et al. suggestion and both de Koning's et al. and Hinrichs' results (Figure 2.5.1). Minkoff reported the tibialis anterior was inactive until the recovery phase. The other studies show that the muscle is active except for a small duration of time in the middle of the stride. This period of muscle inactivity appeared to correspond to the push-off in de Koning's study.

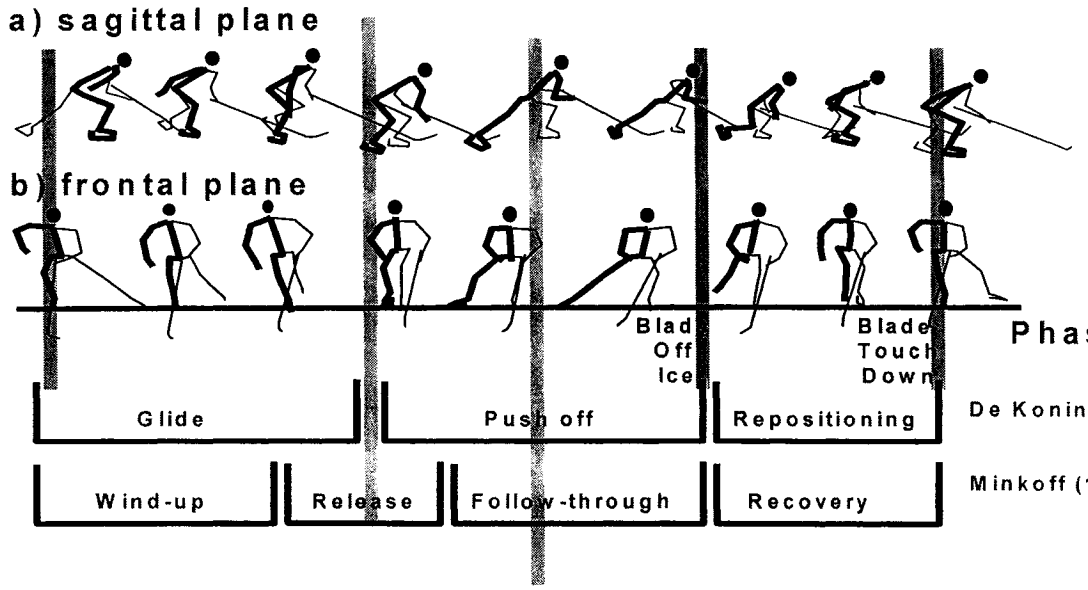

Inactive	Inactive	Inactive	Active Concentric (dorsiflexion

1 (Minkoff et al., 1994)

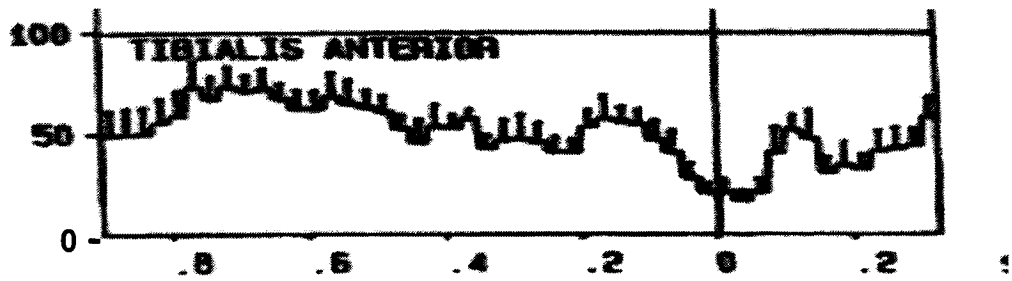

2 (de Koning et al., 1991)

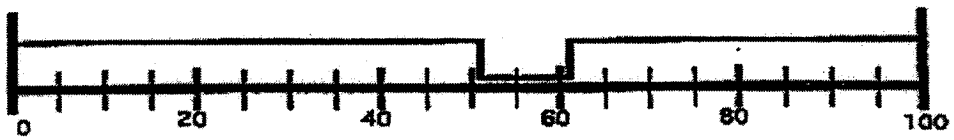

3 (Hinrichs, 1994)

FIGURE 2.5.1: COMPARISON OF MUSCLE ACTIVITY OF THE TIBIALIS ANTERIOR

Goudreault et al. 2002 found that there was usually a significant increase in the peak amplitude at 24 km/hr when compared to 12km/hr see (Tables 2.5.1. – 2.5.4 & Figures 2.5.2 – 2.5.5) which show the muscle activation profiles at speeds 12, 18 and 24

km/hr on the skating treadmill. It is important to note that the markers used to cut the individual strides were different between the treadmill study and this study.

***Table 2.5.1**: m. vastus medialis: normalized measurement parameter values of amplitude (P)*

Parameter	12 km/hr (3.3 m/s)	18 km/hr (5.0 m/s)	24 km/hr (6.7 m/s)
P1	55.6 ± 11.4	63.1 ± 9.1	76.0 ± 13.6*
P2	21.6 ± 10.1	27.6 ± 14.0	34.9 ± 21.6*
P3	78.4 ± 15.3	91.0 ± 18.2	95.1 ± 12.9*
P4	12.3 ± 8.8	12.3 ± 9.3	14.4 ± 9.5

values represent mean ± SD
* indicates a significant difference from speed 12 km/hr ($p < 0.05$)
** indicates a significant difference from speed 18 km/hr ($p < 0.05$)

***Table 2.5.2**: m. tibialis anterior: normalized measurement parameter values of amplitude (P)*

Parameter	12 km/hr (3.3 m/s)	18 km/hr (5.0 m/s)	24 km/hr (6.7 m/s)
P1	58.7 ± 15.5	75.1 ± 24.4	95.0 ± 9.4* **
P3	12.1 ± 6.3	15.1 ± 7.0	16.6 ± 7.3*
P5	61.1 ± 11.7	80.0 ± 21.7*	92.1 ± 8.5*

values represent mean ± SD
* indicates a significant difference from speed 12 km/hr ($p < 0.05$)
** indicates a significant difference from speed 18 km/hr ($p < 0.05$)

***Table 2.5.3**: m. peroneus longus: normalized measurement parameter values of amplitude (P)*

Parameter	12 km/hr (3.3 m/s)	18 km/hr (5.0 m/s)	24 km/hr (6.7 m/s)
P1	59.0 ± 4.8	75.0 ± 13.3	74.7 ± 74.7
P2	32.9 ± 8.8	31.9 ± 8.6	40.3 ± 14.7
P3	68.3 ± 12.3	76.9 ± 17.9	90.9 ± 15.0* **
P4	14.7 ± 9.0	22.9 ± 25.0	24.4 ± 11.0

values represent mean ± SD
* indicates a significant difference from speed 12 km/hr ($p < 0.05$)
** indicates a significant difference from speed 18 km/hr ($p < 0.05$)

***Table 2.5.4**: m. gastrocnemius: normalized measurement parameter values of amplitude (P)*

Parameter	12 km/hr (3.3 m/s)	18 km/hr (5.0 m/s)	24 km/hr (6.7 m/s)
P3	80.1 ± 23.4	92.6 ± 16.3	100.0 ± 1.9*
P4	13.0 ± 9.6	16.3 ± 9.5	19.1 ± 10.3

values represent mean ± SD
* indicates a significant difference from speed 12 km/hr ($p < 0.05$)
** indicates a significant difference from speed 18 km/hr ($p < 0.05$)

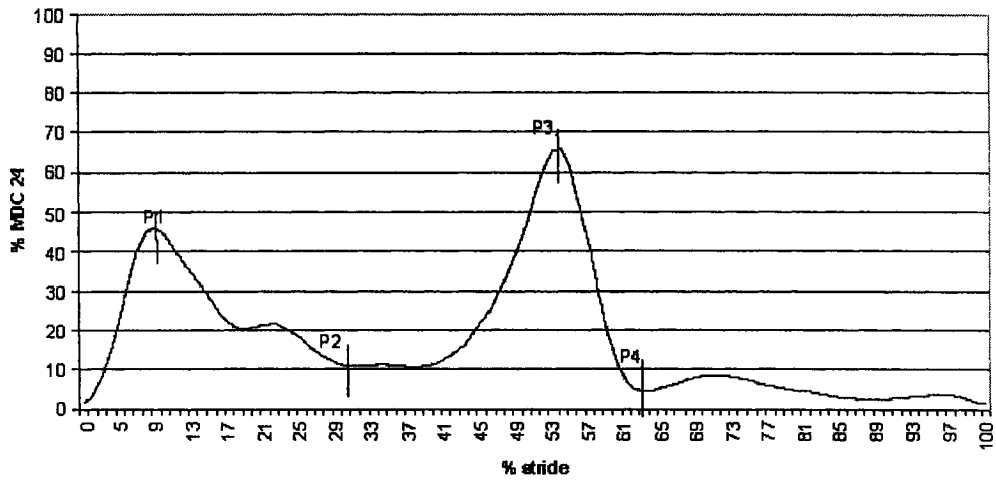

FIGURE 2.5.2: EXAMPLE OF PARAMETER POINTS ON THE M. VASTUS MEDIALIS

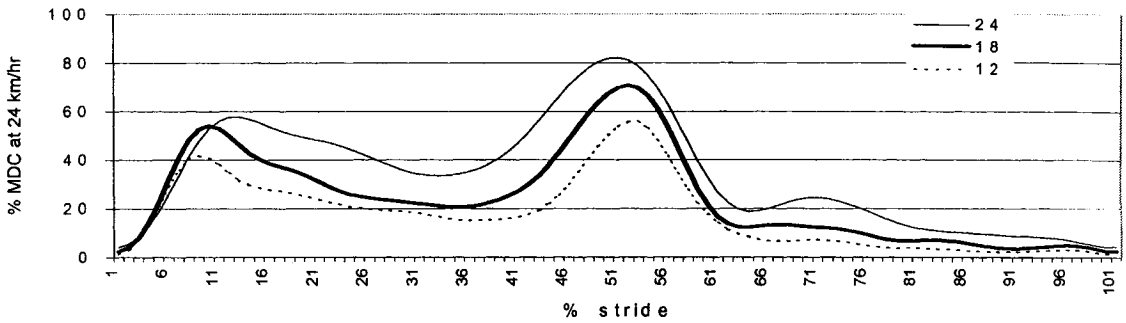

FIGURE 2.5.3 : M. VASTUS MEDIALIS: GROUP AVERAGE EMG PATTERNS OF FORWARD SKATING AT THREE VELOCITIES; 12, 18, and 24 km/hr

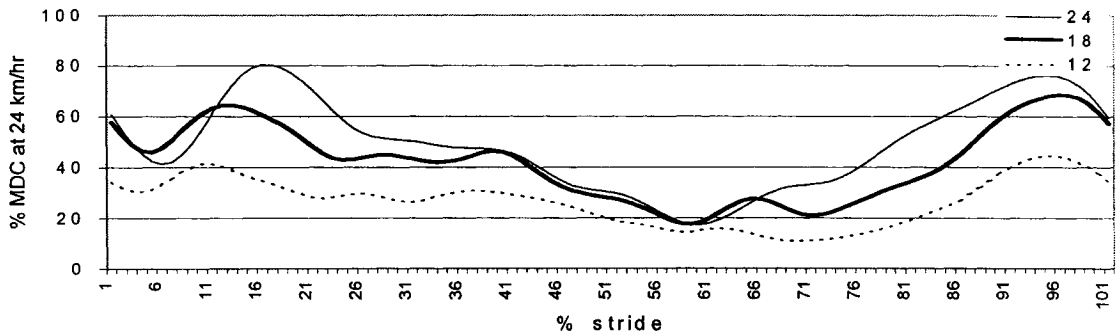

FIGURE 2.5.4: M. TIBIALIS ANTERIOR: GROUP AVERAGE EMG PATTERNS OF FORWARD SKATING AT THREE VELOCITIES; 12,18, AND 24 KM/HR

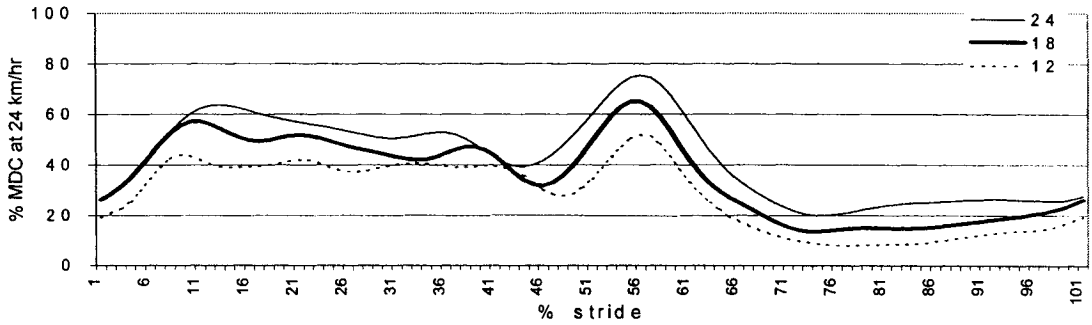

***FIGURE 2.5.5**: PERONEUS LONGUS: GROUP AVERAGE EMG PATTERNS OF FORWARD SKATING AT THREE VELOCITIES; 12, 18, AND 24 KM/HR*

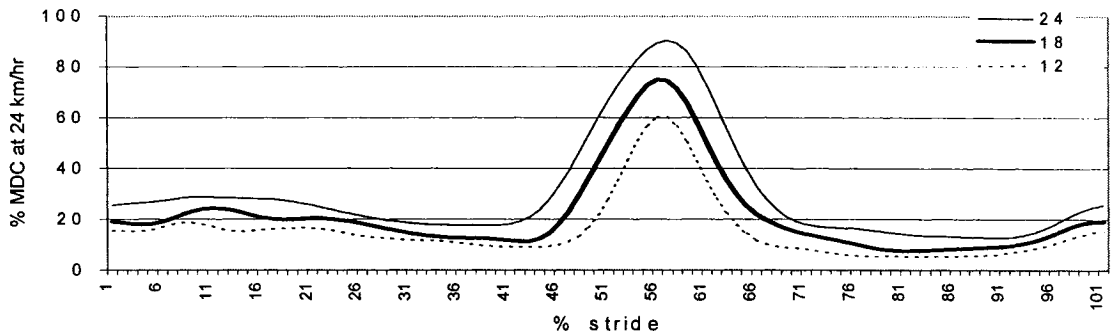

***FIGURE 2.5.6**: M. GASTROCNEMIUS : GROUP AVERAGE EMG PATTERNS OF FORWARD SKATING AT THREE VELOCITIES; 12, 18, and 24 km/hr*

2.6 Goniometry

The goniometer produces an electrical signal linearly related to the angle subtended by the two end blocks. The measured angle is independent of the shape of the bend of the foil strip, and joint angles could be measured regardless of misalignment with the joint's axis of rotation and linear movements due to skin stretch. Thus, it is possible to measure joint motion of polycentric joints such as the wrist and ankle, which are difficult to measure with cinematographic techniques. The commercially available flexible electrogoniometer (Penny & Giles Ltd., Blackwood, UK / Biometrics Ltd.) consists of two plastic end blocks separated by a spring. The spring acts as a protective housing for

the foil strip which is fitted with an array of strain gauges along its surface. It allows measurement in two planes, but is unable to measure rotation about its long axis. Chang et al. (2002) summarizes a study by Ball and Johnson (1993) which measured subtalar movement using flexible electric goniometers. The protocol placed flexible electrogoniometers along the posterior aspect of the lower leg and heel allowing measurement across the ankle and subtalar complex. Both passive and active methods were attempted on twenty-five subjects (n=25) in several different positions (i.e. sitting, standing, and prone). Their results showed that their intra-subject measurements had a standard deviation of less than 3.5 degrees. The standard deviation values were considered highly satisfactory when accounting for the day-to-day variation of the subject and the effects of detachment and reattachment of the device. The results showed too that slight differences in the placement of the goniometer on the lower leg produced negligible effects on the measurement ranges. They concluded that the flexible electrogoniometer was a reliable measurement tool.

Chang et al. (2002) used a design similar to Ball to measure ankle kinematics. Five elite hockey players skated on a treadmill at three velocities (12, 18 and, 24 km/h). The study measured ankle motion in the frontal plane: inversion/eversion and in the sagittal plane: plantar/dorsi flexion. The relevance of calcaneus measurement dates back to 1954 (Hicks) when it was stated that the movements of the subtalar complex are fundamental to the transmission of rotations from the foot to the leg during the early part of the stance phase of gait.

Furthermore, Milani & Hennig (2000) in a review paper stated that in-shoe goniometer measurements were found to be reliable within a series of repetitive trials.

However, it is possible that the shoe or skate movement is slightly influenced mechanically by the goniometer.

Edington et al. (1990) listed kinematic parameters resulting form several studies that were performed mostly using high-speed film techniques. The authors reported maximum eversion values to range between 6.8°- 13.5°

Areblad et al.(1990) compared three-dimensional (3D) rearfoot measurements with two-dimensional (2D) results. The results indicated that the 2D measurements of maximum eversion angles varied between 3° and 10° depending on the foot position relative to the camera axis. Recent 3D studies Reinschmidt et al. (1997) showed that markers that are externally fixed on the shoe overestimate movements occurring at the underlying bone structures. Stacoff et al. (1998) found shoe eversion, and shoe eversion velocity to be approximately twice as large as bone motion data. Thus it could be argued that given the inaccuracies of kinematic analysis using current filming techniques compared to goniometric measurements, and due to the high volume necessity goniometry is the better method to measure ankle kinematics during hockey skating.

The figures below are from Chang et al. (2002); they depict ankle kinematics in the sagittal and frontal planes at speeds at 12, 18, and 24 km/hr on a skating treadmill. Their results showed a generally increasing range of motion at increased velocities.

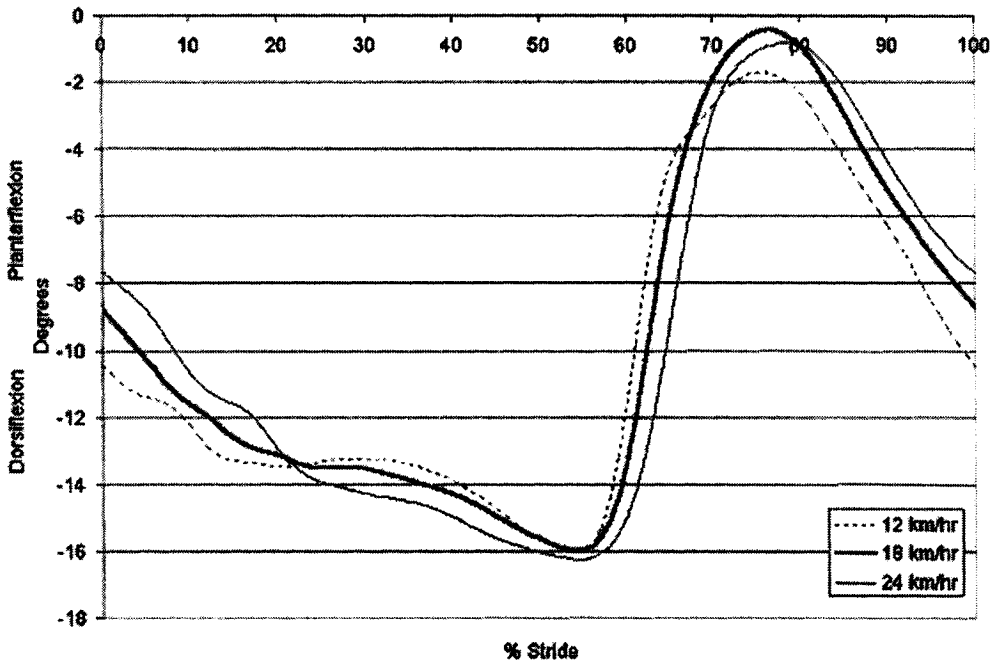

Figure 2.6.1. Mean kinematic profile of ankle plantarflexion and dorsiflexion movements for 5 subjects through one cycle of the skating stride at forward velocities of 12, 18 and 24 km/hr.

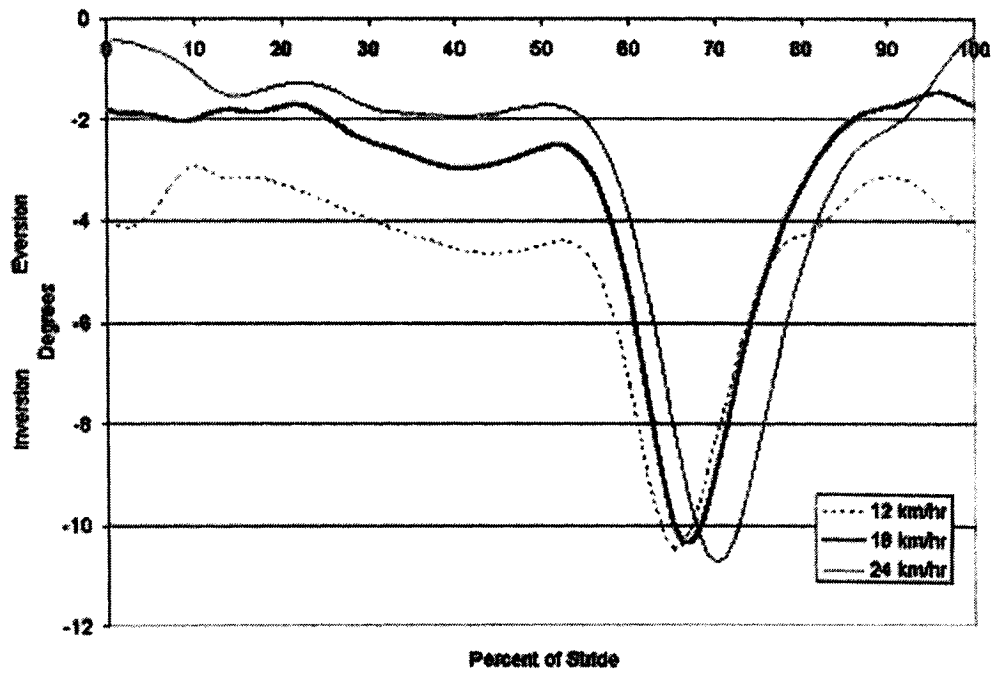

Figure 2.6.2. Mean kinematic profile of ankle inversion and eversion movements for 5 subjects through one cycle of the skating stride at forward velocities of 12, 18 and 24 km/hr.

2.7 Pressure

In speed skating, force-time patterns are repeatable (Jobse et al., 1990, Houdijk et al., 2000, DeBoer et al., 1987.) In these studies, force was measured with strain gauges mounted to the posts of the skate blade holder. Two peaks in the total force during a single speed skating stride were found. The first force peak, of approximately 120 percent of body weight, corresponded to the transfer of body weight from the push-off of the contra lateral skate to the new supporting leg (Jobse et al., 1990, Houdijk et al., 2000, DeBoer et al., 1987.) The second force peak, of approximately 140 percent of body weight, corresponded to the push-off of the measured foot (Jobse et al., 1990, Houdijk et al., 2000, DeBoer et al., 1987.)

Loh et al. (2003) analyzed plantar foot kinetic differences in forward hockey skating on ice and on treadmill at speeds of 22, 24, and 26 km/hr. The conclusions relating to ice skating at 26 km/h follow: 1) there was a heel to toe shifting of force distribution during the skating stride; 2) the force profile of forward skating was bi-modal. de Koning found that during the contra lateral push-off, push-off peaks were intermediated by a minimum support dip in force; 3) the force on the medial and lateral sides of the heel and forefoot essentially mirrored each other; 4) stride rate was the determining factor in regulating forward skating velocity.

As informative as plantar force measurements are Miller (1990), in a review of ground reaction force research, concluded that it is not a particularly sensitive measure because its signals reflect only the acceleration of the body's center of mass. Of particular interest is the loading of individual foot structures which likely play an important role in the occurrence of overuse injuries. Such measures can only be determined using pressure

distribution devices. During skating a slight movement of the bones with respect to the skin may be expected. The use of a limited number of discrete flexible transducers offers an alternative kinetic measure for gathering in-skate pressure information. Fixed with adhesive tape on the anatomical foot structures of interest allows independence for individual foot shape and for measurement of surfaces other than the plantar surface of the foot. It also guarantees that the sensor locations remain independent from skate construction peculiarities, which is a potential problem with some plantar pressure measurement insoles. The major disadvantage with discrete sensor measurements is a resulting incomplete mapping of the foot to shoe interaction pressure knowledge is limited to the chosen sensor locations. Hennig et al., (2000) stated that, the thickness of individual sensors causes a point loading effect that will result in an overestimation of the local pressures, however due to the thickness and flexibility of the fabric piezo resistive sensor a point loading effect is minimal. Depending on the skate construction peak pressure changes may occur at different sites on the foot and ankle. Changes in pressure may be a consequence of skate properties changes but also of different foot landing strategies. Hennig (1996) demonstrated that changes in midsole hardness have a considerable influence on foot loading strategies during ground contact in running.

2.8 Global Pressures of the Foot and Ankle

Few studies have been undertaken that have looked at in boot pressure distribution patterns of the foot at surfaces other than plantar. This may be due to the fact that in most forms of locomotion force vectors run longitudinally about the axis of the hip and lower leg and are transmitted through the plantar surface of the foot. The plantar surface being the location containing the greatest amount of callosities and adipose tissue

in the foot reflects this. Schaff et al. (1987) analyzed pressure distribution in ski boots with flexible mats. They concluded' Dynamic measurement of pressure distribution using a flexible mat as a capacitor can yield valuable additional information, on the static and dynamic stress acting on the human locomotor system'. By applying the measuring of pressure distribution in alpine ski sports the influence the construction of ski boots on the stress exercised on the human leg could be objectively quantified in man for the first time. The analysis focussed on the pressure distribution along the tibia, with the intention to provide the basis for a new guideline for the testing of ski boots. The only other known study looking at pressure at alternative surfaces to the plantar surface was published by Hillmann et al., (2000). Plantar and dorsal foot pressures in subjects who had undergone rotationplasty surgeries were measured with PEDAR (Novel GmbH, Munich, Germany) capacitive pressure distribution insoles. Their findings showed that plantar and dorsal pressure measurements inside the shaft of the prosthesis are feasible and reproducible and that peaks in the pressure patterns correspond to callosities in the foot. These are the only studies that have examined the issue of pressures at the different regions of the foot and ankle in skating.

2.9 Equipment

2.9.1 Goniometry

The goniometers, two lead wires, one per plane, protruding from an end block transfer the produced electrical signal to an amplifier for increased measurement resolution. The signal is then sent to a data logger. The opposing end block has a built in telescoping mechanism allowing a variable distance between the two blocks. This feature

is important during rotations with changing axes and also prevents overstretching or buckling of the spring (Boocock et al., 1994) (Figure 2.9.1).

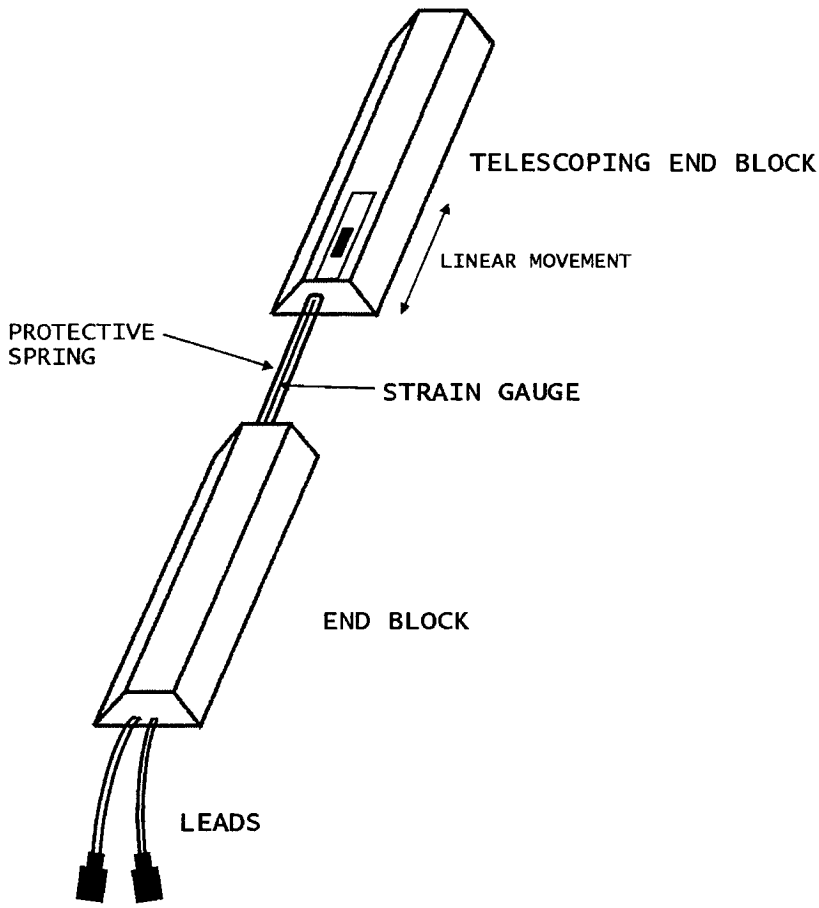

Figure 2.9.1. Commercially available flexible electrogoniometer (adapted from Boocock & Jackson, 1994).

The flexible electrogoniometer is non-invasive, light and fits under clothing easily which make it very suitable for the clinical and research setting. The flexible spring provides very little restriction to movement of joints (Nicol 1987, 1989, Rowe et al. 1989). Biometrics Ltd., the manufacturers of the goniometer give the following specifications: has a life span of 300,000 cycles, an accuracy of ±2° measured, a range of 90°, the repeatability is better than ±1° when measured over a range of 90°, the recommended operating temperature range is 10 - 40°C.

2.9.2 Electromyography

The signal from the 2.5 cm shaped disposable bipolar differential electrodes (Meditrace Inc., conductive adhesive electrodes) was transmitted to a portable data collection unit using EMG amplifier cables (The gain of the preamplifiers is 375. The resolution is 2.95 uV per bit). The EMG, and goniometric signals were measured with the MegaWin Multi Signal System ME3000P8 muscle tester unit (Mega Electronics, Finland). Raw signals were recorded at 1 kHz to avoid aliasing. The portable data logger collects and records data onto a Mitsubishi Electric Memory Card: 32 MB Model MF832M-GMCAV01 ; data were subsequently downloaded into a computer through a an edgeport serial to USB converter.

2.8.3 Pressure Sensors

Semiconductor components that use new signal processing techniques for piezoresistive pressure sensors have enabled precise, automatic, and low-cost electronic compensation of the standard error parameters.

Because most control systems operate with electrical signals, pressure or force must be converted to current or voltage before further processing or analysis. Capacitive and resistive signal transducers are commonly used for this purpose. Capacitive sensors detect pressure as a capacitance associated with the distance between two (or more) diaphragms, which changes in response to a change in pressure. To provide useful output, this capacitance change is usually expressed as attenuation of an AC signal or as a frequency shift in a resonant circuit.

In resistive sensors, pressure changes the resistance by mechanically deforming the sensor, enabling the resistors in a bridge circuit, for example, to detect pressure as a

proportional differential voltage across the bridge. Conventional resistive pressure measurement devices include film resistors, strain gauges, metal alloys, and polycrystalline semiconductors.

Monocrystalline silicon pressure sensors have come into wide use in recent years. Though manufactured with semiconductor technology, they also operate on the resistive principle. The resistance change in a monocrystalline semiconductor (a piezoelectric effect) is substantially higher than that in standard strain gauges, whose resistance changes with geometrical changes in the structure. Conductivity in a doped semiconductor is influenced by a change--compression or stretching of the crystal grid--that can be produced by an extremely small mechanical deformation. As a result, the sensitivity of monocrystalline sensors is higher than that of most other types. Specific advantages are:

- High sensitivity, >10 mV/V
- Good linearity at constant temperature
- Ability to track pressure changes without signal hysteresis, up to the destructive limit

Reference: (http://www.maxim-ic.com/appnotes.cfm/appnote_number/871/ln/en)

Pressure signals quantified forces normal to the surface were collected with flexible piezoresistive sensors dimensions (1.8 X 1.8 X 0.2 cm). The raw signals were recorded at 100 Hz and the data were stored on a portable data logger (FSA Verg Inc. Winnipeg, Manitoba). The stored data were subsequently downloaded onto a PC via a serial port connection.

Chapter 3

Methods

A total of 5 subjects voluntarily participated in the study. All of the subjects were varsity hockey players from McGill University (mean ± SD: age = 21.8 ± 1.9 years, height = 1.81 ± 0.05 m, mass = 83.3 ± 8.0 kg.) Subjects had varying playing experience at the intercollegiate level (i.e. 1 to 5 years). Upon arrival, a verbal explanation of the procedures was given to subjects, as well as informing them of any potential risks or benefits inherent to the research. The consent form was signed to demonstrate that the subjects were aware of the physical demands of the testing protocol, and their willingness to participate.

For EMG measures, bipolar surface electrodes were placed on the muscles of interest using the guidelines from Anatomical Guide for the Electromyographer (Delagi et al., 1980) and oriented with respect to the direction of the muscle fibre. Pilot testing verified the procedure and protocols for the study, as well as to determine the method of processing EMG signals and analysing data. Electrode site locations on the right leg were prepared by removing local hair, abrading the skin with abrasive scrub pads, then cleaning the area with rubbing alcohol. One-inch disc (2.5 cm) shaped disposable bipolar differential electrodes (Meditrace Inc., conductive adhesive electrodes) were placed with the centres 2.5 cm apart. The equipment set up was limited to collecting only four muscles simultaneously, reserving four additional channels for goniometer measures.

The goniometers measured kinematic parameters of right ankle. At the ankle, the device was placed on the posterior aspect of the leg and foot, along the long axis of the Achilles tendon. Height of the placement was adjusted so that approximately the lower

third portion of the lower end block was placed at the height of the calcaneal tuberosity. The goniometers were secured to the subjects with athletic tape (Jaybird & Mais, Inc. Lawrence, MA, USA.)

The EMG and goniometer signals were measured using the Multi Signal System ME3000P8 muscle tester unit (Mega Electronics, Finland). Data were sampled at 1000 Hz. An online measurement was taken to ensure that all channels were receiving signals from the appropriate muscle sources.

Transpose surgical tape (3M) was used to fix the flexible piezo resistive sensors, (FSA Verg Inc. Winnipeg, Manitoba) to the skin. Hair from the area around the skin was removed to restrict displacement of the piezo resistive sensors. All wires from the respective measurement systems were secured to the skaters with athletic tape and bandages to remove a movement artifact from swinging cables and to avoid entanglement between the cables and the subjects. The value of the neutral laced skate weight bearing condition was used as the reference offset for the pressures produced by stance, and lacing of the skates. Subjects were allowed to select their own preferential skate size and were instructed to lace the skates with the tension they deemed sufficient to provide the fit they are usually accustomed to. All subjects skated in the same skate model, the Bauer Vapor XX.

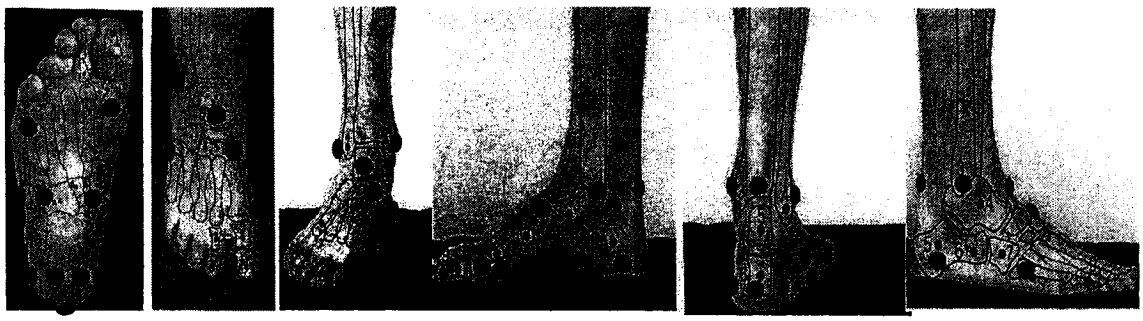

Figure 3.0.1 The locations of the piezo resistive sensor placements. From right to left: Plantar foot, Dorsal Foot (2), Medial Foot, Posterior Foot, Lateral Foot

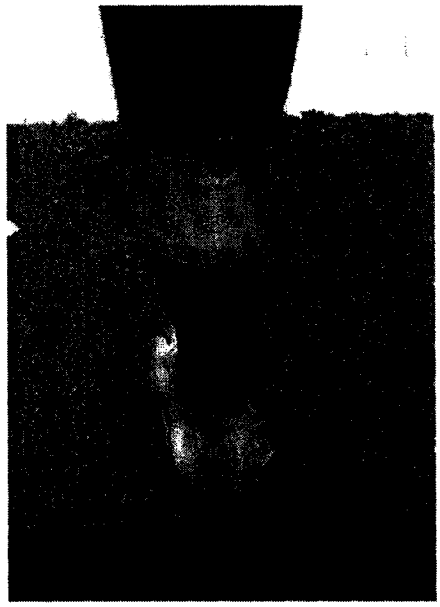

Figure 3.0.2 Goniometer placement and alignment.

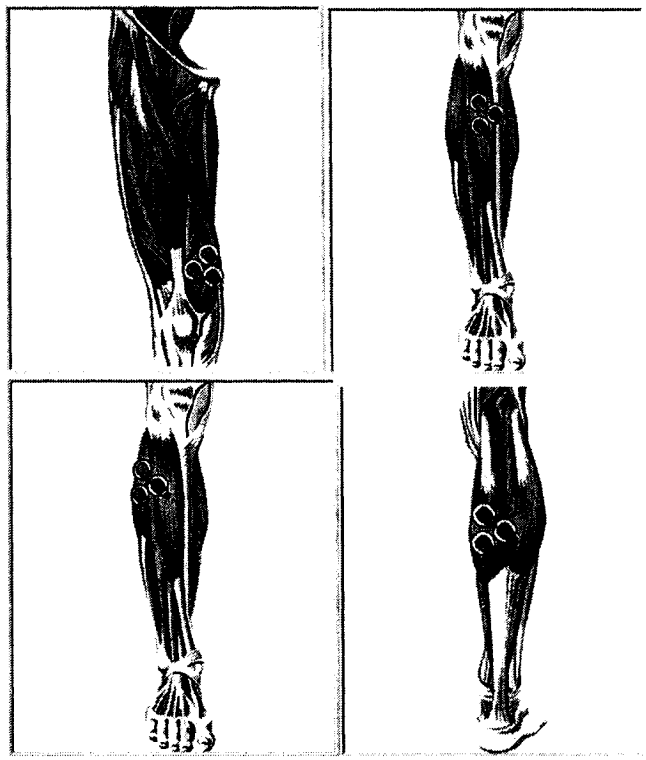

Figure 3.0.3 Illustration of electrode placements sites for 1) Vastus Medialis top left, 2) Tibialis Anterior top right, 3) Peroneus Longus bottom left, and 4) Medial Gastrocnemius bottom right.

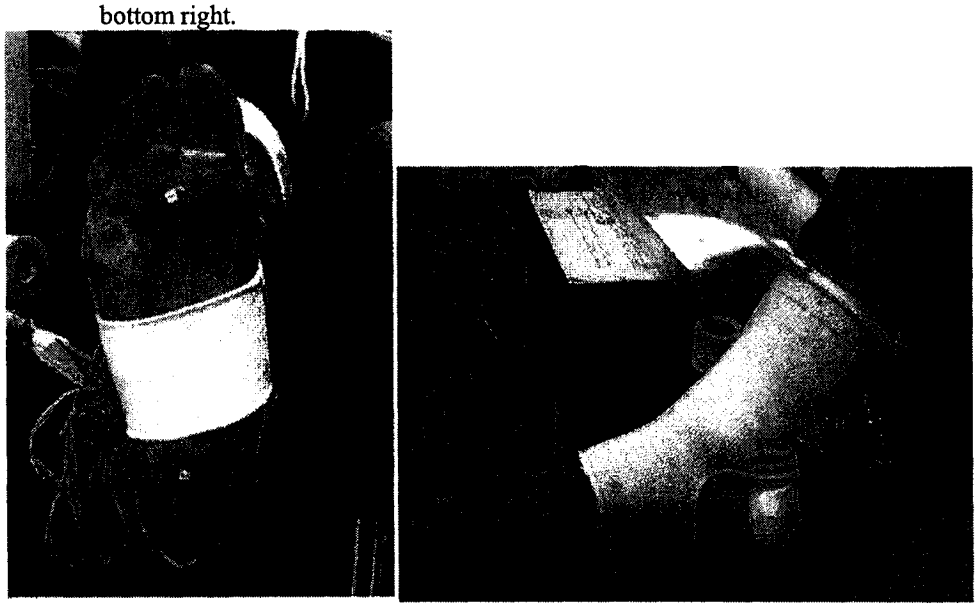

Figure 3.0.4 Sagittal and transverse view of the foot and ankle with goniometer and piezo resistive pressure sensors.

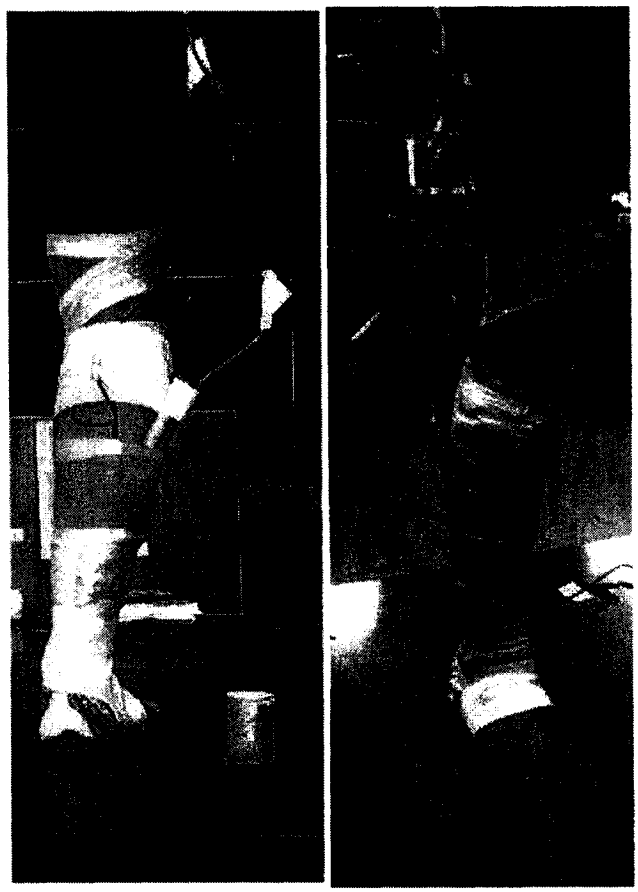

Figure 3.0.5 Posterior and anterior view of the right leg with goniometer, EMG and piezo resistive pressure sensors.

Figure 3.0.6 View of the subject prior to performing the skating tasks.

Prior to the commencement of trials, the subjects were required to stand in a neutral comfortable position during a base line measurement. The ME3000P8 was inserted into a padded casing and then into a waist level backpack. While skating, subjects held their own hockey stick to replicate typical skating conditions.

Subjects were permitted to warm up until they felt prepared and comfortable skating with a goniometer inside the skate. A previous study undertaken investigated whether a warm up of 10 minutes on a stationary bike is enough to reach the end of range of motion measured in weight bearing. The results clearly indicated that the warm up was sufficient and no further functional stress was needed. Thus the author is confident that enough warm up time was given to the subjects. Subjects performed ten trials of constant velocity skating at approximately ninety percent of the maximal skating velocity. In between trials subjects took approximately a fifteen second rest. After the trials were completed, data were downloaded by interfacing the ME3000P8 with an IBM Thinkpad (Pentium III) computer, via an optic transfer cable. Additional video recorded logs were kept.

3.1 Calibration of the Electrogoniometer

The linear relationship between the voltage potential produced by the device and the subtended angle between the end blocks were examined. This was achieved by flexion the goniometer at known angles. A scatter plot of the concurrent output voltages was noted. Resolutions and accuracy of the channels are presented below.

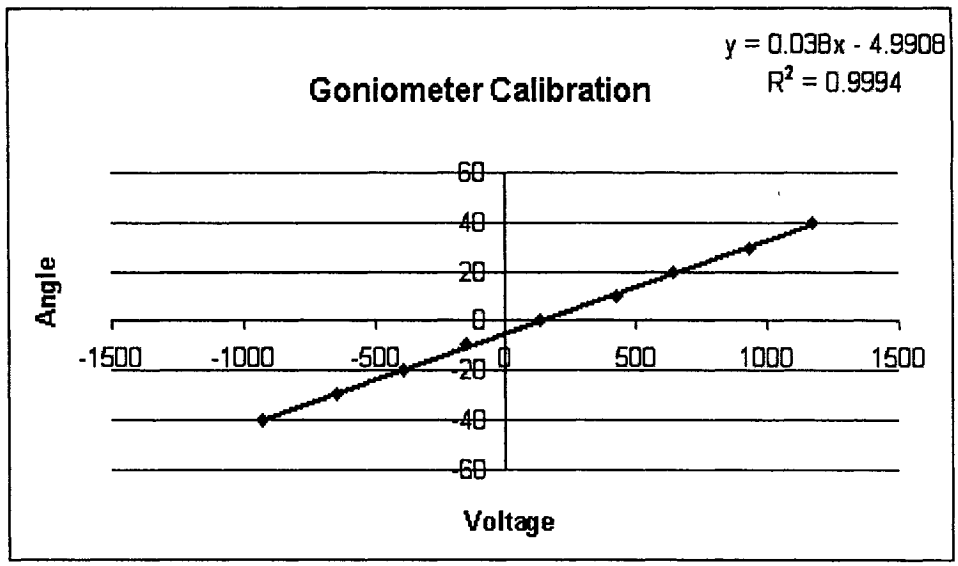

Figure 3.1.1. Calibration of a uniaxial measurement of a flexible electric goniometer shows a high degree of linearity reflected by the determination coefficient. Y axis values represent degrees of flexion.

The two independent measurement systems the Multi Signal System ME3000P8 muscle tester unit (Mega Electronics, Finland and the FSA) were triggered by the tester through a backpack mounted apparatus that held both triggering devices. The trigger events were later used to align the start and stop points of the two measurement systems; subsequently, a linear interpolation was performed in Matlab^{tm} (vrs. 6.1, Mathworks, USA) processing modules to fit the FSA 100 Hz data with the Biomation 1000 Hz data.

3.2 Calibration of the Pressure Sensors

The piezo resistive sensors were calibrated by utilizing an air bladder (Tekscan, West Boston, MA, USA) that applied uniform force on each sensor. The calibration process, a function of the FSA software, corrects to some degree for the phenomena of creep and hysteresis. The linearity of the sensors to both rising and falling pressure over a considerable length of time is shown below (±3 PSI over a 100 PSI range). Pressure

sensors were calibrated each day of data collection thereby eliminating day to day variability in the sensor gain.

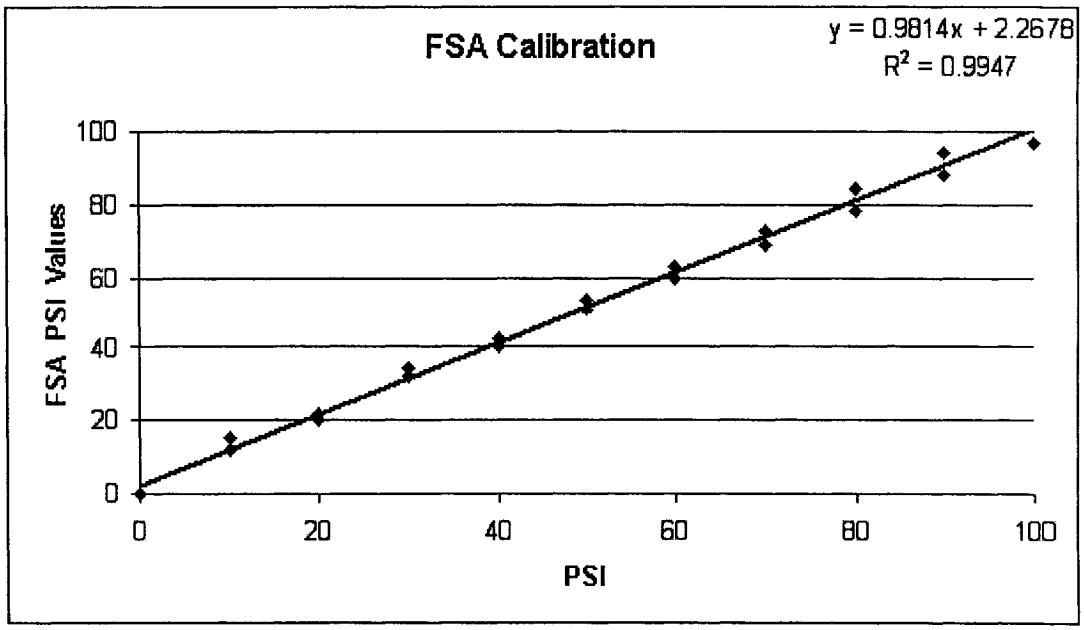

Figure 3.2.1. Calibration of piezo resistive sensors shows a high degree of linearity reflected by the determination coefficient.

3.3 Measuring skating velocity using photocells

To determine the skaters' velocities photocell emitters were used (Brower Timing Systems). The beam from the photocell emitter goes to a reflector, located directly opposite, and is reflected back to the photocell sensor where it is detected. Two emitter-reflector pairs were arranged at equal separations along the ice surface (length = 18.3m) to identify the beginning and end of steady state velocity intervals. Given the beam separation distance and the time history of the beam breaks it was possible to calculate the average velocity of the skater between any two beams.

For this study, skating velocity is defined as the mean velocity of the skater over a specific distance. Based on the significant photocell separation (18.3 m), velocity

estimates obtained from photocell systems in this study are associated with an error margin < than 0.1 m.s-1.

3.4 Skating Task

During the forward skating trials, each subject initiated forward skating via a parallel start from their respective defensive zone face-off circle. The subjects' trailing foot was set on the goal line for each trial. The subjects were instructed to 'accelerate to the blue line and skate at a constant velocity (~90% of maximum skating velocity' (See figure 3.4.1). This velocity corresponds to speed typically observed in game play.

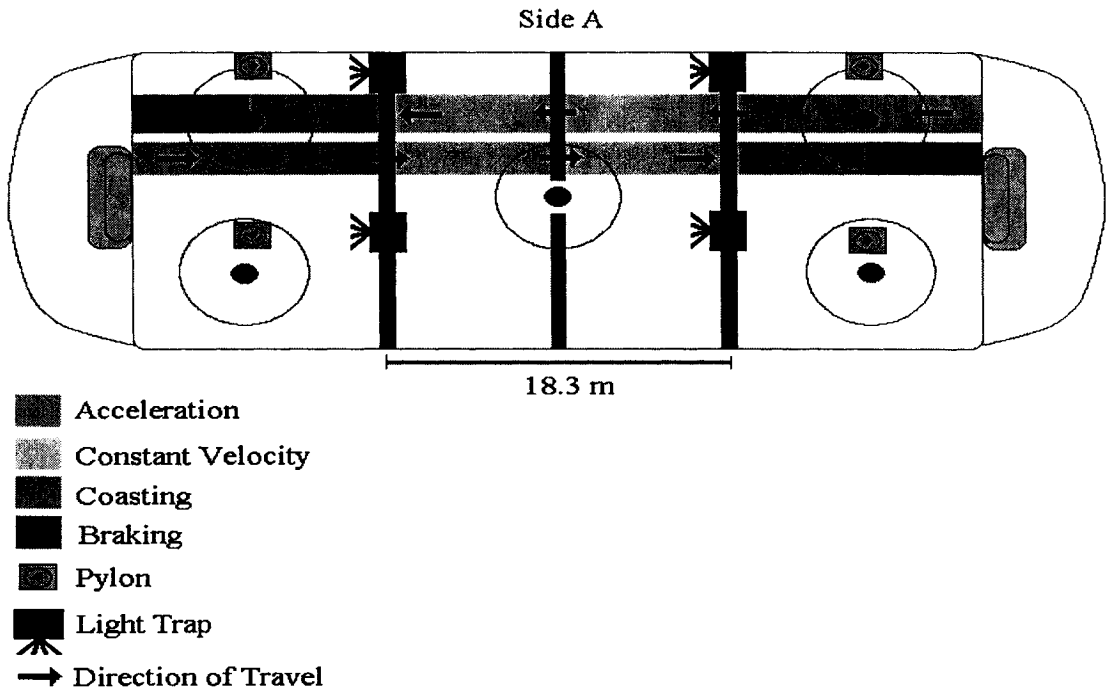

Figure 3.4.1 Diagram of the arena setup.

The trial was completed when the subjects reached the respective offensive face-off circle, where they used a parallel stop (See figure 3.4.2). The subjects repeated this exercise for a period of ten trials and were given ample time to recover in between trials (i.e. 15 - 20 sec.) The timed data were gathered continuously throughout all the trials by the two data loggers. The exact demands and standards of the subject were explained

thoroughly and practiced before data were collected. Photocells (Brower Timing Systems) were used to measure the blue-line to blue-line intervals.

In each trial condition the stride measures of were parsed and imported into Acorn, a Matlab[tm] based graphical user interface. A description below lists the steps involved in the processing of the data modified from Loh et al. (2003.)

3.5 Data Processing and Software Development

Specialized software subroutines in Matlab[tm] were developed to process the data. Five modules divided the processing in the following steps: (1) aligning and interpolating module (2) loading module, (3) the preference panel, (4) the partitioning module, and (5) the ensembler. The following summarizes the sequence involved with each module.

3.5.1 The Aligning and Interpolating Module

The start and stop points of data collection for the two data collection systems were aligned and the data were linearly interpolated with a Matlab[tm] based subroutine to create an appended ASCII file containing all measured values.

3.5.2 The Loading Module

The loading module read the ASCII output files of the FSA software and the MegaWin Software. The loading module read the files simultaneously and separated the input data into 24 channels (channels 1-8 MegaWin and 9 – 24 FSA Pressure).

3.5.3 The Preference Panel

The preference panel was developed to apply the linear application procedure to the first two goniometric channels of the data. The process of linear application was to multiply all the points within a specified channel, by a constant determined by the calibration of the goniometers as described above and then input the slope and y-intercept

values from the neutral offset procedure into the linear application formula. EMG channels four to eight were rectified and a fourth order Butterworth filter was applied after inputting the parameters into the preference panel. No manipulation of the pressure data, channels nine to 24, occurred.

3.5.4 The Partitioning Module.

Once all the channels were correctly processed, they were then parsed into separate strides by the partitioning module. The strides were cut from the myoelectric activity of the Vastus Medialis. Pilot testing indicated that the initial heel-loading event consistently corresponded to the initial peak in myoelectric activity of the vastus medialis. Once the partioning module defined a stride, the pressure, EMG, and kinematic measures were normalized to 1001 points along the time scale. The following text describes the normalization procedure. The first point begins at initial heel (blade) contact of the stride and the last point was identified as the next consecutive heel contact of the same foot. All points between these two points were calculated as follows.

$$Xp = X/(S-1)$$

Where:
Xp was the calculated percent of stride for a particular point.
X was the number of the point (e.g. if calculating the percent of stride for the third point, X is 3)
S was the size the entire stride (i.e. S was the number of points of the stride)

After defining the percent of stride of each point, the profile was interpolated to estimate the variables at specific intervals (0%, 0.1%, 0.2%, etc). The result from these calculations always yielded a variable profile of 1001 points. This process of normalization set all strides to the same length to eliminate the variance of stride to stride temporal differences. Ensemble averages for the 1001 points for pressure, EMG and

kinematics measures were calculated. The parsed stride was saved as a separate file for the plotting module.

3.5.5 The Ensembler Module

The Ensembler recorded a list of all the files processed in the previous four modules. This study parsed and identified four unique strides for each of the five subjects. These consisted of the first three strides during acceleration (i.e. A1, A2, A3) and for strides collected at constant velocity (i.e. CONST.) The Ensembler grouped these 20 files according to stride. The grouped data were ensembled according to preceding guidelines Winter (1980). The ensembling process resulted in the mean, standard deviation and standard error of each curve parameter plotted and the mean, standard deviation, and standard error of each profile within each channel.

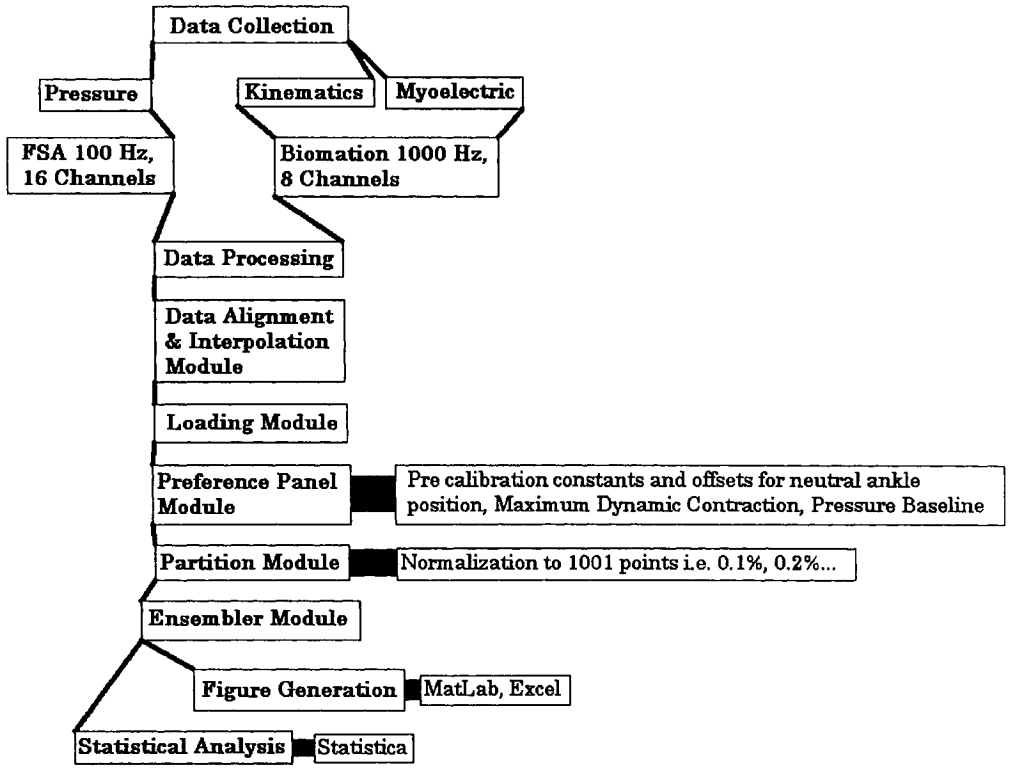

Figure 3.5.1 Flow chart diagramming the steps involved in data collection, processing and presentation.

3.6 Research Design for Statistical Analysis

The stride parameters, the independent variable, were tested at four strides: A1, A2, A3, and CONST. Dependent variables included the minimum and maximum measured values for the kinematic, myoelectric and pressure variables. To enable comparison of the kinematic data, curve parameters were derived; specifically, parameters defining orientation of the joint (i.e. angle).

To determine differences in the measured values, curve parameters were assessed using a one-way repeated measures ANOVA followed by a *post hoc* Tukey HSD using a significance value of $p < 0.05$ via a statistical package (Statistica Release 5.0, Statsoft, Inc., Tulsa, USA).

Chapter 4

4. Results

Despite restricting the objective of this study to the seemingly simplified task of forward skating analysis, the processing of data was considerably time consuming and involved numerous steps, given the large number of independent variables. Adding to the difficulty was the task of deciding on an effective manner of presentation among the numerous ways to represent the figures and skating profiles. Subjects skated at an average velocity of 27.8 km/h ± 1.5 km/h between blue lines for the Constant Velocity (CONST) condition. First angular kinematic results will be presented followed by myoelectric results and finally pressure results. There is a brief explanation provided before each of the figures presented below and text referring to the tables that showed significant differences between variables.

- Ankle Kinematics
- Electromyography
- Pressure
- Stride Duration

EMG data obtained were normalized to the Maximum Dynamic Contraction (MDC) that occurred during the data collection period. The MDCs were found after the data were filtered (fourth order Butterworth with a lowpass set at ten Hz.) The goniometry data were filtered with the same specifications as the EMG data. Pressure data collected from the FSA system were unfiltered. The pressure data are represented according to both its (1) absolute value and (2) relative to the 'neutral' weight bearing condition. The data presented in this study represent a sample size of five subjects (n=5).

4.1 Ankle Kinematics

The following figures present the mean kinematic profiles for the ankle motion. They are accompanied by the tables which contain the minimum and maximum point values observed in the sagittal and frontal planes.

4.1.1. Sagittal: Plantar-Dorsi Flexion

Figures 4.1.1 & 4.1.3 show the motions of plantar flexion and dorsi flexion during the stride. Some general observations were evident: 1) the overall shape of the curve was similar for the four conditions; 2) although there was no statistical significance, plantar flexion increases though A1- A3 and reaches it's peak at 'Constant Velocity'; 3) ankle plantar flexion peak occured at approximately 63 percent of stride, when the foot was in swing phase; 4) the ankle was near maximal dorsi flexion at terminal stance; and 5) subtle variations in the skating profiles produce marked variations in the timing of the maximum dorsi flexion values, however no statistically significant differences were found between strides for this maximum dorsi flexion value.

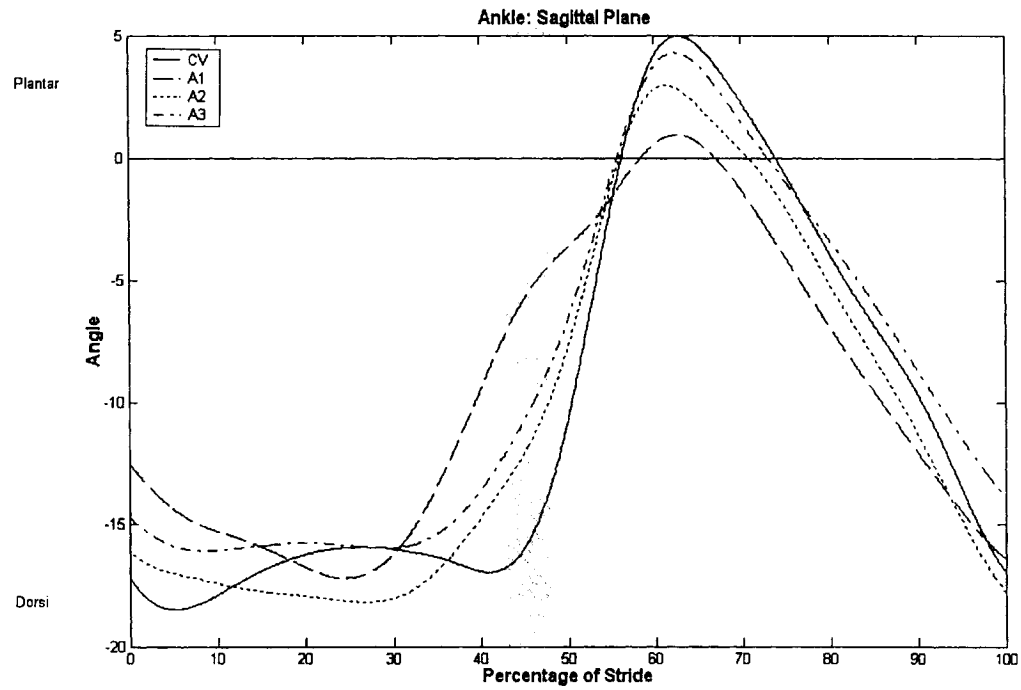

Figure 4.1.1 Mean sagittal kinematic profiles of ankle movements for 5 subjects performing forward skating strides. Different patterned lines represent different strides First Acceleration (A1), Second Acceleration (A2), Third Acceleration (A3), and Constant Velcoity (CONST). The striped area represents the approximate time phase at which the blade left the ice surface. The horizontal line depicts neutral frontal ankle position.

Table 4.1.1. Tukey's HSD Post Hoc Test Results from ANOVA comparing maximum (a) and minimum (b) values representing peak Ankle Plantar / Dorsi Flexion angles for strides A1, A2, A3, and CONST Velocity.

a) Maximum

	A1	A2	A3	CONST
	2.93	3.28	5.07	5.69
A1				
A2	0.99			
A3	0.43	0.57		
CONST	0.23	0.33	0.97	

b) Minimum

	A1	A2	A3	CONST
	-18.55	-19.43	-20.74	-19.34
A1				
A2	0.70			
A3	0.079	0.41		
CONST	0.76	0.99	0.36	

a)

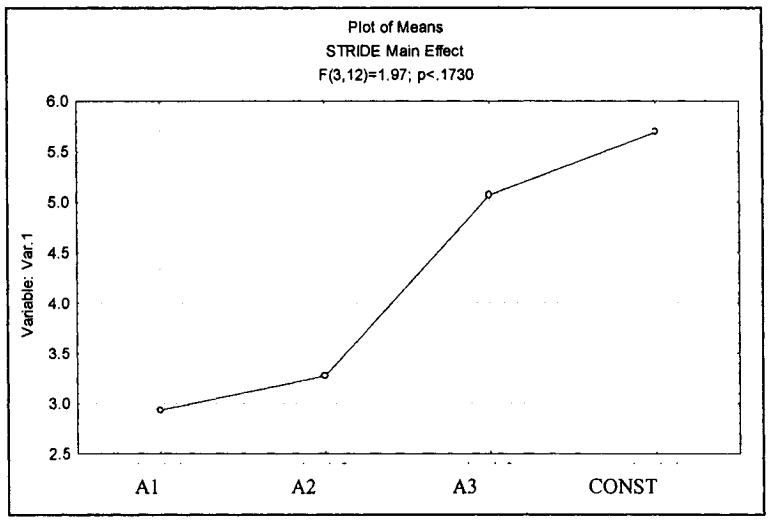

b)

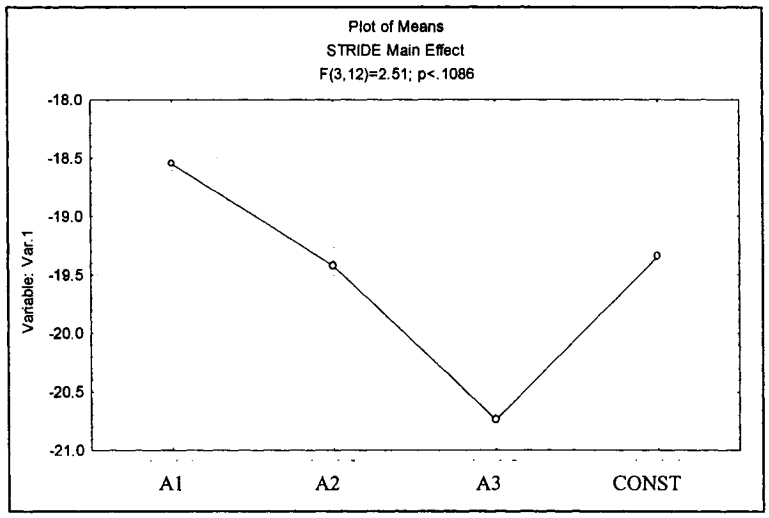

Figure 4.1.2 Profiles of mean ankle maximum (a) and minimum (b) dorsi / plantar flexion for 5 subjects performing forward skating strides. Different values represent different strides A1, A2, A3, and CONST. Negative values indicate greater dorsi flexion.

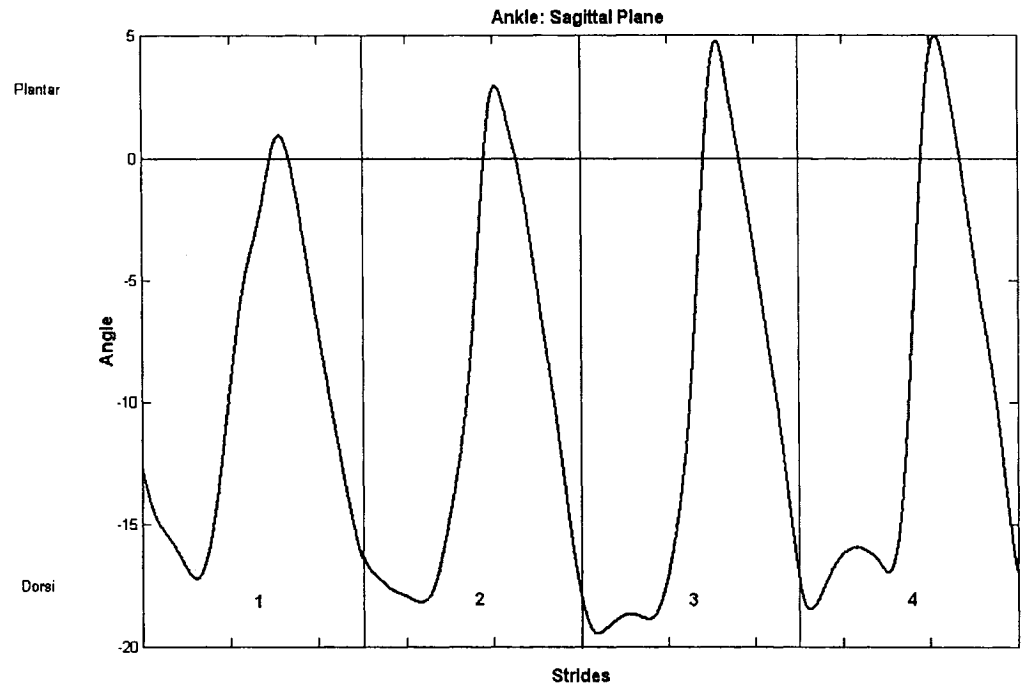

Figure 4.1.3 Mean kinematic profiles of sagittal ankle movements for 5 subjects performing forward skating strides. Vertical lines represent different strides 1 (A1), 2 (A2), 3 (A3), and 4 (CONST). The horizontal lines depict neutral sagittal ankle position.

4.1.2 Frontal: Inversion-Eversion

Figures 4.1.4 & 4.1.6 show the motions of inversion and eversion during the stride. Some observations are evident: 1) the overall shape of the curve is similar for the four conditions; 2) although there is no statistical significance inversion in the swing phase increases though A1- A3 and reaches it's peak at CONST; 3) peak eversion values decrease from strides A1 – A3 however peak eversion for CONST is closer to the values of A1 & A2 than A3. Although the temporal aspects of the minimum and maximum values for the dependent variable were not analyzed statistically these figures show the timing of peak inversion values in the swing phase occurring progressively later on the normalized time scale from strides A1 – CONST. The occurrence of peak eversion is noticeably earlier in stride A1 than in all other strides.

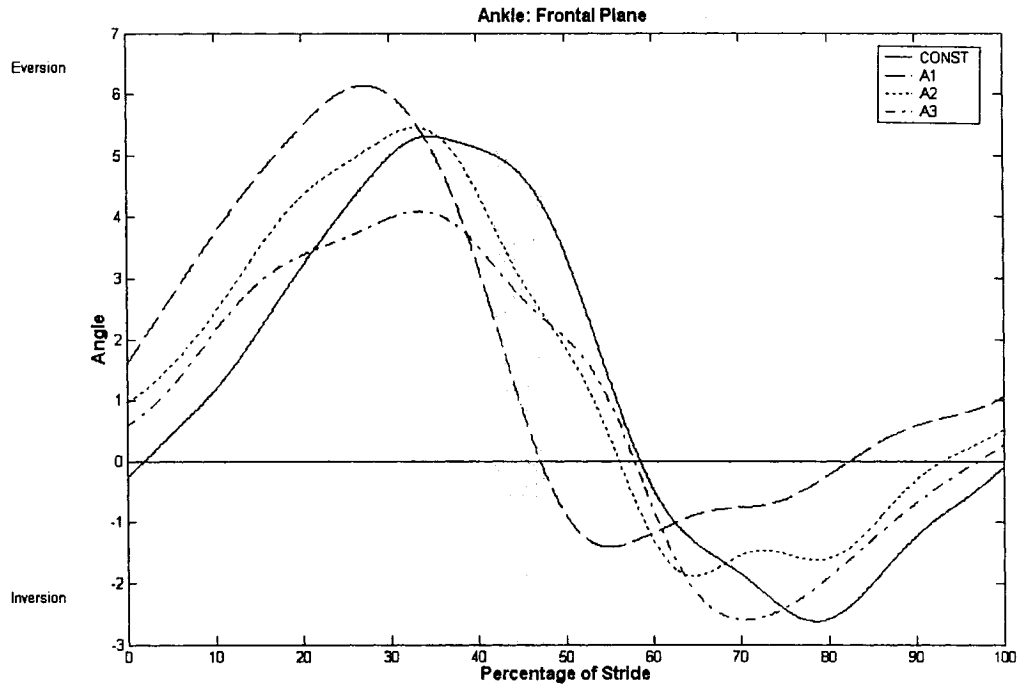

Figure 4.1.4 Mean frontal kinematic profiles of ankle movements for 5 subjects performing forward skating strides. Different patterned lines represent different strides First Acceleration (A1), Second Acceleration (A2), Third Acceleration (A3), and Constant Velcoity (CONST). The striped area represents the approximate time phase at which the blade left the ice surface. The horizontal line depicts neutral frontal ankle position.

Table 4.1.2. Tukey's HSD Post Hoc Test Results from ANOVA comparing maximum (a) and minimum (b) values representing peak Ankle Inversion/Eversion angles for strides A1, A2, A3, and CONST Velocity.

a) Maximum

	A1	A2	A3	CONST
	6.94	6.33	6.48	5.82
A1				
A2	0.70		0.99	0.81
A3	0.85	0.99		0.65
CONST	0.25	0.81	0.65	

b) Minimum

	A1	A2	A3	CONST
	-3.38	-4.17	-4.32	-4.24
A1				
A2	0.33			
A3	0.20	0.98		
CONST	0.27	0.99	0.99	

a)

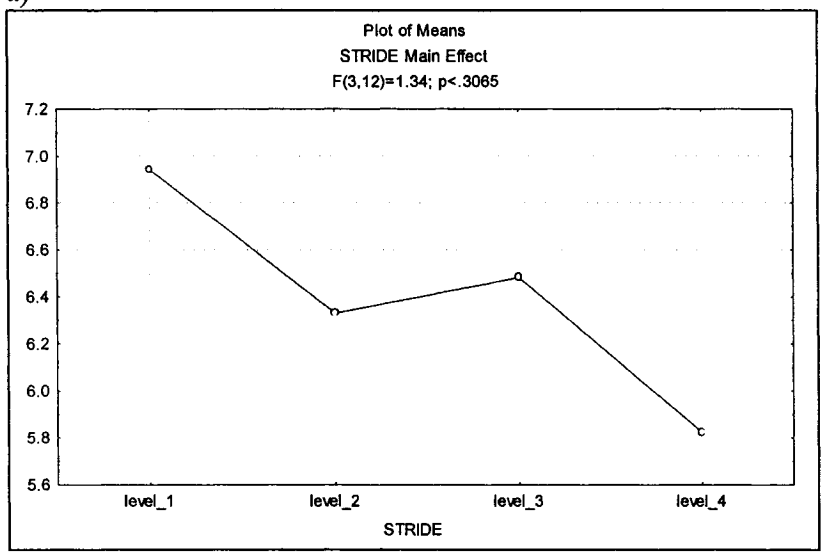

b)

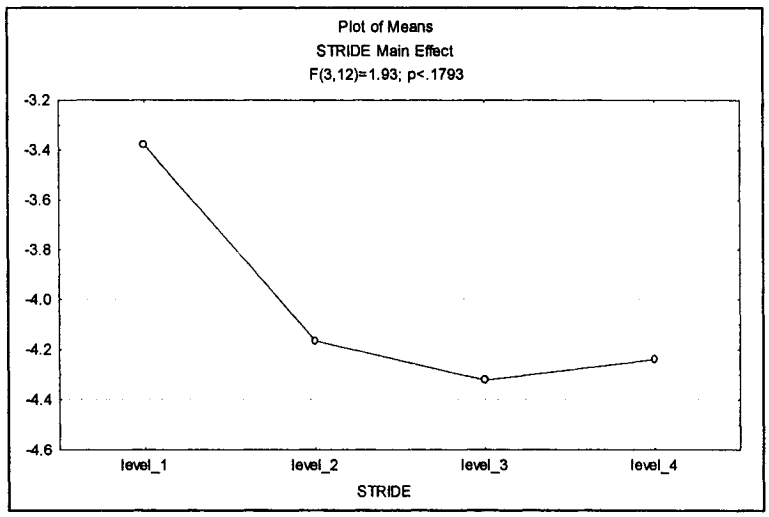

Figure 4.1.5. Profiles of mean ankle maximum (a) and minimum (b) inversion-eversion angles for 5 subjects performing forward skating strides. Different values represent different strides level_1 (A1), level_2 (A2), level_3 (A3), and level_4 (CONST). Negative values indicate inversion.

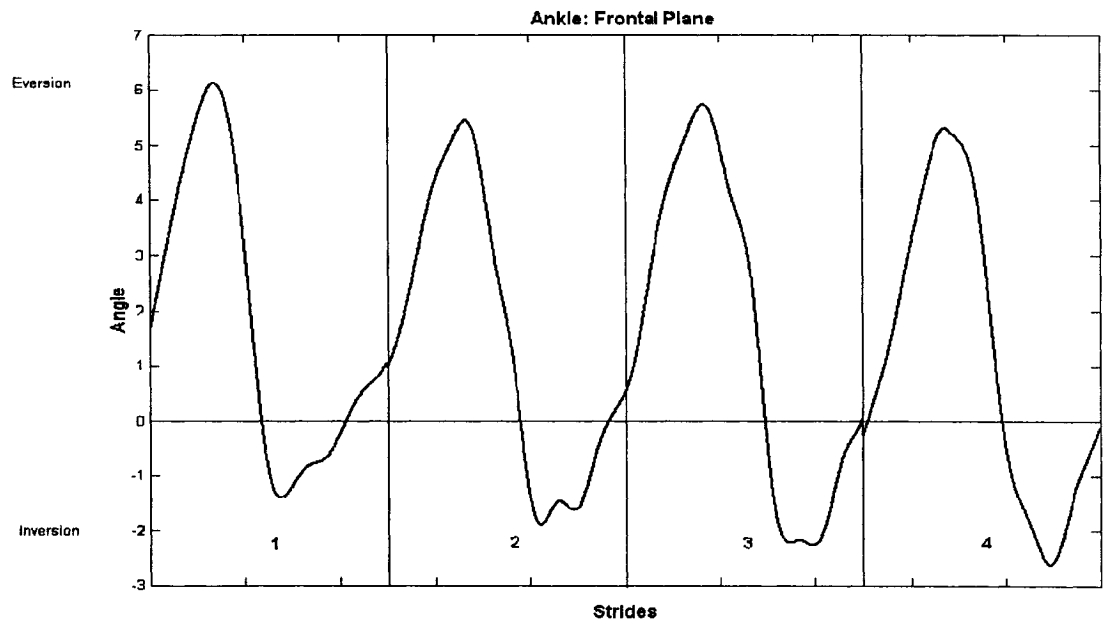

Figure 4.1.6. Mean kinematic profiles of frontal ankle movements for 5 subjects performing forward skating strides. Vertical lines represent different strides 1 (A1), 2 (A2), 3 (A3), and Const (4). The horizontal line depicts neutral frontal ankle position.

4.1.3 Sagittal Angle – Frontal Angle

An ankle angle-angle diagram demonstrating the motion of the sagittal and frontal plane is seen in **Error! Reference source not found.**.7 contrasts ankle kinematics throughout the transition strides of acceleration in forward skating to a relatively constant velocity condition. The open loops of the first, second and third acceleration strides represent the different ankle alignment at the start and endpoints of the stride, and the subsequent task demand differences. In this diagram it is plain to see that the foot inverts as it plantar flexes through the majority of all strides.

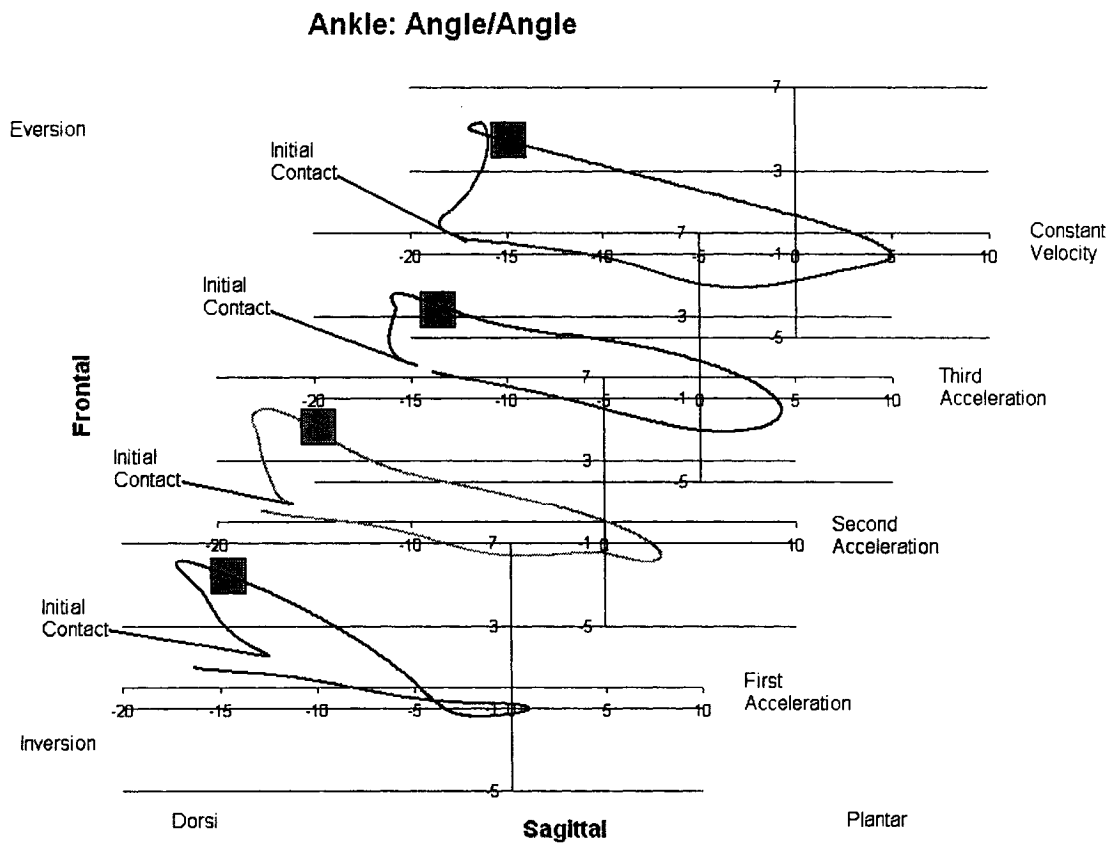

Figure 4.1.7 Mean frontal-sagittal profiles for 5 subjects during forward skating. Moving up and to the right the lines depict (A1), (A2), (A3), and (CONST). The grey shaded regions depict the end of foot contact and the beginning of swing.

4.2 Electromyography

4.2.1 Vastus Medialis

Figure 4.2.1 shows vastus activity has a steep increase at approximately 87 percent of stride in preparation for foot contact. The second peak for strides A1 – A3 occur before the 33 percent of stride at which peak vastus medialis activation occurs at CONST. The shape of the curve remains similar for all strides, the exception being A1 which doesn't have a prominent second peak in the curve after its initial peak. In addition the myoelectric activity at the start of stride for strides A1 –A3 is noticeably greater than at CONST. The slope during the decline in myoelectric activity in the vastus

medialis are similar during all strides, however the decline occurs later in strides A3 and CONST than for strides A1 – A2.

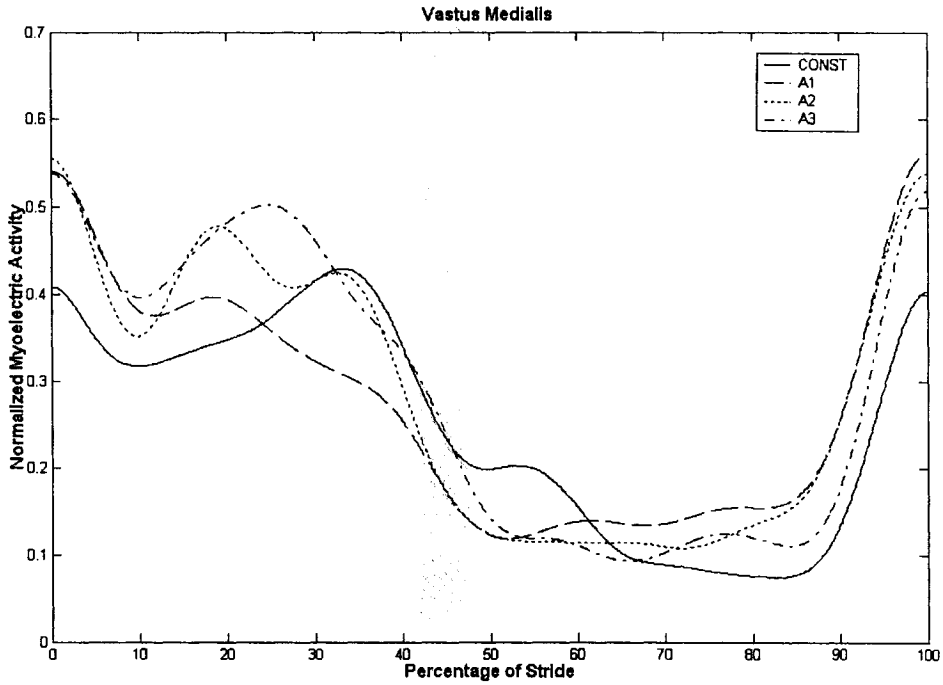

Figure 4.2.1. Mean myoelectric profiles of the vastus medialis for 5 subjects performing forward skating strides. Different patterned lines represent different strides First Acceleration (A1), Second Acceleration (A2), Third Acceleration (A3), and Constant Velcoity (CONST). The striped area represents the approximate time phase at which the blade left the ice surface.

Table 4.2.1. Tukey's HSD Post Hoc Test Results from ANOVA comparing maximum (a) and minimum (b) values representing Vastus Medialis muscle activity for strides A1, A2, A3, and CONST Velocity. * denotes a significant difference between conditions

a) Maximum

	A1	A2	A3	CONST
	.61	.58	.59	.52
A1				
A2	0.78			
A3	0.91	0.99		
CONST	0.05 *	0.23	0.15	

b) Minimum

	A1	A2	A3	CONST
	.088	.088	.057	.067
A1				
A2	0.99			
A3	0.15	0.15		
CONST	0.44	0.45	0.87	

a)

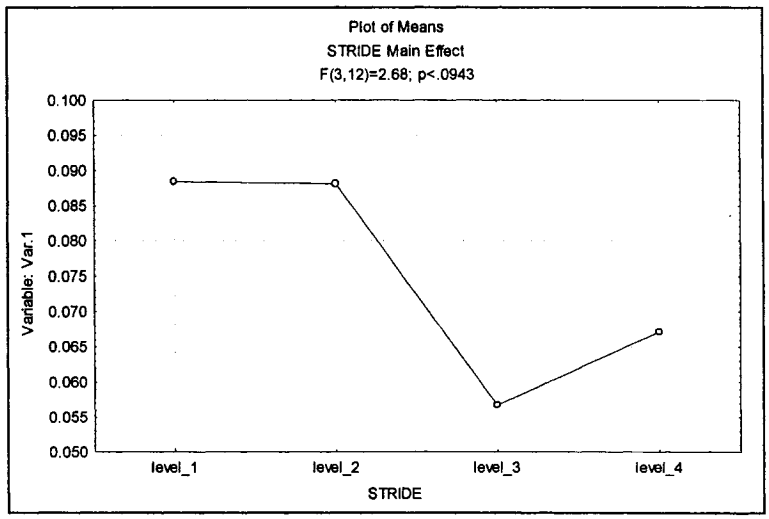

b)

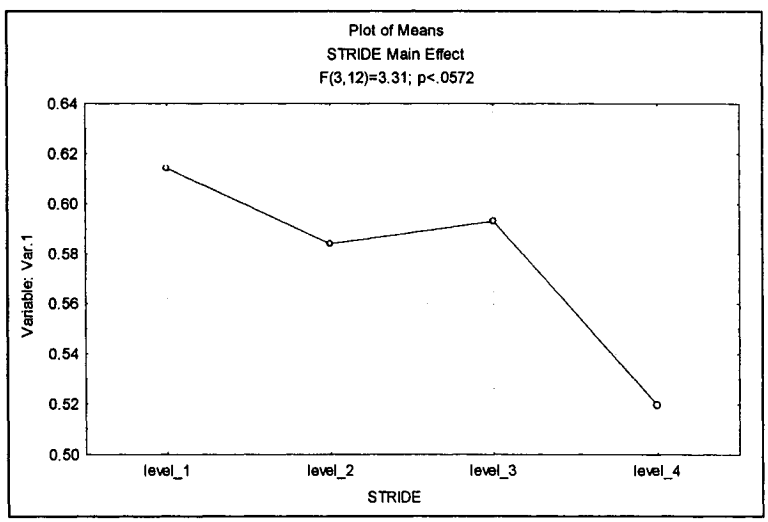

Figure 4.2.2. Profiles of mean maximum (a) and minimum (b) Vastus Medialis muscle activity for 5 subjects performing forward skating strides. Different values represent different strides level_1 (A1), level_2 (A2), level_3 (A3), and level_4 (CONST). Y-axis values are normalized to the Maximum Dynamic Contraction.

4.2.2 Tibialis Anterior

Figure 4.2.3 (A) shows peak tibialis anterior activity occurs during swing phase. A dorsiflexion movement of the ankle is seen at this peak. Peak tibialis activation occurs at approximately 78 percent of stride at CONST. The tibialis anterior activity in stance is at its lowest level during 15 – 40 percent of stride. This is the time when the foot is in contact with the ice and the foot is near maximal eversion.

The tibialis anterior profiles are similar throughout the different strides however this is a temporal shift in the peak myoelectric activity from earlier to later respectively for strides A1 – CONST.

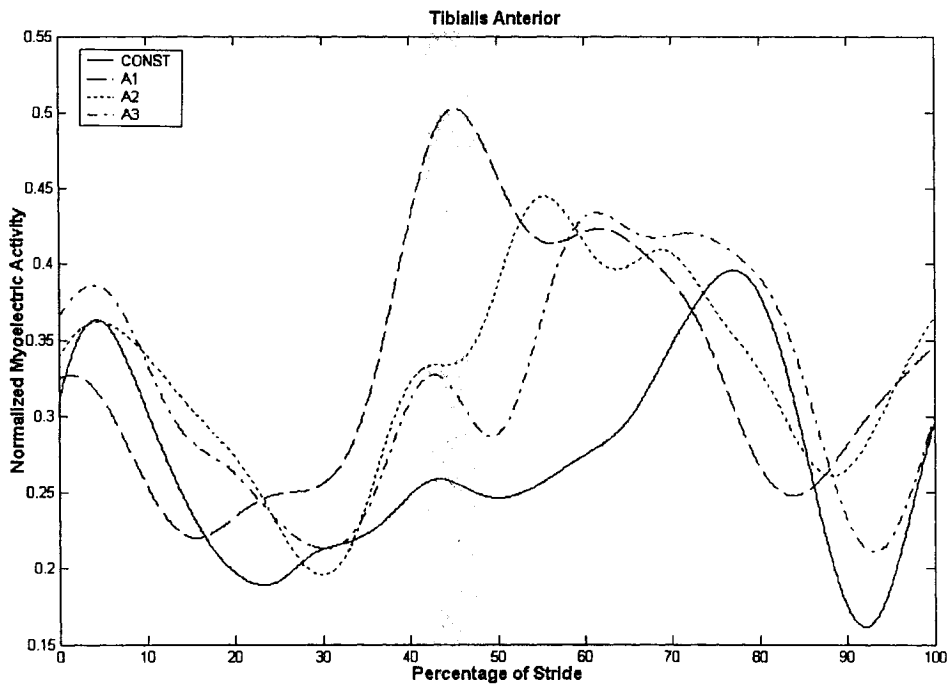

Figure 4.2.3 (A). Mean myoelectric profiles of the tibialis anterior for 5 subjects performing forward skating strides. Different patterned lines represent different strides First Acceleration (A1), Second Acceleration (A2), Third Acceleration (A3), and Constant Velcoity (CONST). The striped area represents the approximate time phase at which the blade left the ice surface.

Table 4.2.2. Tukey's HSD Post Hoc Test Results from ANOVA comparing maximum (a) and minimum (b) values representing Tibialis Anterior muscle activity for strides A1, A2, A3, and CONST Velocity.

a) Maximum

	A1	A2	A3	CONST
	.58	.55	.56	.49
A1				
A2	0.91			
A3	0.99	0.98		
CONST	0.18	0.46	0.29	

b) Minimum

	A1	A2	A3	CONST
	.14	.15	.14	.13
A1				
A2	0.97			
A3	0.99	0.91		
CONST	0.69	0.45	0.82	

a)

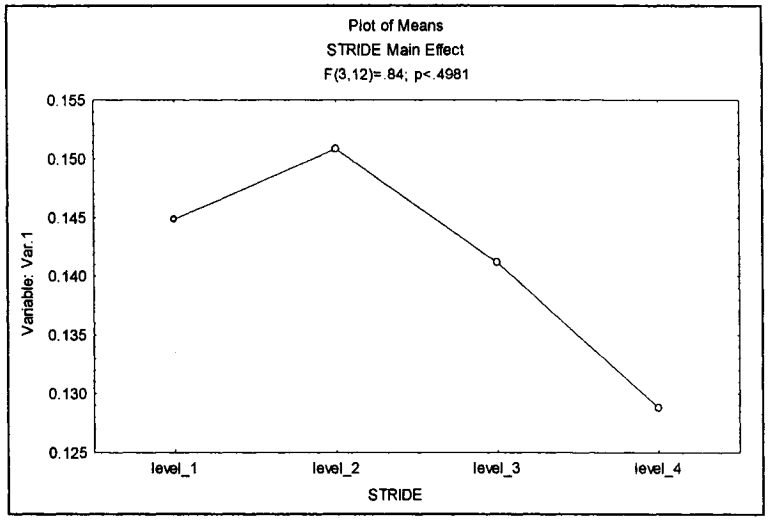

b)

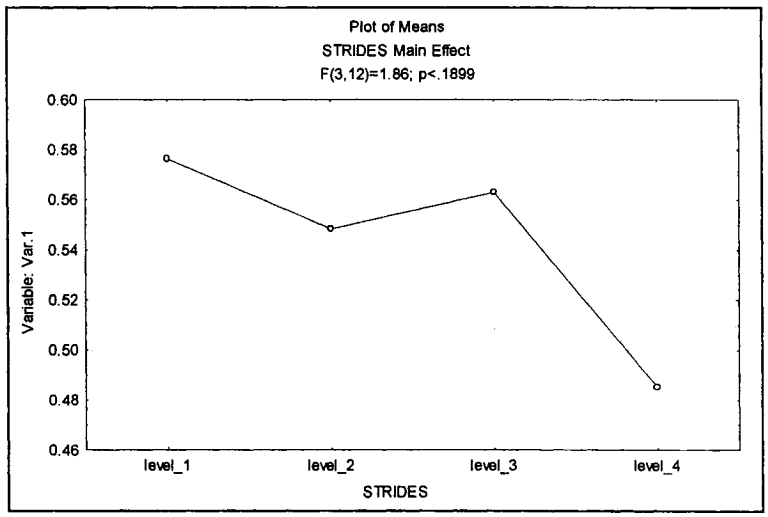

Figure 4.2.3 (B) Profiles of mean maximum (a) and minimum (b) Tibialis Anterior muscle activity for 5 subjects performing forward skating strides. Different values represent different strides level_1 (A1), level_2 (A2), level_3 (A3), and level_4 (CONST). Y-axis values are normalized to the Maximum Dynamic Contraction.

4.2.3 Peroneus Longus

Figure 4.2.4 shows peak peroneus longus activity occurs just prior or just after the weight acceptance event. The exception being at constant velocity in which the peak Peroneus Longus activity occurs at approximately 40 percent of stride, or near push off. Worth noting is that at approximately 40 percent of stride all profiles with the exception of A1 there is a marked increase in activity. The differences in peroneus longus

myoelectric profiles between strides A1 and A2 – CONST are quite similar to the differences in the vastus medialis profile seen between the respective strides.

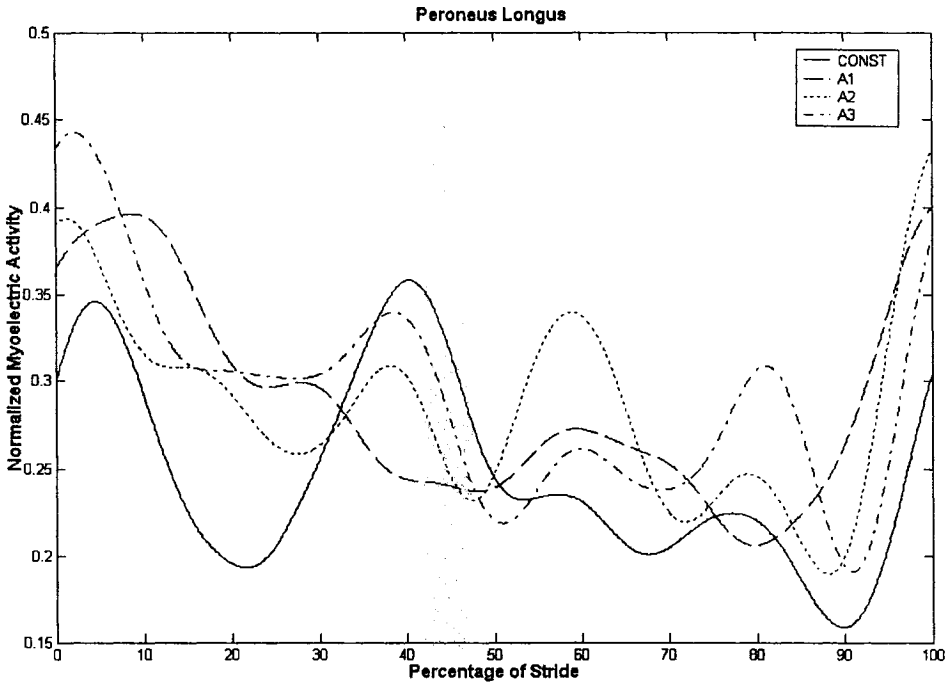

Figure 4.2.4. Mean myoelectric profiles of the Peroneus Longus for 5 subjects performing forward skating strides. Different patterned lines represent different strides First Acceleration (A1), Second Acceleration (A2), Third Acceleration (A3), and Constant Velocity (CONST). The striped area represents the approximate time phase at which the blade left the ice surface.

Table 4.2.3. Tukey's HSD Post Hoc Test Results from ANOVA comparing maximum (a) and minimum (b) values representing Peroneus Longus muscle activity for strides A1, A2, A3, and CONST Velocity.

a) Maximum

	A1	A2	A3	CONST
	.54	.52	.56	.44
A1				
A2	0.99			
A3	0.97	0.88		
CONST	0.33	0.50	0.18	

b) Minimum

	A1	A2	A3	CONST
	.12	.13	.13	.13
A1				
A2	0.99			
A3	0.99	0.99		
CONST	0.99	0.99	0.99	

a)

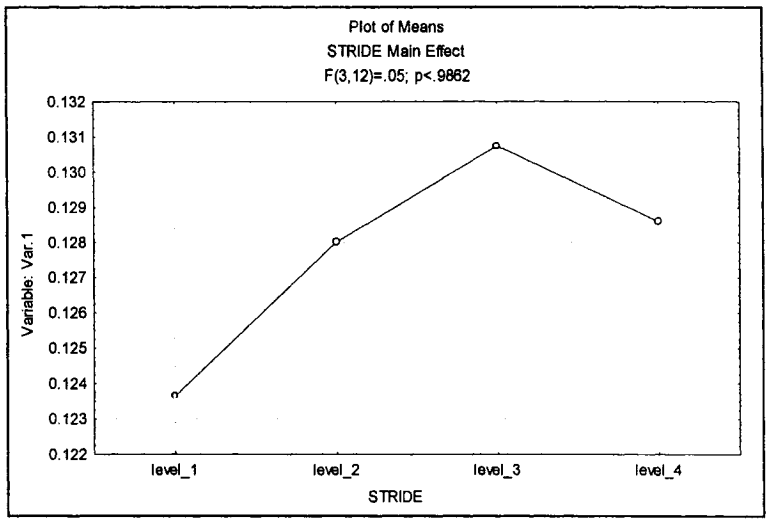

b)

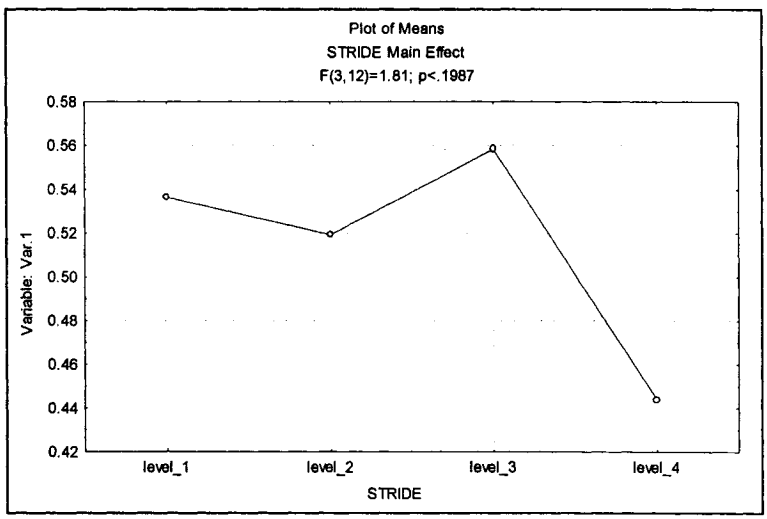

Figure 4.2.5. Profiles of mean maximum (a) and minimum (b) Peroneus Longus muscle activity for 5 subjects performing forward skating strides. Different values represent different strides level_1 (A1), level_2 (A2), level_3 (A3), and level_4 (CONST). Y-axis values are normalized to the Maximum Dynamic Contraction.

4.2.4 Medial Gastrocnemius

Figure 4.2.6 shows medial gastrocnemius peak activation occurs at approximately 42 percent of stride. This peak coincides with increased muscle activation of the peroneus longus at this time. Medial gastrocnemius activation peak occurs approximately 20 percent prior to the plantar flexion peak. Medial gastrocnemius activation is quite low during 60 – 90 percent of stride when the leg is in the swing phase. Again, there are differences in medial gastrocnemius myoelectric profiles between strides A1 and strides

A2 – CONST; this is congruent with the findings of the vastus medialis, and peroneus longus between the respective strides.

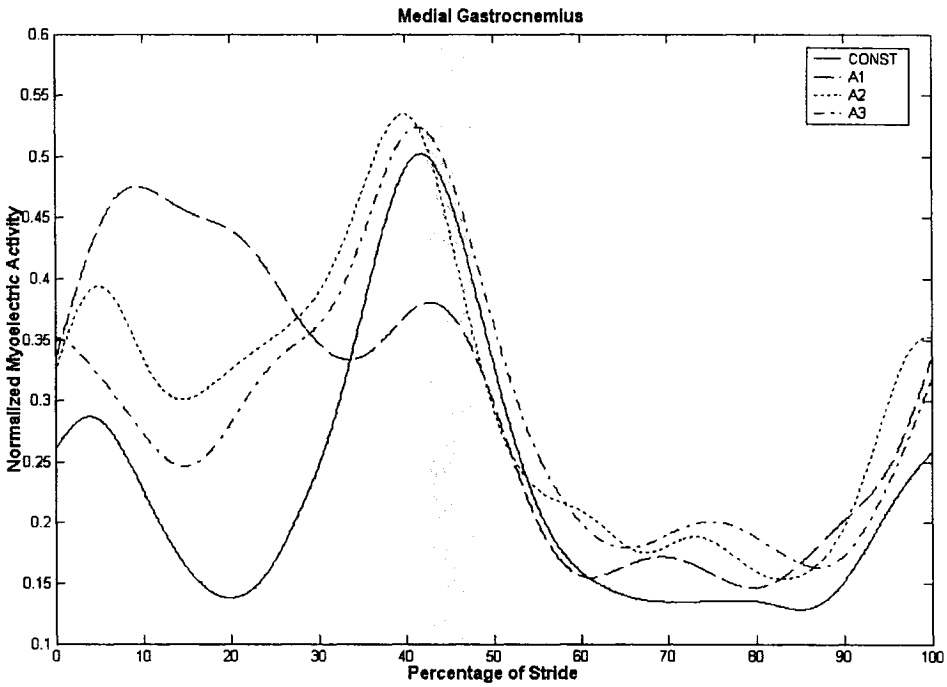

Figure 4.2.6. Mean myoelectric profiles of the medial gastrocnemius for 5 subjects performing forward skating strides. Different patterned lines represent different strides First Acceleration (A1), Second Acceleration (A2), Third Acceleration (A3), and Constant Velcoity (CONST). The striped area represents the approximate time phase at which the blade left the ice surface.

Table 4.2.4. Tukey's HSD Post Hoc Test Results from ANOVA comparing maximum (a) and minimum (b) values representing Medial Gastrocnemius muscle activity for strides A1, A2, A3, and CONST Velocity.

a) Maximum

	A1	A2	A3	CONST
	.6556755	.6202273	.5859574	.5319377
A1				
A2	0.896488			
A3	0.539748	0.905188		
CONST	0.123611	0.348985	0.718159	

b) Minimum

	A1	A2	A3	CONST
	.1099617	.1080530	.1083756	.0964436
A1				
A2	0.999691			
A3	0.999822	0.999999		
CONST	0.90269	0.935027	0.930055	

a)

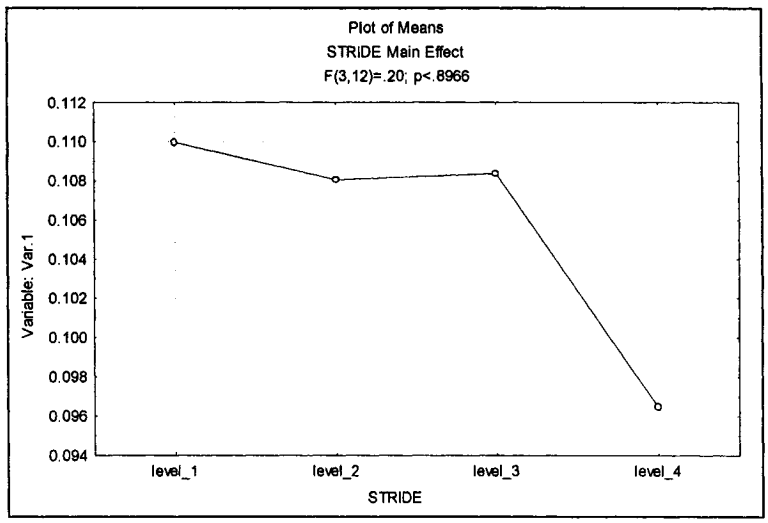

b)

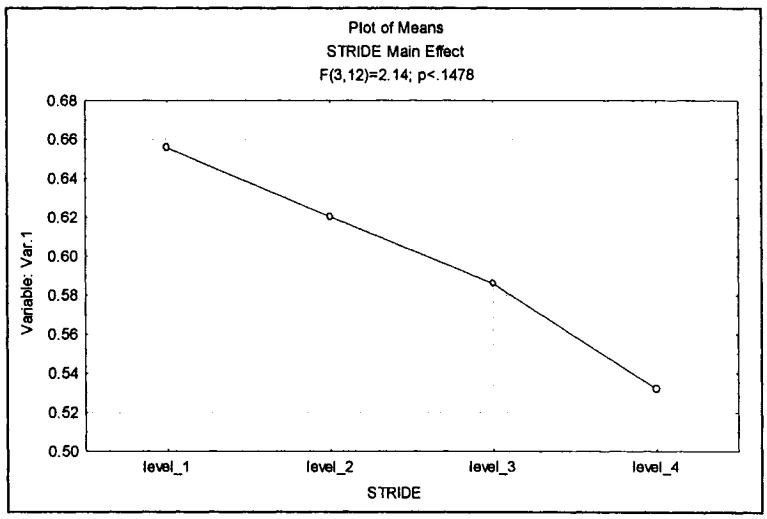

Figure 4.2.7. Profiles of mean maximum (a) and minimum (b) Medial Gastrocnemius muscle activity for 5 subjects performing forward skating strides. Different values represent different strides level_1 (A1), level_2 (A2), level_3 (A3), and level_4 (CONST). Y-axis values are normalized to the Maximum Dynamic Contraction.

4.3 Pressure

Table 4.3.1 denotes the average pressure measurements between subjects while standing in skates with a defined neutral posture. Pressure values were presented in kilopascals. The largest pressure points are found at the plantar surface of the foot: plantar: first metatarsal head, plantar: medial heel, plantar: lateral heel; and at the ankle: medial: malleolus, lateral malleolus, these were also the regions with the largest standard deviation values. The posterior region of the foot and ankle: posterior calcaneus, achilles tendon were the locations that had the least pressure.

Table4.3.1. Descriptive statistics comparing of neutral weight bearing pressure measurements (kPa).

Sensor Placement	**Mean**	**SD**
Plantar: First Metatarsal Head	15.68	9.45
Plantar: Fifth Metatarsal Head	5.79	4.30
Plantar: Medial Arch	3.55	3.20
Plantar: Lateral Arch	8.78	2.44
Plantar: Medial Heel	11.73	5.15
Plantar: Lateral Heel	10.27	6.47
Posterior Calcaneus	.12	.26
Achilles Tendon	.85	.60
Medial: Malleolus	17.64	13.80
Medial Calcaneus	1.75	2.02
Medial: First Metatarsal Head	5.93	5.24
Lateral Malleolus	10.18	8.55
Lateral Calcaneus	3.90	3.41
Lateral: Fifth Metatarsal Base	4.17	4.47
Dorsalis Pedis	2.47	1.77
Dorsal: First Metatarsal Base	7.41	3.37

4.3.1 Plantar Medial Foot

Figure 4.3.1 (A) shows the absolute pressure values of the medial plantar foot were consistent with the offset pressure values in that the highest pressure values were in order of 1, forefoot 2, heel and 3, arch.

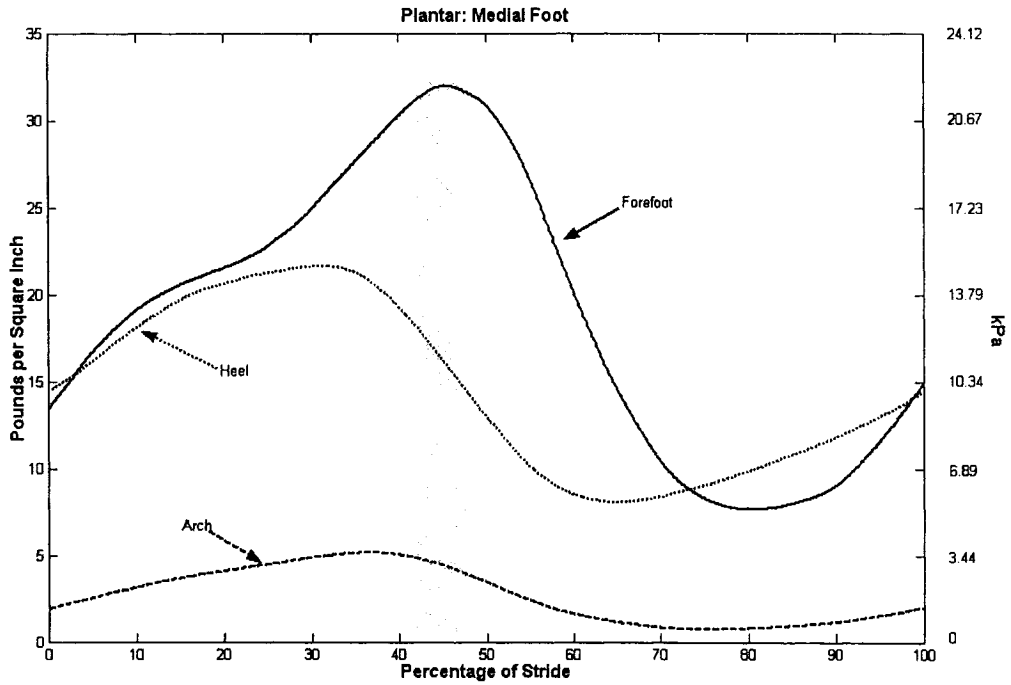

Figure 4.3.1 (A). Mean pressure profiles of the Medial: Plantar Foot for 5 subjects performing forward skating strides at Constant Velocity. The striped area represents the approximate time phase at which the blade left the ice surface.

Figure 4.3.1 (B) shows the plantar medial forefoot pressures were highest compared to the pressures obtained from the sensors placed on the medial side of the foot when the pressure values were offset to the neutral weight bearing value. The occurrence of peak pressure is delayed from proximal to distal sensors on the plantar foot. This delay in onset of peak values represents the movement of the center of mass and centre of pressure anteriorly during the stance phase of the skating stride.

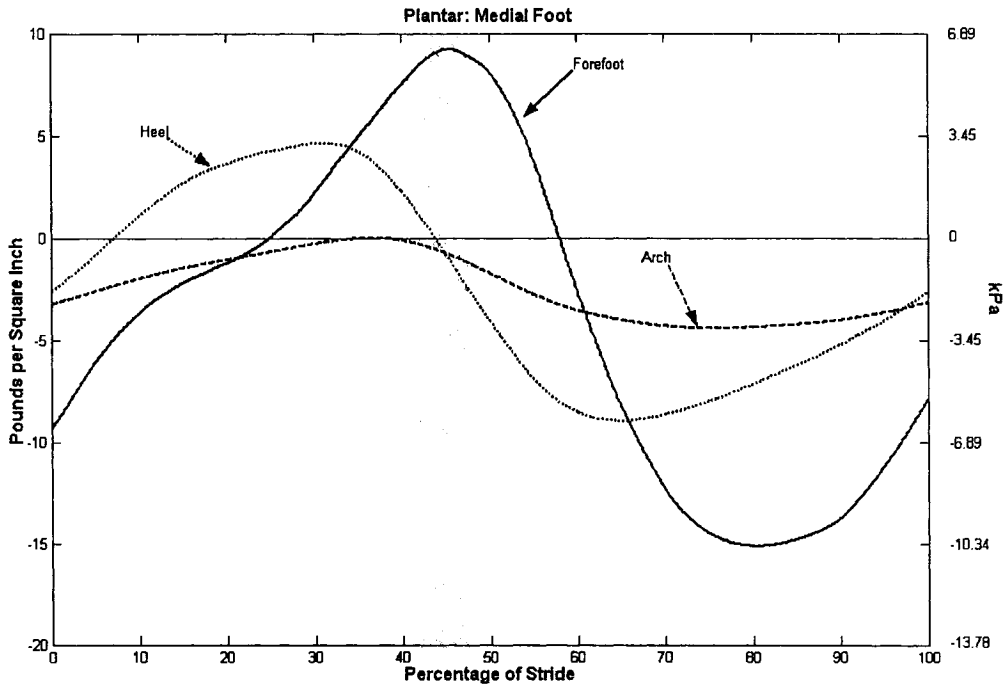

Figure 4.3.1 (B). Mean pressure profiles of the Medial: Plantar Foot for 5 subjects performing forward skating strides at Constant Velocity. Values are represented relative to their neutral weight bearing value. The striped area represents the approximate time phase at which the blade left the ice surface.

Table 4.3.2. Tukey's HSD Post Hoc Test Results from ANOVA comparing maximum (a) and minimum (b) values representing Plantar: First Metatarsal pressure for strides A1, A2, A3, and CONST Velocity.

a) Maximum

	A1	A2	A3	CONST
	47.7	35.9	42.9	40.8
A1				
A2	0.4			
A3	0.9	0.8		
CONST	0.8	0.9	0.9	

b) Minimum

	A1	A2	A3	CONST
	6.4	6.5	5.9	7.2
A1				
A2	0.9			
A3	0.9	0.9		
CONST	0.9	0.9	0.7	

a)

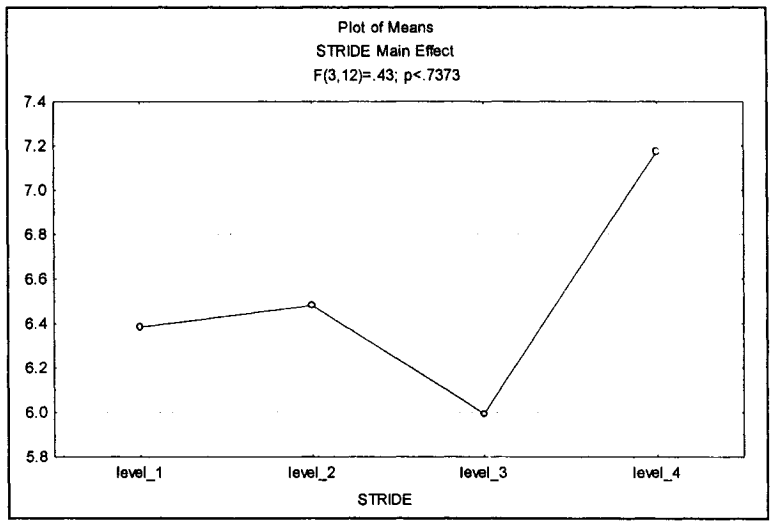

b)

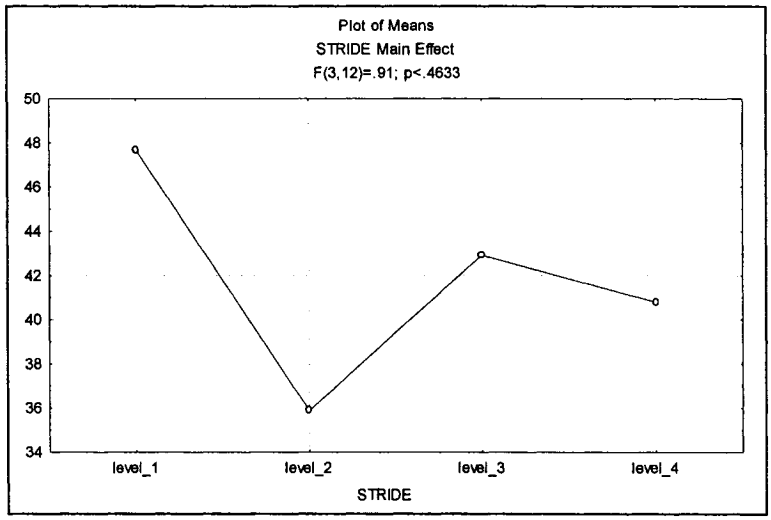

Figure 4.3.2. Profiles of mean maximum (a) and minimum (b) Plantar: First Metatarsal pressure for 5 subjects performing forward skating strides. Different values represent different strides level_1 (A1), level_2 (A2), level_3 (A3), and level_4 (CONST).

Table 4.3.3. Tukey's HSD Post Hoc Test Results from ANOVA comparing maximum (a) and minimum (b) values representing Plantar: Medial Arch pressure for strides A1, A2, A3, and CONST Velocity.

a) Maximum

	A1	A2	A3	CONST
	5.125221	5.644631	4.841968	5.539507
A1				
A2	0.884074			
A3	0.977904	0.681896		
CONST	0.93606	0.998843	0.764459	

b) Minimum

	A1	A2	A3	CONST
	.7857279	.5723904	.5380611	.6259502
A1				
A2	0.513535			
A3	0.392357	0.995662		
CONST	0.718632	0.983902	0.935236	

a)

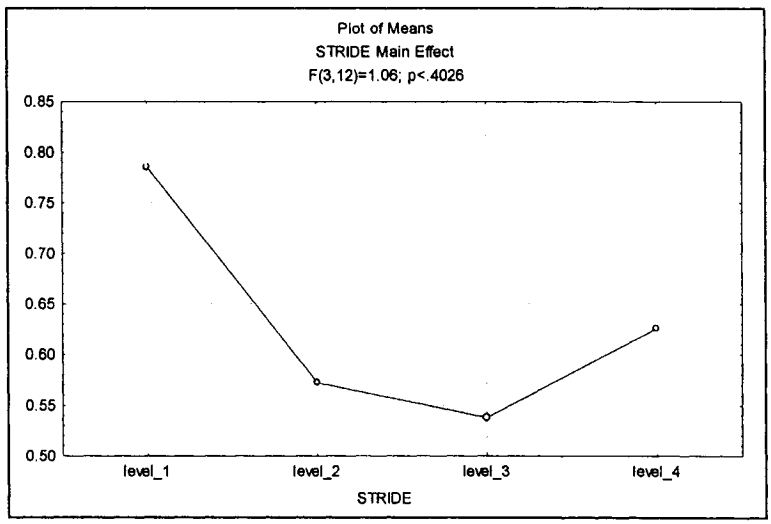

b)

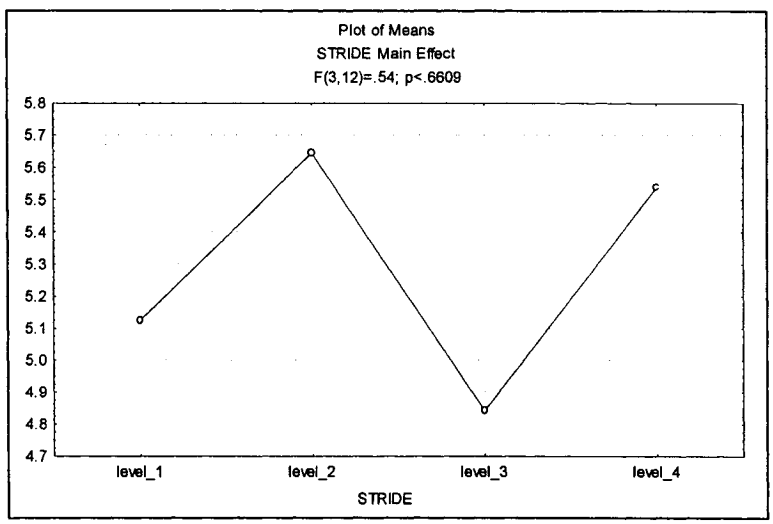

Figure 4.3.3. Profiles of mean maximum (a) and minimum (b) Plantar: Medial Arch pressure for 5 subjects performing forward skating strides. Different values represent different strides level_1 (A1), level_2 (A2), level_3 (A3), and level_4 (CONST).

Table 4.3.4. Tukey's HSD Post Hoc Test Results from ANOVA comparing maximum (a) and minimum (b) values representing Plantar: Medial Heel pressure for strides A1, A2, A3, and CONST Velocity.

a) Maximum

	A1	A2	A3	CONST
	26.14873	28.67290	28.28581	22.26348
A1				
A2	0.805689			
A3	0.87032	0.999062		
CONST	0.531986	0.156882	0.194291	

b) Minimum

	A1	A2	A3	CONST
	7.830324	7.056797	7.989242	7.487625
A1				
A2	0.882674			
A3	0.998773	0.814301		
CONST	0.987701	0.976198	0.963371	

a)

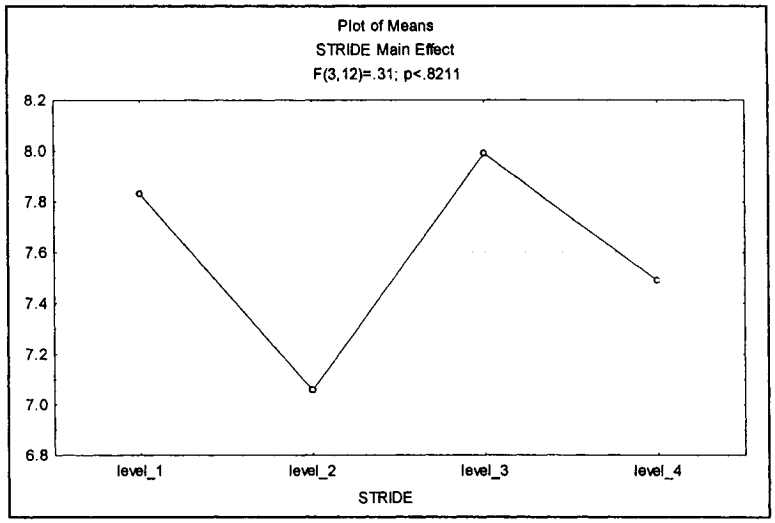

b)

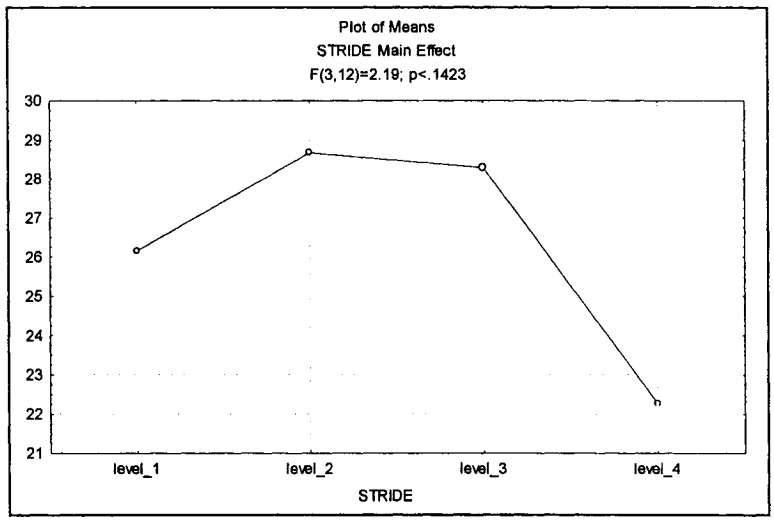

Figure 4.3.4. Profiles of mean maximum (a) and minimum (b) Plantar: Medial Heel pressure for 5 subjects performing forward skating strides. Different values represent different strides level_1 (A1), level_2 (A2), level_3 (A3), and level_4 (CONST).

4.3.2 Plantar: Lateral Foot

Figure 4.3.5 (A) shows that plantar lateral pressures were lower the more distal the sensor was located. The succession of peak pressures from proximal to distal was before and aft respectively for each sensor placement.

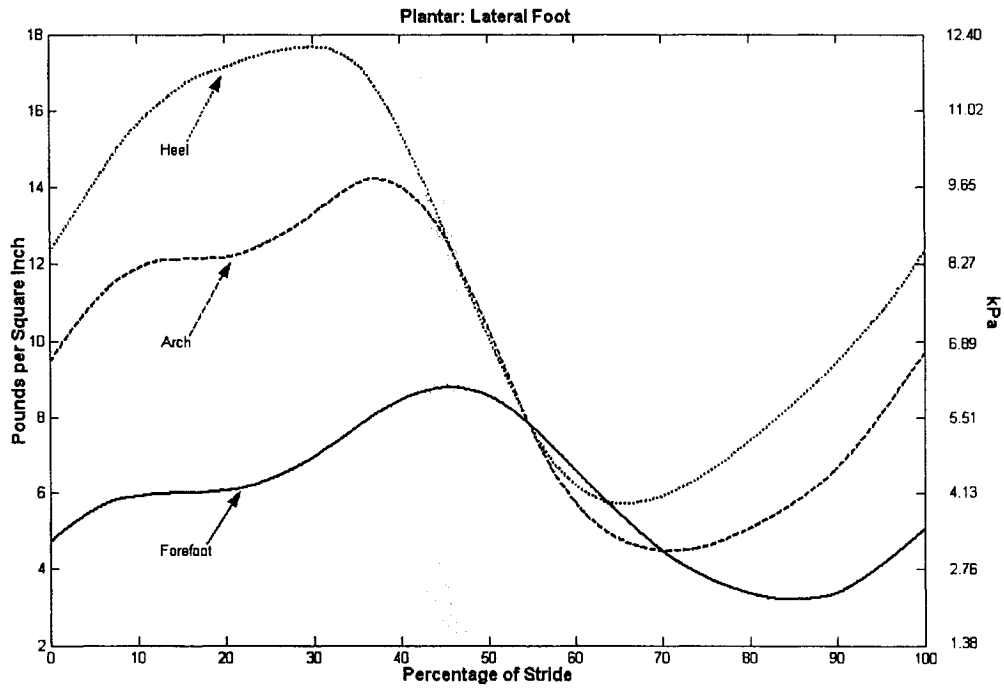

Figure 4.3.5 (A). Mean pressure profiles of the Lateral: Plantar Foot for 5 subjects performing forward skating strides at Constant Velocity. The striped area represents the approximate time phase at which the blade left the ice surface.

Figure 4.3.5 (B). shows that with respect to the plantar lateral foot pressures, the arch pressure was highest during stride relative to the offset neutral weight bearing pressure collected from the subjects. Heel pressure was in between arch and forefoot pressure in respect to this magnitude. Forefoot pressures were the lowest of the lateral foot pressure they reach their peak value at approximately 45 percent of stride. The relative pressure at the forefoot during the stride was small; peak pressures reached approximately 1 PSI or 6.89 kPa.

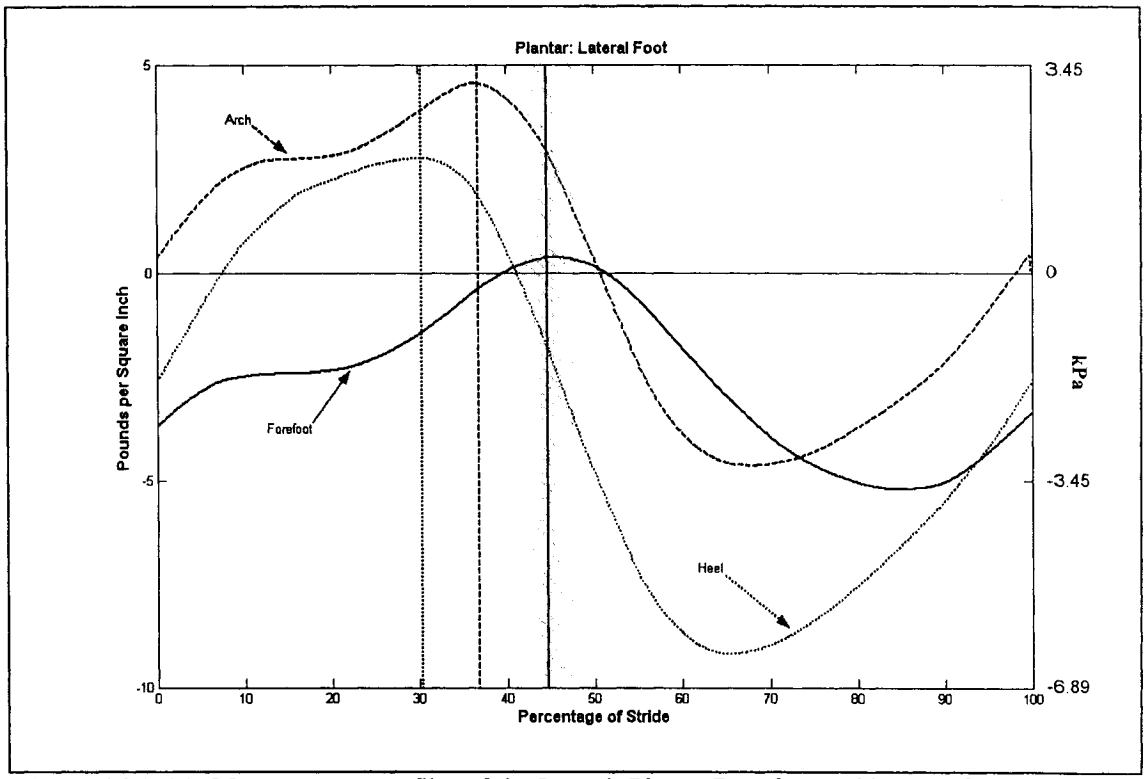

Figure 4.3.5 (B). Mean pressure profiles of the Lateral: Plantar Foot for 5 subjects performing forward skating strides at Constant Velocity. Values are represented relative to their neutral weight bearing value. The striped area represents the approximate time phase at which the blade left the ice surface. Vertical lines represent time of peak pressure for the respective pattern line.

Table 4.3.5. Tukey's HSD Post Hoc Test Results from ANOVA comparing maximum (a) and minimum (b) values representing Plantar: Fifth Metatarsal pressure for strides A1, A2, A3, and CONST Velocity. Tukey's High Significant Difference Post Hoc test revealed a significant difference between the duration of stride time between A1 and CONST (p = 0.05), and A1 and A2 (p = 0.02). Near significant differences are seen between strides A1 and A3 (p = 0.06) in all cases, maximum pressure was highest at A1.

a) Maximum

	A1	A2	A3	CONST
	12.3	8.3	9.1	9.0
A1				
A2	0.02 *			
A3	0.06	0.87		
CONST	0.05 *	0.91	0.99	

b) Minimum

	A1	A2	A3	CONST
	3.068395	2.778793	2.609744	3.024810
A1				
A2	0.77545			
A3	0.458652	0.942408		
CONST	0.99893	0.847187	0.538686	

* denotes a significant difference between conditions

a)

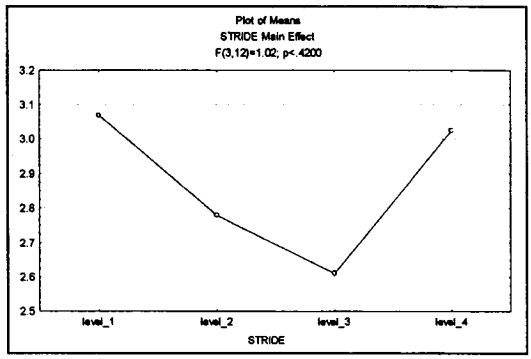

b)

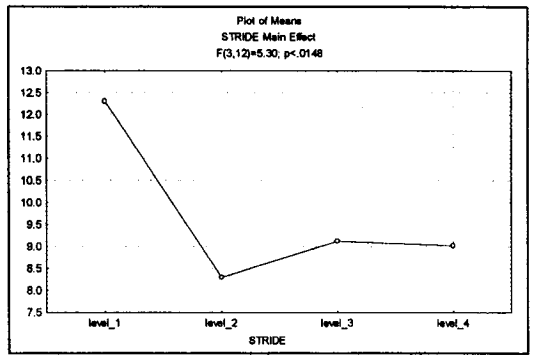

Figure 4.3.6. Profiles of mean maximum (a) and minimum (b) Plantar: Fifth Metatarsal pressure for 5 subjects performing forward skating strides. Different values represent different strides level_1 (A1), level_2 (A2), level_3 (A3), and level_4 (CONST).

Table 4.3.6. Tukey's HSD Post Hoc Test Results from ANOVA comparing maximum (a) and minimum (b) values representing Plantar: Lateral Arch pressure for strides A1, A2, A3, and CONST Velocity.

a) Maximum

	A1	A2	A3	CONST
	15.74088	15.00170	15.31131	15.06876
A1				
A2	0.95041			
A3	0.989467	0.996016		
CONST	0.961906	0.999961	0.998102	

b) Minimum

	A1	A2	A3	CONST
	4.490271	3.915140	3.992103	4.173992
A1				
A2	0.755006			
A3	0.824037	0.999165		
CONST	0.945578	0.968849	0.988726	

a)

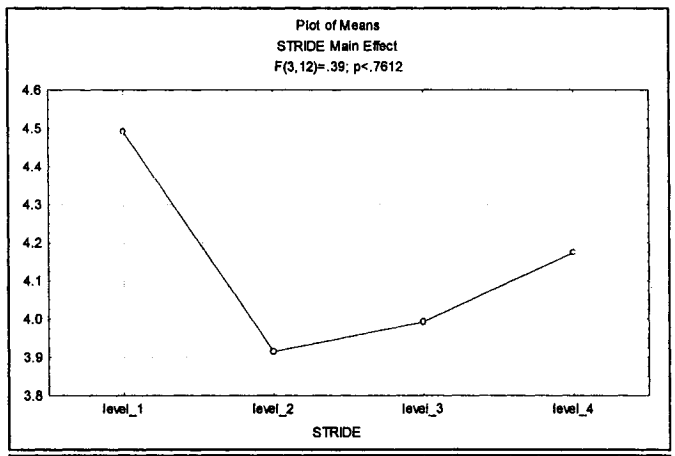

b)

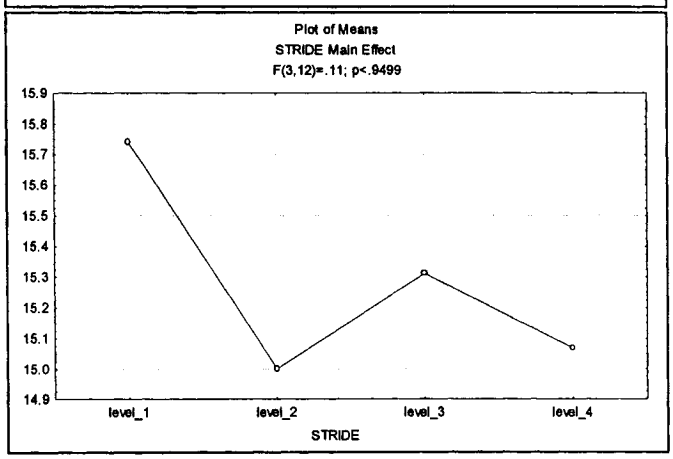

Figure 4.3.7. Profiles of mean maximum (a) and minimum (b) Plantar: Lateral Arch pressure for 5 subjects performing forward skating strides. Different values represent different strides level_1 (A1), level_2 (A2), level_3 (A3), and level_4 (CONST).

Table 4.3.7. Tukey's HSD Post Hoc Test Results from ANOVA comparing maximum (a) and minimum (b) values representing Plantar: Lateral Arch pressure for strides A1, A2, A3, and CONST Velocity.

a) Maximum

	A1	A2	A3	CONST
	20.31247	20.84522	21.23508	18.36218
A1				
A2	0.976886			
A3	0.895819	0.990665		
CONST	0.480218	0.286706	0.185623	

b) Minimum

	A1	A2	A3	CONST
	5.814214	4.666981	4.977678	5.096604
A1				
A2	0.703427			
A3	0.856336	0.990716		
CONST	0.902668	0.976224	0.9995	

a)

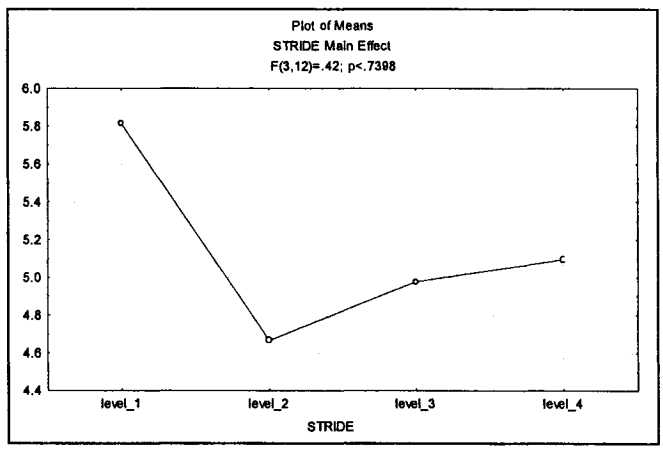

b)

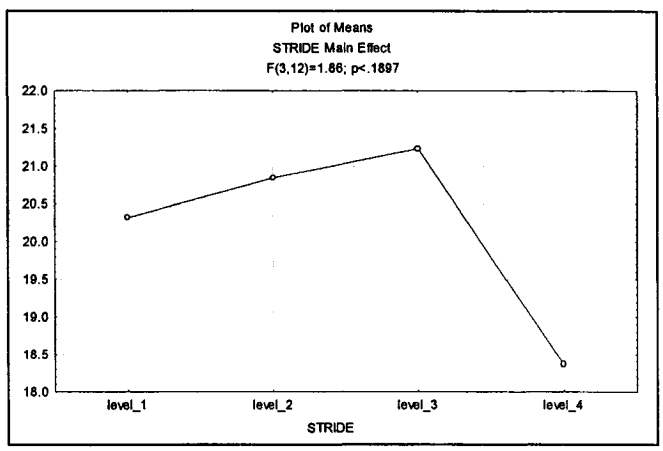

Figure 4.3.8. Profiles of mean maximum (a) and minimum (b) Plantar: Lateral Heel pressure for 5 subjects performing forward skating strides. Different values represent different strides level_1 (A1), level_2 (A2), level_3 (A3), and level_4 (CONST).

Figure 4.3.9 shows the plantar: medial foot is the region of the plantar foot where the greatest difference with its lateral equivalent. Despite the extremely different pressure the onset of peak pressure occurs at approximately the same instance.

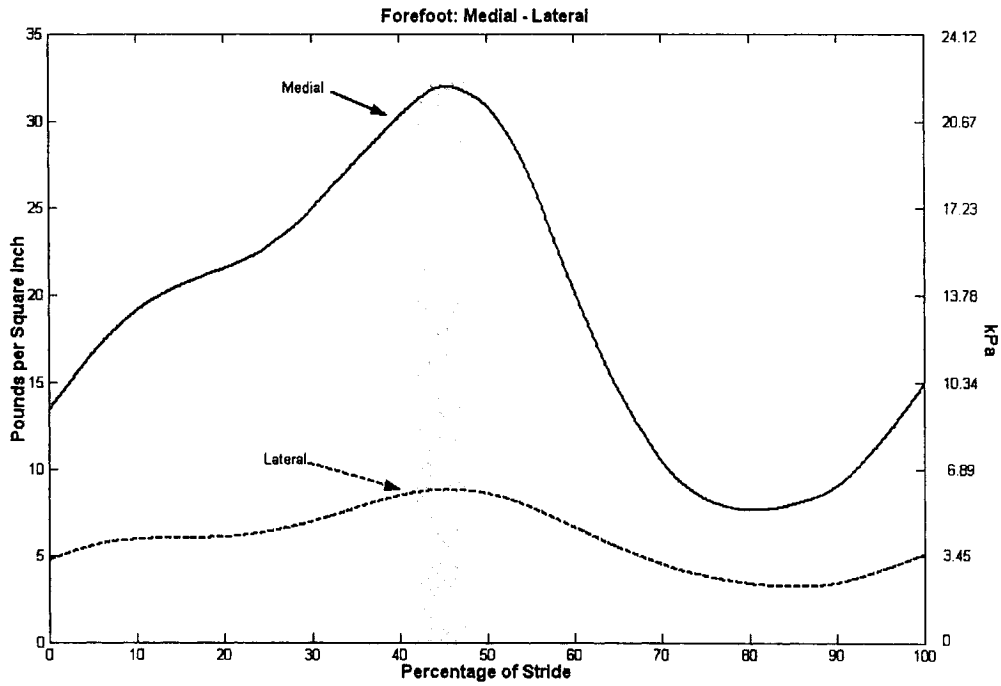

Figure 4.3.9. Mean pressure profiles of the Forefoot for 5 subjects performing forward skating strides at Constant Velocity. The striped area represents the approximate time phase at which the blade left the ice surface.

Figure 4.3.10 shows that more proximally than the forefoot the arch area of the plantar foot shows the second greatest discrepancy of the plantar foot medially-laterally; however in this region pressures on the lateral border of the foot are larger than pressures on the medial border. Again as seen with the forefoot the occurrence of peak pressure in this region occurs at approximately at the same instance.

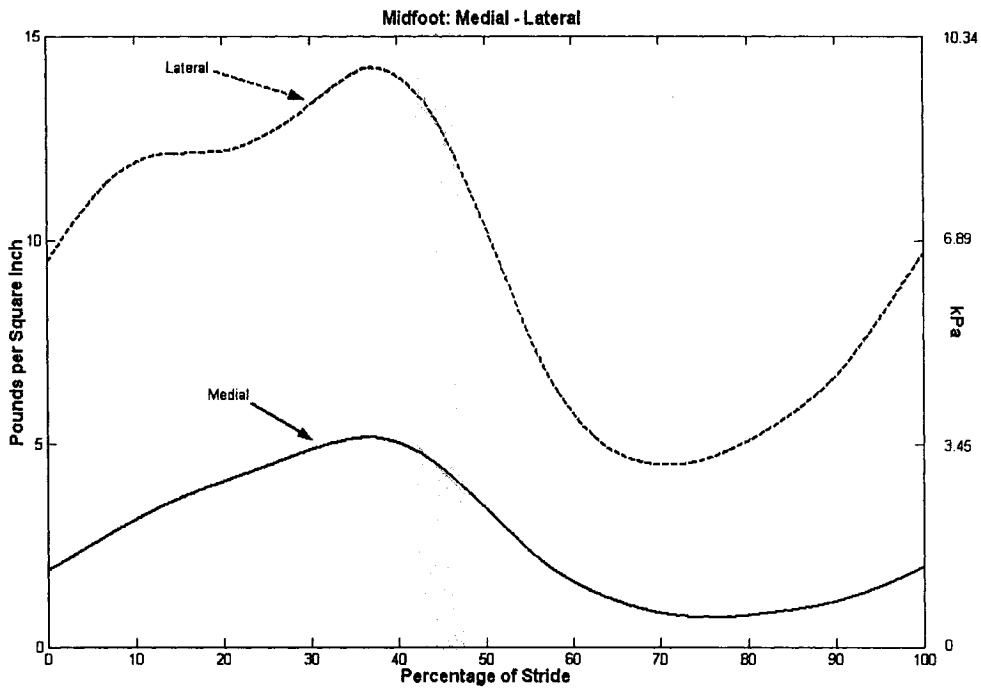

Figure 4.3.10. Mean pressure profiles of the Midfoot for 5 subjects performing forward skating strides at Constant Velocity. The striped area represents the approximate time phase at which the blade left the ice surface.

Figure 4.3.11 shows that the Heel values of the Plantar Foot being the most proximal measure of the plantar foot show the greatest similarity in terms of a medial-lateral comparison. Medial heel pressures were larger on average than Lateral heel pressure.

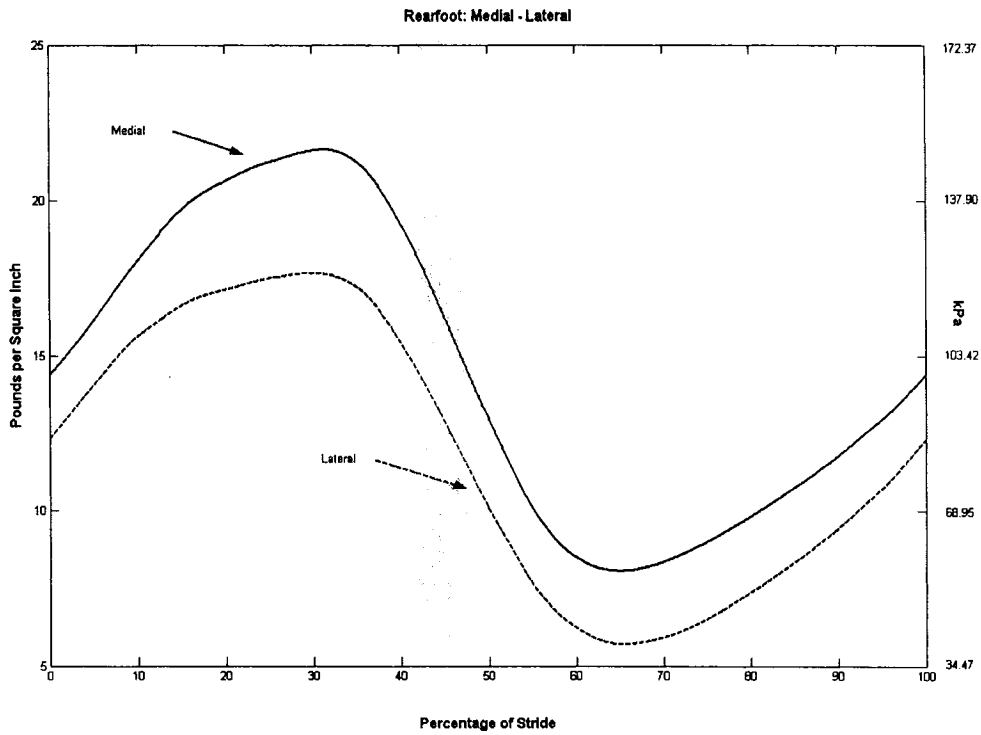

Figure 4.3.11. Mean pressure profiles of the Rearfoot for 5 subjects performing forward skating strides at Constant Velocity. The striped area represents the approximate time phase at which the blade left the ice surface.

4.3.3 Medial Foot

Figure 4.3.12 (A) shows very low pressure at the medial calcaneus throughout the skating stride. In addition to this there was very minimal fluctuation at the area. In contrast medial malleolus pressures were extremely high, a finding that was congruent with the values obtained during the neutral weight bearing phase. Medial malleolus pressure peaked at approximately 10 percent of stride, in the stance phase and declined fairly steadily to a low in swing phase at approximately 63 percent of stride. Medial forefoot pressures increased substantially during the last part of stance phase and peaked at approximately 48 percent of stride. During late swing phase and early stance medial forefoot pressure remained relatively low and stable.

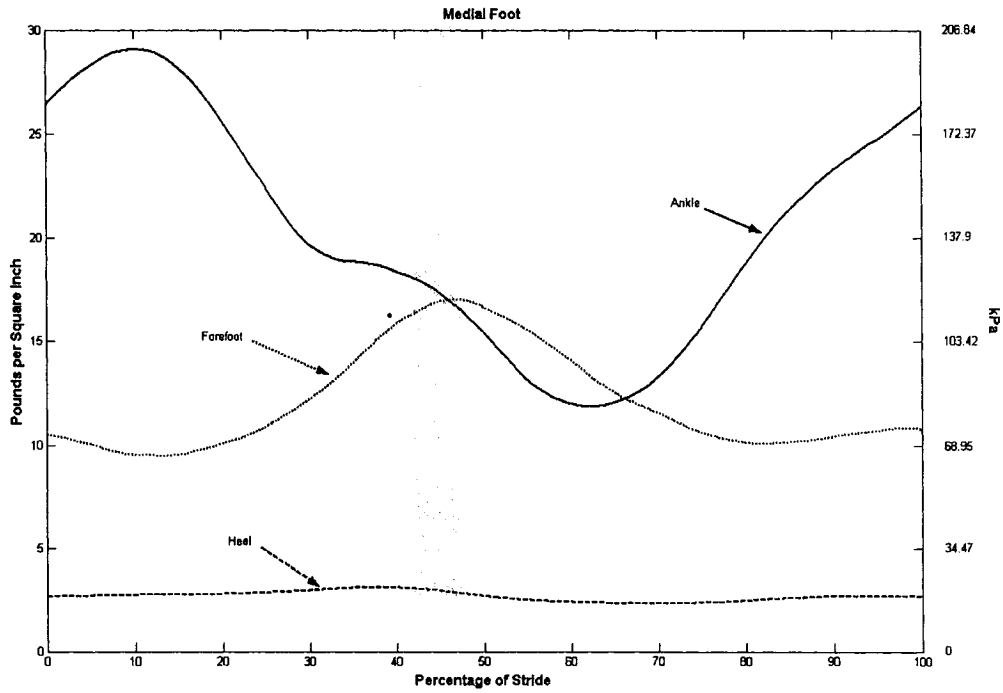

Figure 4.3.12 (A). Mean pressure profiles of the Medial foot for 5 subjects performing forward skating strides at Constant Velocity. The striped area represents the approximate time phase at which the blade left the ice surface.

Figure 4.3.12 (B) shows very low pressure at the medial calcaneus throughout the skating stride. Again, there was very minimal pressure fluctuation at the area. Medial malleolus pressures were below the neutral weight bearing value during most of the stride. Medial forefoot pressures on the other hand were greater than at the neutral weight bearing value throughout stride.

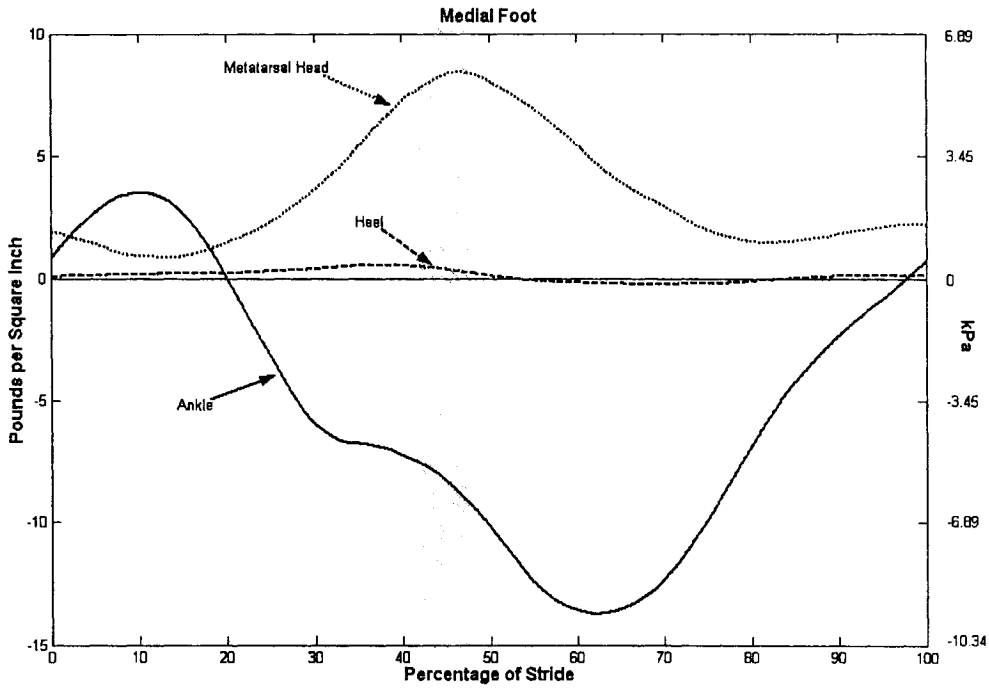

Figure 4.3.12 (B). Mean pressure profiles of the Medial foot for 5 subjects performing forward skating strides at Constant Velocity. Values are represented relative to their neutral weight bearing value. The striped area represents the approximate time phase at which the blade left the ice surface.

Table 4.3.8. Tukey's HSD Post Hoc Test Results from ANOVA comparing maximum (a) and minimum (b) values representing Medial Malleolus pressure for strides A1, A2, A3, and CONST Velocity.

a) Maximum

	A1	A2	A3	CONST
	37.43056	37.08578	36.46938	35.83973
A1				
A2	0.991038			
A3	0.848072	0.952656		
CONST	0.555465	0.723729	0.949801	

b) Minimum

	A1	A2	A3	CONST
	9.440003	10.84118	11.76701	11.06478
A1				
A2	0.704199			
A3	0.318244	0.888243		
CONST	0.603695	0.99811	0.946367	

a)

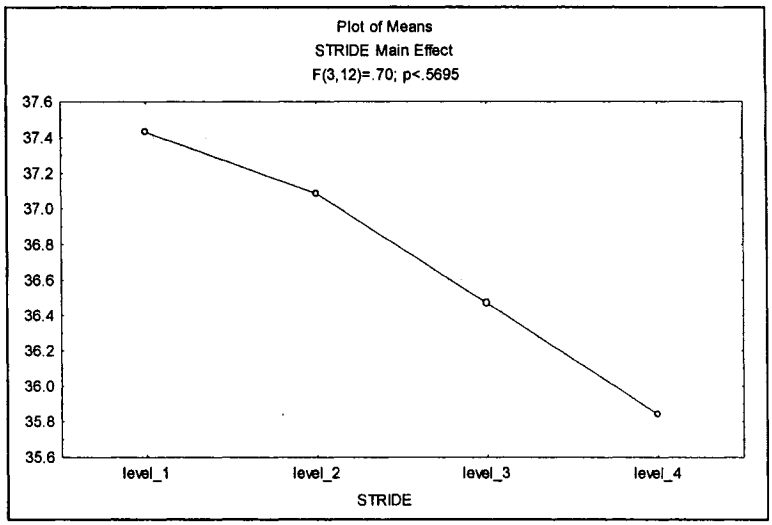

b)

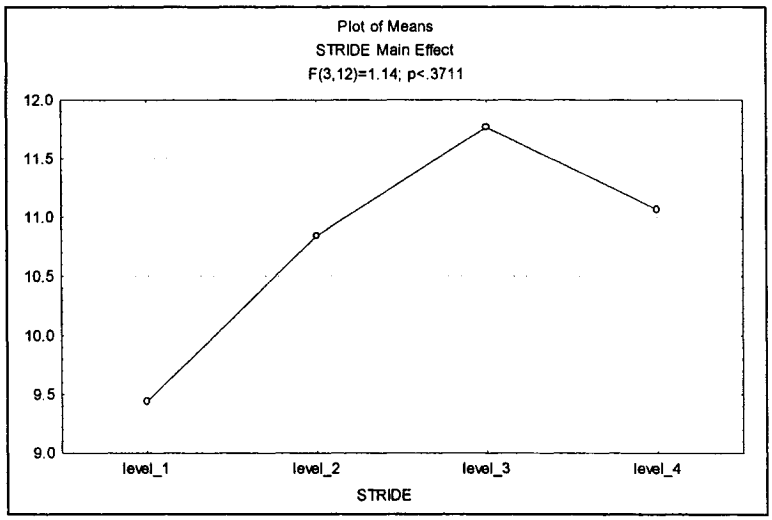

Figure 4.3.13. Profiles of mean maximum (a) and minimum (b) Medial Malleolus pressure for 5 subjects performing forward skating strides. Different values represent different strides level_1 (A1), level_2 (A2), level_3 (A3), and level_4 (CONST).

Table 4.3.9. Tukey's HSD Post Hoc Test Results from ANOVA comparing maximum (a) and minimum (b) values representing Medial Calcaneus pressure for strides A1, A2, A3, and CONST Velocity.

a) Maximum

	A1	A2	A3	CONST
	3.731304	3.864596	3.559086	3.613351
A1				
A2	0.985176			
A3	0.969105	0.856671		
CONST	0.989625	0.913074	0.999003	

b) Minimum

	A1	A2	A3	CONST
	1.321795	1.621306	1.636773	1.648811
A1				
A2	0.189862			
A3	0.159678	0.999516		
CONST	0.139137	0.99713	0.999771	

a)

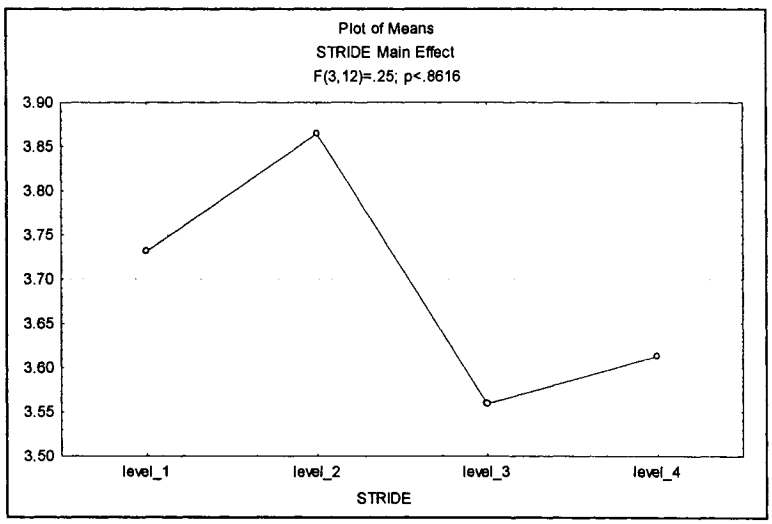

b)

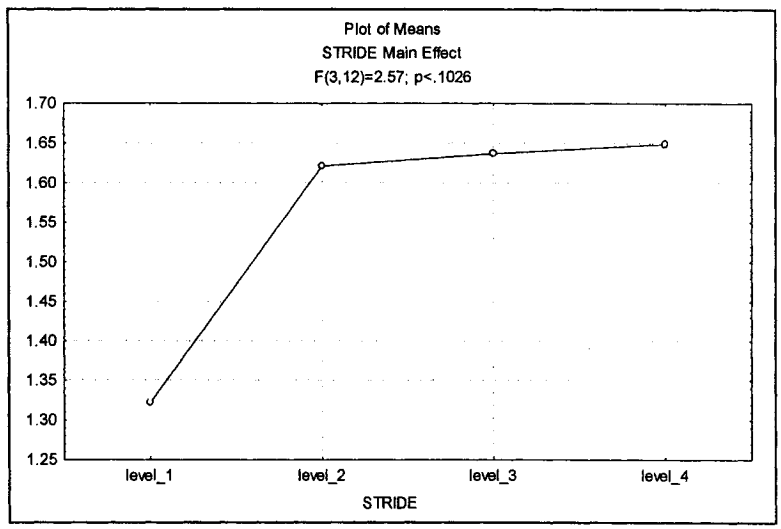

Figure 4.3.14. Profiles of mean maximum (a) and minimum (b) Medial Calcaneus pressure for 5 subjects performing forward skating strides. Different values represent different strides level_1 (A1), level_2 (A2), level_3 (A3), and level_4 (CONST).

Table 4.3.10. Tukey's HSD Post Hoc Test Results from ANOVA comparing maximum (a) and minimum (b) values representing Medial: First Metatarsal pressure for strides A1, A2, A3, and CONST Velocity.

a) Maximum

	A1	A2	A3	CONST
	29.76635	15.02654	22.38936	20.65932
A1				
A2	0.068172			
A3	0.525141	0.526661		
CONST	0.354513	0.715809	0.987341	

b) Minimum

	A1	A2	A3	CONST
	4.116076	3.251215	3.573981	5.447003
A1				
A2	0.925546			
A3	0.979734	0.99558		
CONST	0.781502	0.435119	0.562185	

a)

b)

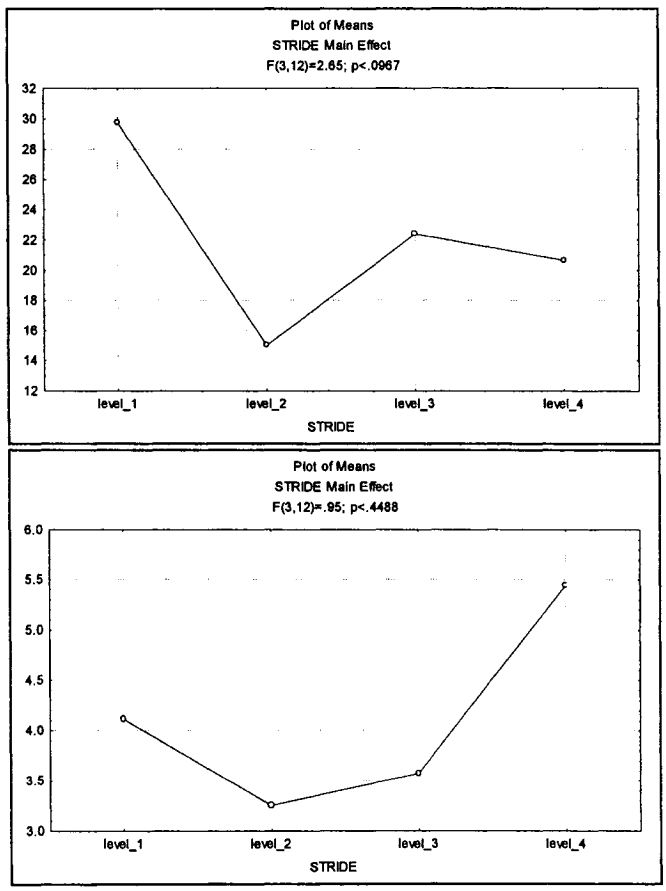

Figure 4.3.15. Profiles of mean maximum (a) and minimum (b) Medial: First Metatarsal pressure for 5 subjects performing forward skating strides. Different values represent different strides level_1 (A1), level_2 (A2), level_3 (A3), and level_4 (CONST).

4.3.4 Lateral Foot

Figure 4.3.16 (A) shows the lateral malleolus pressure increased steadily throughout the beginning of stride, reaching a peak at approximately 33 percent of stride after which time it remained at a relative plateau; a noticeable decrease in pressure occured at approximately 55 percent of stride. In general lateral malleolus pressures increased as the ankle everted and decreased as the foot inverted in swing phase. A decrease in pressure at the lateral: fifth metatarsal base occurred during peak eversion of the calcaneus. Peak lateral: fifth metatarsal base pressure occurred at approximately the same time as peak ankle inversion, during swing phase. Pressure at the lateral calcaneus reached a maximum at approximately 10 percent of stride and slowly decreased to a low at approximately 65 percent of stride. As stated above lateral calcaneus pressure fluctuated reciprocally with medial calcaneus pressure.

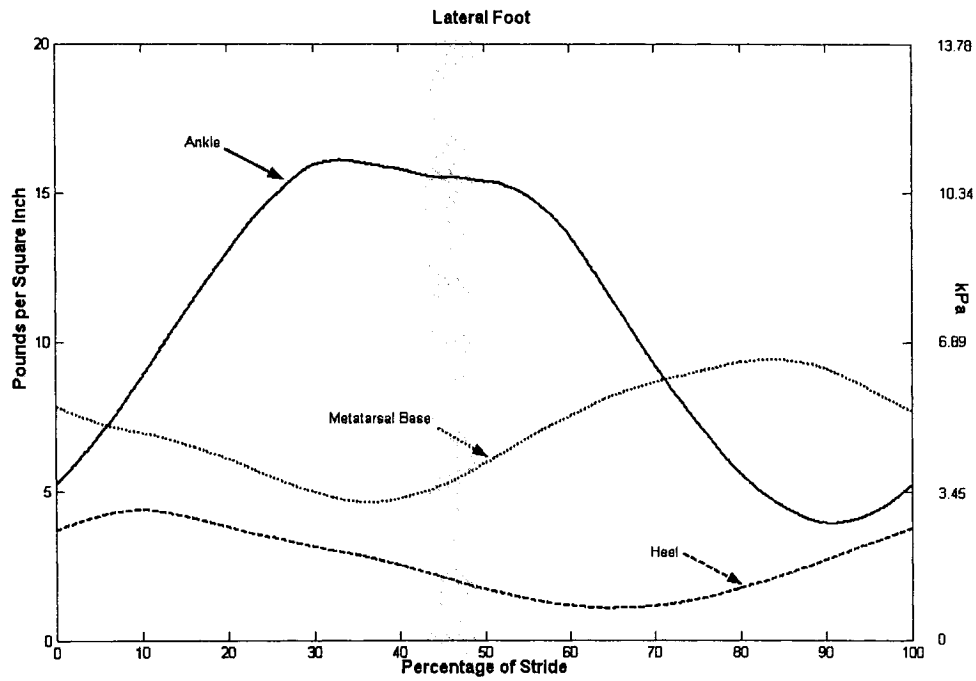

Figure 4.3.16 (A). Mean pressure profiles of the Lateral foot for 5 subjects performing forward skating strides at Constant Velocity. The striped area represents the approximate time phase at which the blade left the ice surface.

Figure 4.3.16 (B) shows the lateral malleolus pressure remained below the neutral weight bearing value throughout most of stride. Pressure values at terminal swing were approximately 7 kPa below neutral values. Pressure at the lateral: fifth metatarsal base was above neutral weight bearing values throughout most of the stride with the exception of the time between 20 and 50 percent of stride. Interestingly, it was during this time that lateral malleolus pressure climbed above neutral values. Pressure values at the lateral calcaneus were below neutral weight bearing value throughout the entire stride.

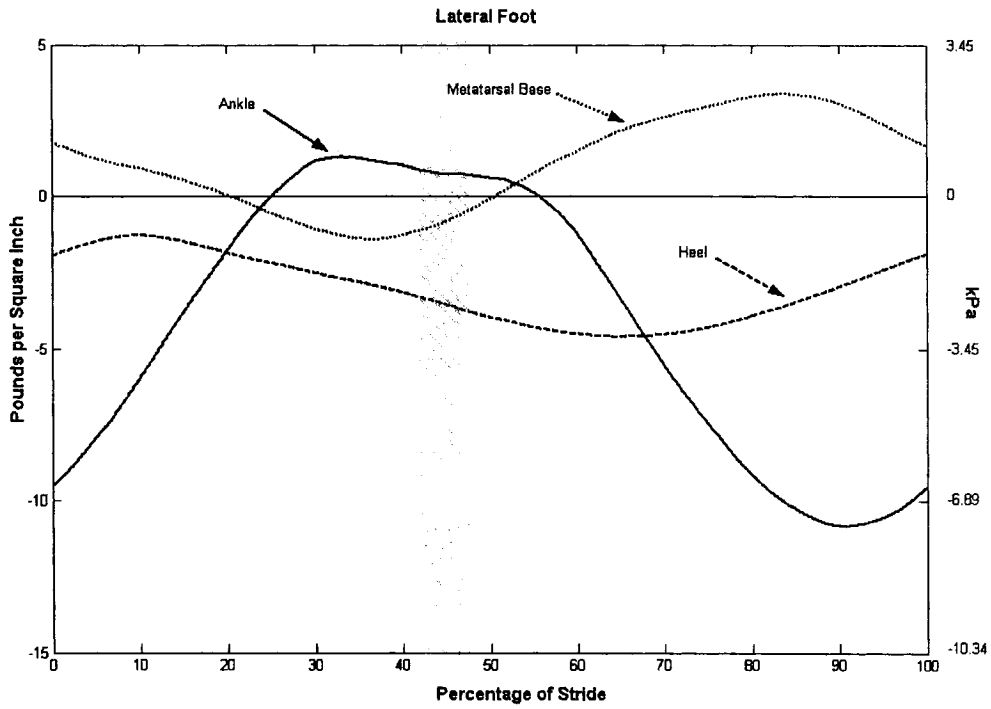

Figure 4.3.16 (B). Mean pressure profiles of the Medial Foot for 5 subjects performing forward skating strides at Constant Velocity. Values are represented relative to their neutral weight bearing value. The striped area represents the approximate time phase at which the blade left the ice surface.

Table 4.3.11. Tukey's HSD Post Hoc Test Results from ANOVA comparing maximum (a) and minimum (b) values representing Lateral Malleolus pressure for strides A1, A2, A3, and CONST Velocity.

a) Maximum

	A1	A2	A3	CONST
	22.46847	16.52999	17.85828	18.04852
A1				
A2	0.544891			
A3	0.720937	0.989767		
CONST	0.745234	0.984868	0.999971	

b) Minimum

	A1	A2	A3	CONST
	3.567191	3.855050	2.324934	3.470857
A1				
A2	0.984737			
A3	0.463785	0.296446		
CONST	0.999444	0.965175	0.528606	

a)

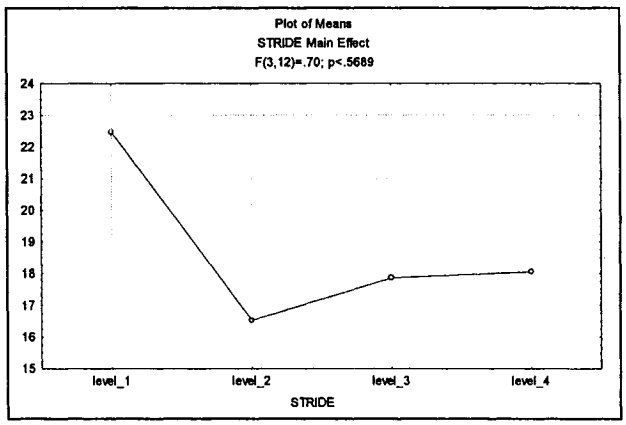

b)

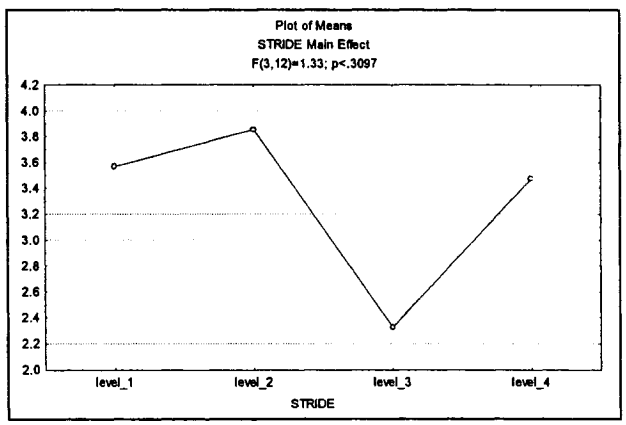

Figure 4.3.17. Profiles of mean maximum (a) and minimum (b) Lateral Malleolus pressure for 5 subjects performing forward skating strides. Different values represent different strides level_1 (A1), level_2 (A2), level_3 (A3), and level_4 (CONST).

Table 4.3.12. Tukey's HSD Post Hoc Test Results from ANOVA comparing maximum (a) and minimum (b) values representing Lateral Calcaneus pressure for strides A1, A2, A3, and CONST Velocity.

a) Maximum

	A1	A2	A3	CONST
	5.212561	6.637348	5.041604	5.181011
A1				
A2	0.505407			
A3	0.998163	0.413387		
CONST	0.999989	0.487785	0.999018	

b) Minimum

	A1	A2	A3	CONST
	1.099913	.8847601	1.053782	.8872702
A1		0.89114	0.998723	0.894375
A2	0.89114		0.942602	1
A3	0.998723	0.942602		0.944897
CONST	0.894375	1	0.944897	

a)

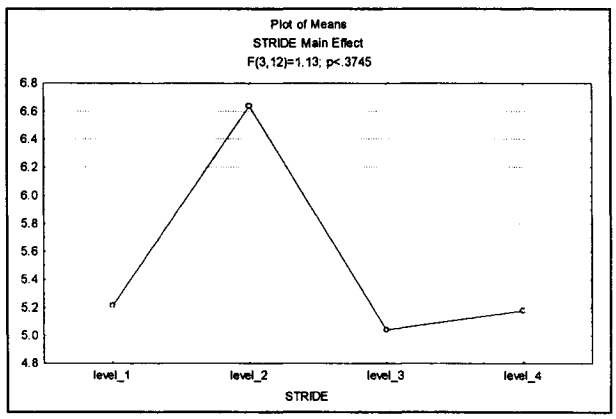

b)

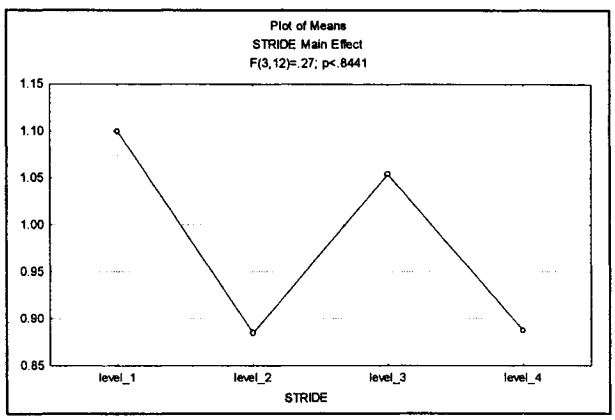

Figure 4.3.18. Profiles of mean maximum (a) and minimum (b) Lateral Calcaneus pressure for 5 subjects performing forward skating strides. Different values represent different strides level_1 (A1), level_2 (A2), level_3 (A3), and level_4 (CONST).

Table 4.3.13. Tukey's HSD Post Hoc Test Results from ANOVA comparing maximum (a) and minimum (b) values representing Lateral: Fifth Metatarsal base pressure for strides A1, A2, A3, and CONST Velocity.

a) Maximum

	A1	A2	A3	CONST
	11.96547	11.04952	10.16748	9.846818
A1				
A2	0.955281			
A3	0.752193	0.959727		
CONST	0.65081	0.906769	0.997931	

b) Minimum

	A1	A2	A3	CONST
	5.559724	4.587803	2.694062	3.908350
A1				
A2	0.960137			
A3	0.499346	0.77786		
CONST	0.839002	0.985648	0.926743	

a)

b)

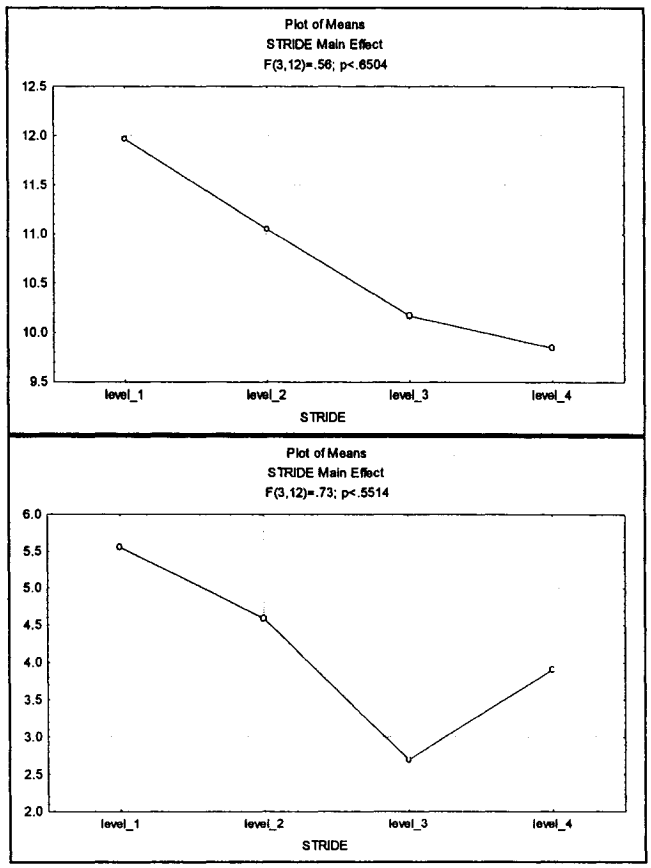

Figure 4.3.19. Profiles of mean maximum (a) and minimum (b) Lateral: Fifth Metatarsal base pressure for 5 subjects performing forward skating strides. Different values represent different strides level_1 (A1), level_2 (A2), level_3 (A3), and level_4 (CONST).

4.3.5 Dorsal Foot

Figure 4.3.20 (A) shows that peak pressure at the dorsalis pedis occurred at approximately 17 percent of stride. Peak pressure at the dorsal: first metatarsal base reached maximum at approximately 58 percent of stride and its minimum at approximately the beginning of stride.

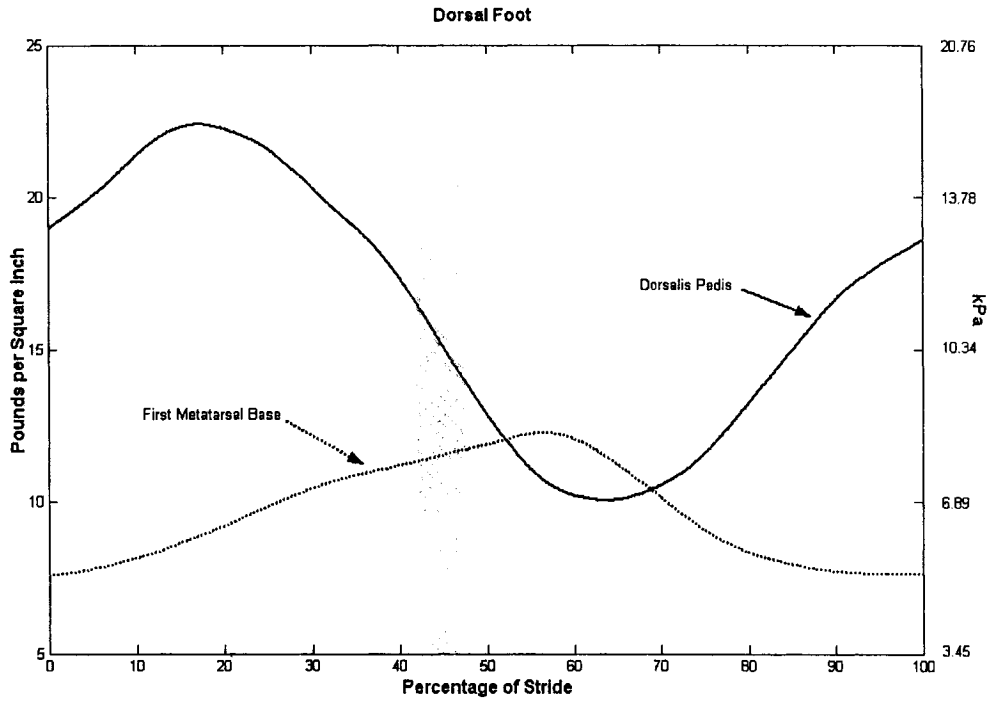

Figure 4.3.20 (A). Mean pressure profiles of the Dorsal foot for 5 subjects performing forward skating strides at Constant Velocity. The striped area represents the approximate time phase at which the blade left the ice surface.

Figure 4.3.20 (B) shows the dorsalis pedis pressure was considerably higher during skating than during the neutral weight bearing posture. This may be explained by the fact that the ankle was considerably dorsi-flexed during the skating stride relative to the standing weight bearing value, causing compression with the skate tongue; in addition a bending effect of the sensor similar to that of the achilles tendon sensor may have

occurred. At peak plantar flexion of the ankle the dorsalis pedis pressure was over 5 kPa over the neutral weight bearing dorsalis pedis value.

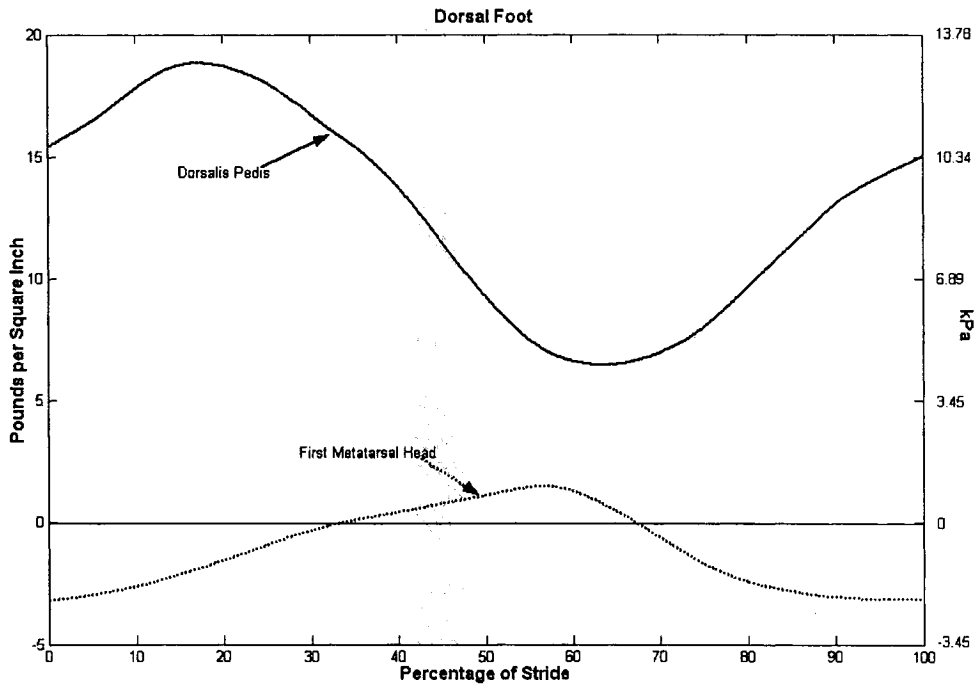

Figure 4.3.20 (B). Mean pressure profiles of the Dorsal Foot for 5 subjects performing forward skating strides at Constant Velocity. Values are represented relative to their neutral weight bearing value. The striped area represents the approximate time phase at which the blade left the ice surface.

Table 4.3.14. Tukey's HSD Post Hoc Test Results from ANOVA comparing maximum (a) and minimum (b) values representing Dorsalis pedis pressure for strides A1, A2, A3, and CONST Velocity.

a) Maximum

	A1	A2	A3	CONST
	19.99890	24.69436	26.02372	23.38745
A1				
A2	0.508576			
A3	0.307674	0.97685		
CONST	0.73669	0.977964	0.85313	

b) Minimum

	A1	A2	A3	CONST
	9.733797	10.20365	10.39088	9.340465
A1				
A2	0.971585			
A3	0.928183	0.998128		
CONST	0.982918	0.854753	0.769002	

a)

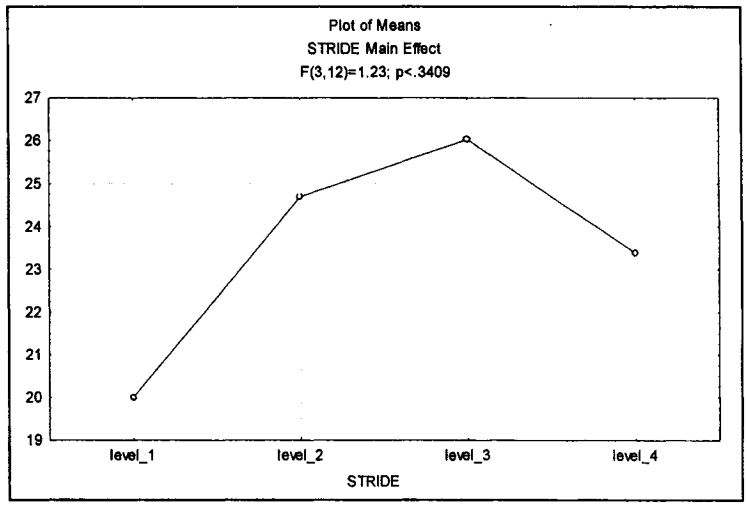

b)

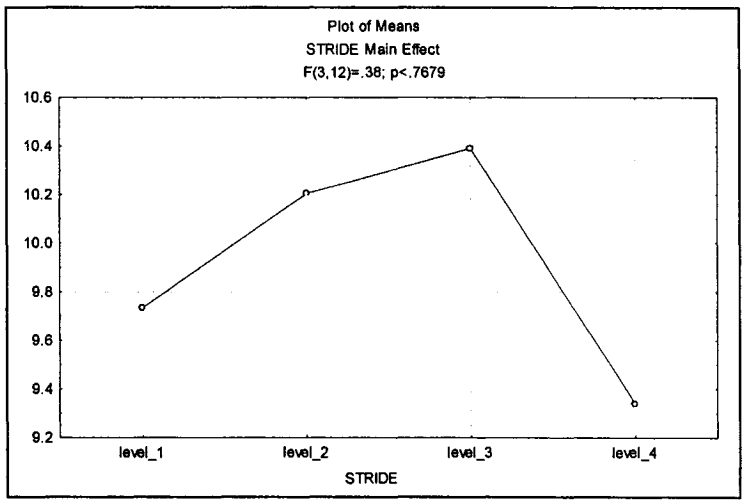

Figure 4.3.21. Profiles of mean maximum (a) and minimum (b) Dorsalis pedis pressure for 5 subjects performing forward skating strides. Different values represent different strides level_1 (A1), level_2 (A2), level_3 (A3), and level_4 (CONST).

Table 4.3.15. Tukey's HSD Post Hoc Test Results from ANOVA comparing maximum (a) and minimum (b) values representing Dorsal: First Metatarsal base pressure for strides A1, A2, A3, and CONST Velocity.

a) Maximum

	A1	A2	A3	CONST
	12.47902	12.38570	13.55007	12.62563
A1				
A2	0.999651			
A3	0.668798	0.610547		
CONST	0.998599	0.993788	0.757473	

b) Minimum

	A1	A2	A3	CONST
	6.999392	7.103148	7.031248	7.050412
A1				
A2	0.995263			
A3	0.999869	0.998449		
CONST	0.999465	0.999409	0.999972	

a)

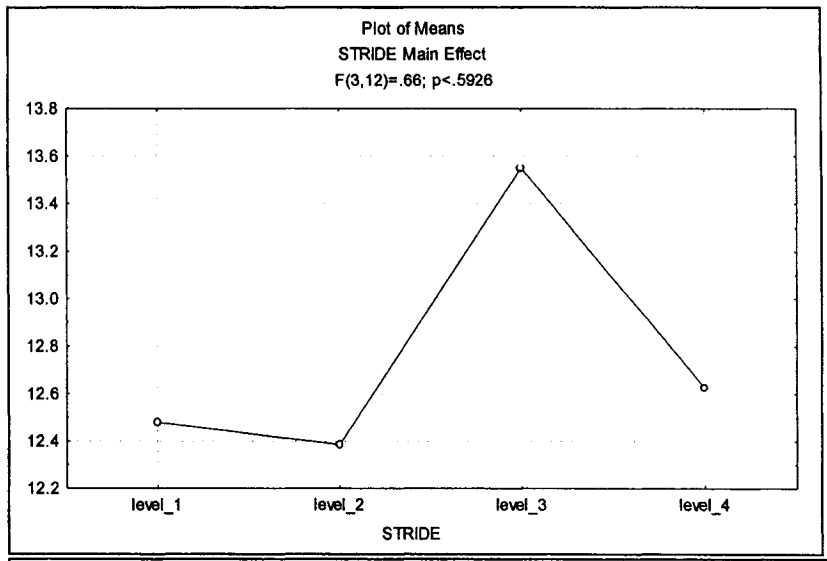

b)

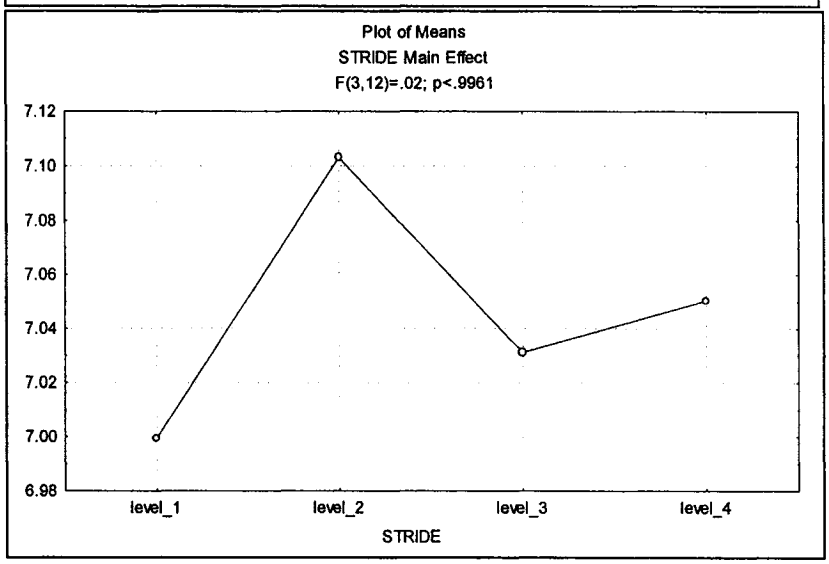

Figure 4.3.22. Profiles of mean maximum (a) and minimum (b) Dorsal: First Metatarsal base pressure for 5 subjects performing forward skating strides. Different values represent different strides level_1 (A1), level_2 (A2), level_3 (A3), and level_4 (CONST).

4.3.6 Posterior Foot

Figure 4.3.23 (A) shows peak posterior calcaneus pressures occurred at approximately 12 percent of stride during foot contact. Pressures at the achilles tendon region were minimal. Posterior calcaneus and achilles tendon peak pressure were approximately 50 percent out of phase with each other. Measurements at both regions showed very small pressure values.

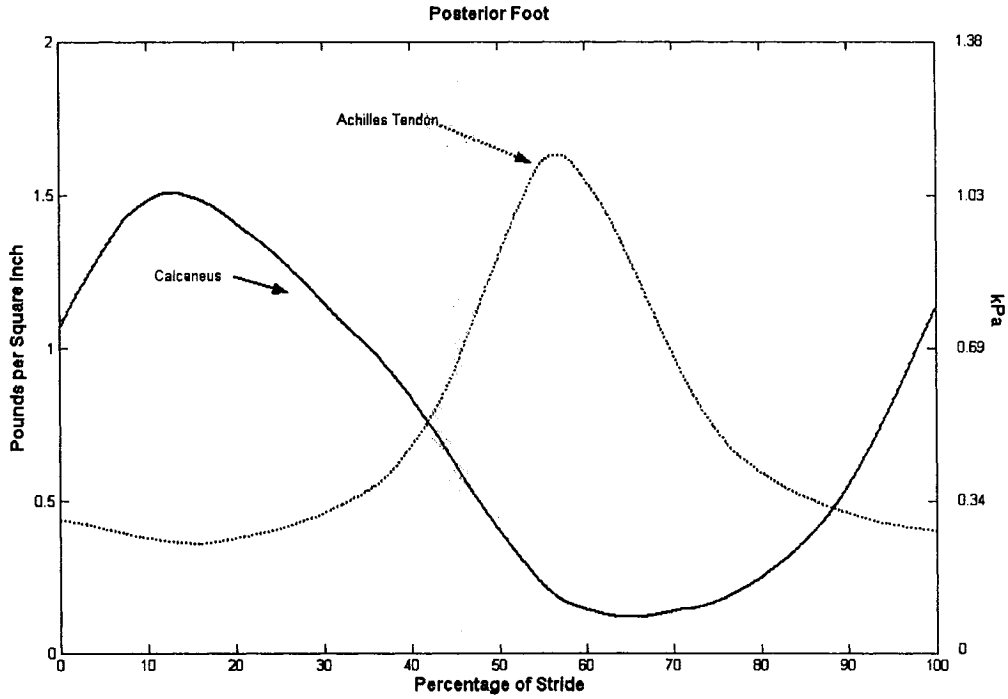

Figure 4.3.23 (A). Mean pressure profiles of the Posterior foot for 5 subjects performing forward skating strides at Constant Velocity. The striped area represents the approximate time phase at which the blade left the ice surface.

Figure 4.3.23 (B) shows posterior calcaneus pressure was above neutral weight bearing values throughout most of stride with the exception of a period of early swing at approximately 58 – 75 percent of stride. Conversely, achilles tendon pressure remained below neutral weight bearing values for most of stride with the exception of the period of 48 – 65 percent of stride.

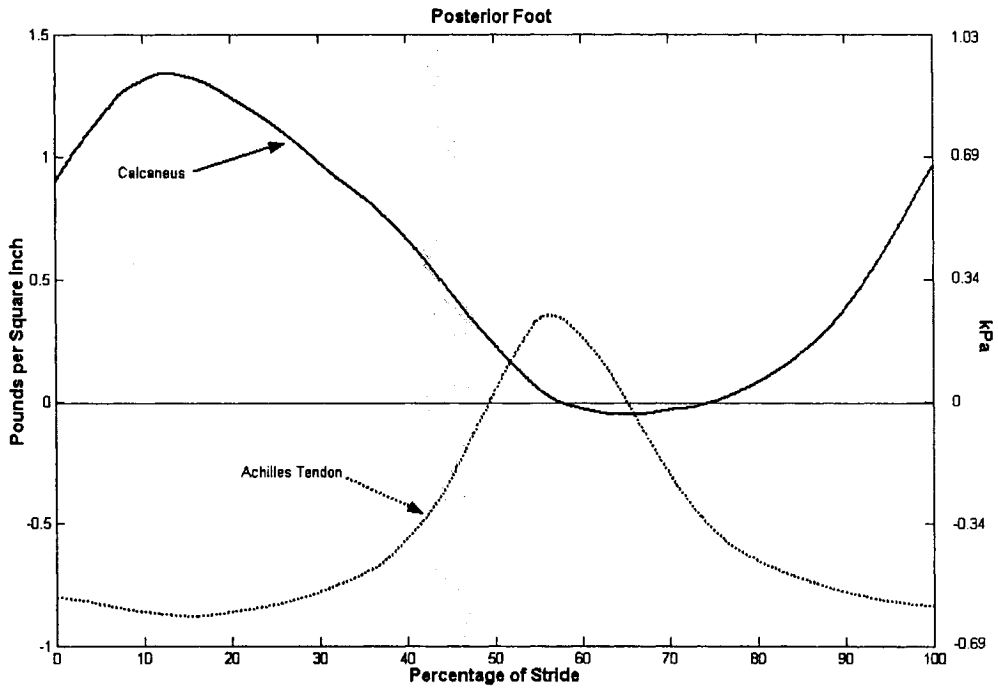

Figure 4.3.23 (B). Mean pressure profiles of the Posterior Foot for 5 subjects performing forward skating strides at Constant Velocity. Values are represented relative to their neutral weight bearing value. The striped area represents the approximate time phase at which the blade left the ice surface.

Table 4.3.16. Tukey's HSD Post Hoc Test Results from ANOVA comparing maximum (a) and minimum (b) values representing Posterior: Calcaneus pressure for strides A1, A2, A3, and CONST Velocity.

a) Maximum

	A1	A2	A3	CONST
	2.371046	2.858936	3.494869	1.723145
A1				
A2	0.901243			
A3	0.427104	0.809364		
CONST	0.800864	0.418457	0.113458	

b) Minimum

Matrix cannot be inverted.

a)

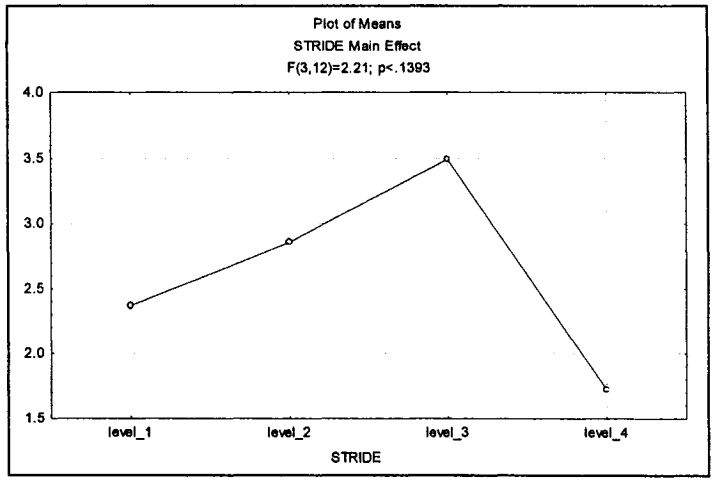

b)

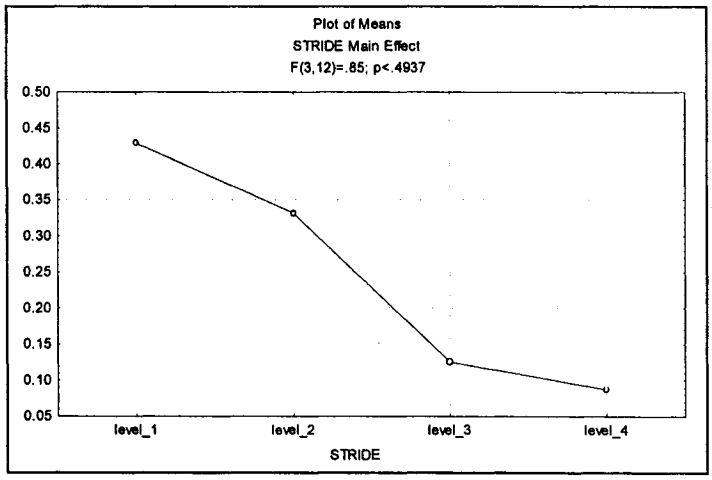

Figure 4.3.24. Profiles of mean maximum (a) and minimum (b) Posterior: Calcaneus pressure for 5 subjects performing forward skating strides. Different values represent different strides level_1 (A1), level_2 (A2), level_3 (A3), and level_4 (CONST).

Table 4.3.17. Tukey's HSD Post Hoc Test Results from ANOVA comparing maximum (a) and minimum (b) values representing Achilles tendon pressure for strides A1, A2, A3, and CONST Velocity.

a) Maximum

	A1	A2	A3	CONST
	1.925700	1.592674	1.637967	1.693544
A1				
A2	0.800475			
A3	0.859657	0.999341		
CONST	0.919182	0.99238	0.998737	

b) Minimum

	A1	A2	A3	CONST
	.4915480	.1428354	.1422682	.2948447
A1				
A2	0.286744			
A3	0.285518	1		
CONST	0.718964	0.844374	0.842947	

a)

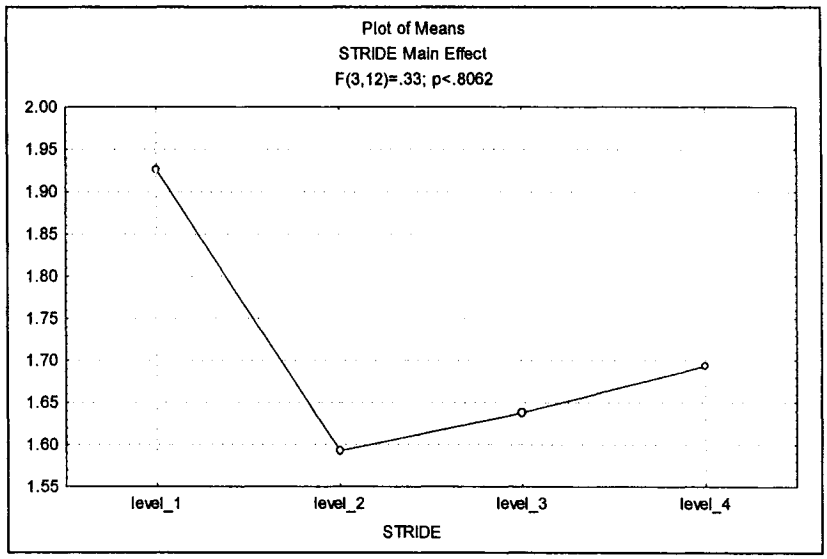

b)

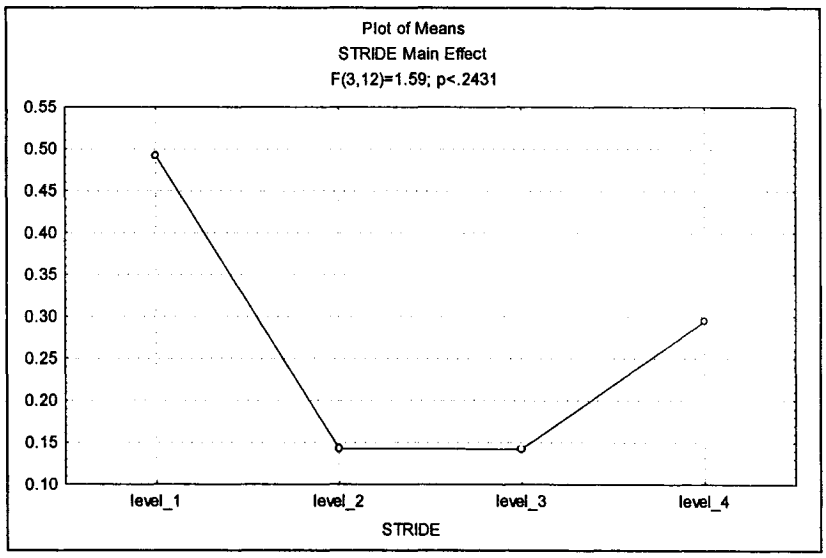

Figure 4.3.25. Profiles of mean maximum (a) and minimum (b) Achilles tendon pressure for 5 subjects performing forward skating strides. Different values represent different strides level_1 (A1), level_2 (A2), level_3 (A3), and level_4 (CONST).

4.4 Stride Duration

Table 4.4 shows a Tukey's High Significant Difference Post Hoc test revealed a significant difference between the duration of stride time between A1 and CONST ($p = 0.005$) where CONST strides consume more time. Near significant differences were seen

between strides A2 and CONST (p = 0.07) and with A3 and CONST (p = 0.05) in both cases, again CONST strides consumed more time.

Table 4.4.1. Tukey's HSD Post Hoc Test Results from ANOVA comparing duration of stride in seconds for strides A1, A2, A3, and CONST Velocity. Mean Values denote milliseconds.

Stride Duration Comparison

	A1	A2	A3	CONST
	558.9	612.6	606.7	706.3
A1				
A2	0.43			
A3	0.52	0.99		
CONST	0.005 *	0.07	0.05	

* denotes a significant difference between conditions.

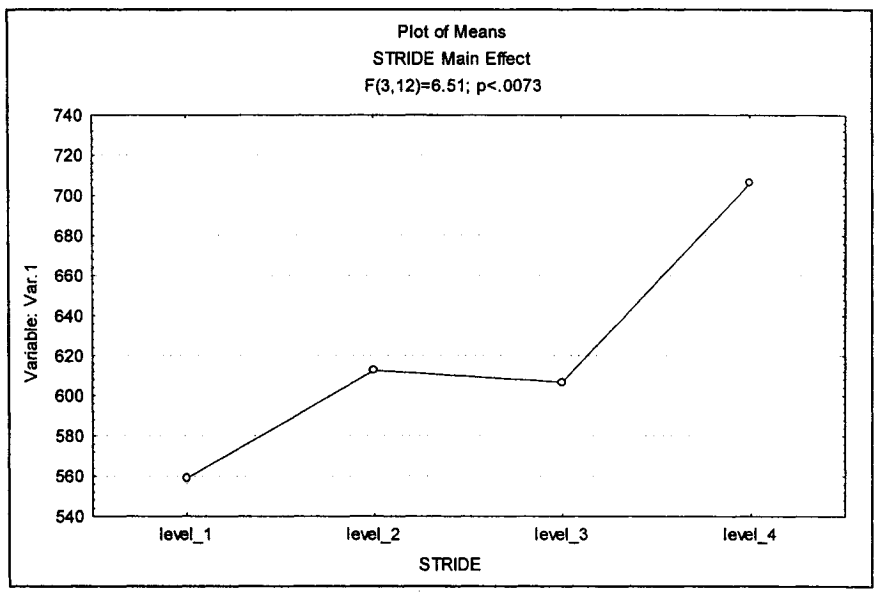

Figure 4.4.1. Profiles of mean duration of stride for 5 subjects performing forward skating strides. Different values represent different strides level_1 (A1), level_2 (A2), level_3 (A3), and level_4 (CONST). Y-axis values denote milliseconds.

Chapter 5

5. Discussion

The purposes of this study were (1) to present kinematic and dynamic pressure profiles the foot and ankle mechanics during forward hockey skating of elite skaters at a high velocity (25 to 30 km/hr), as well as (2) to identify the muscle activation profiles of some of the prime movers of the foot and ankle. Furthermore foot and ankle parameters during acceleration and constant velocity strides were compared.

In general, the equipment and protocol adopted succeeded in identifying repeatable pressure and kinematic patterns. Though few statistical differences were observed in the latter comparison due to the relatively small sample size ($n = 5$) clear trends in the foot/ankle mechanics during this transitional phase were observed. This section will attempt to (1) evaluate the prior stated hypotheses formed with respect to observations and (2) to synthesize the various observations to explain the functional mechanics by the lower limb necessary to produce this unique form of locomotion. The hypothesis that there would be significant differences in the stride duration between respective acceleration and constant velocity strides was found to be true, in part, for A1 vs. CONST ($p = 0.005$). In general stride duration increased from stride A1 – CONST. It was found that the mean stride duration was longer at CONST than at A2 ($p = 0.07$) and A3 ($p = 0.06$). Further, it was found that the mean stride duration for strides A2 and A3 were longer than A1

The hypothesis that there would be differences in minimum and maximum kinetic, kinematic and myolectric measurements among strides was also found to be in part true. Significant differences were found in vastus medialis maximum muscle activity amplitudes ($p = 0.049$) between strides A1 and CONST, where A1 values were greater

than CONST values. No significant differences in minimum and maximum movements at the ankle existed among strides. Differences in the pressure at the plantar: lateral forefoot existed between strides A1 versus CONST ($p = 0.047$), and A1 versus A2, ($p = 0.015$). Near significant differences were also seen between strides A1 and A3 ($p = 0.06$). Despite the few statistically significant differences among strides, some trends were evident. The following text explores in more detail the change in patterns observed and speculates on some of the functional relationships possibly existing between the kinetic, kinematic and myoelectrical measure parameters.

5.1 Electromyography

Without exception myoelectric activity of all muscles measured showed increased activity for the initial phase of acceleration strides compared to the constant velocity skating stride. In general the myoelectric profiles showed pronounced activity at foot strike (even between antagonistic muscles) followed by a pronounced reduction in myoelectric activity during mid support. The difference in myoelectric amplitude between strides was pronounced in all muscles except in the tibialis anterior. The role of this myoelectric co-activation is likely to both (1) increase 'joint stability' and (2) tune the muscle to reduce the deleterious effects of soft tissue vibration (Wakeling et al. 2002). Differences in these myoelectric amplitudes may be due to different foot strike characteristics.

The peak of the vastus medialis activity corresponded to blade contact and of push off phases during skating stride, respectively. Corresponding myoelectric activity of the vastus medialis indicates a shorter percentage of foot contact during strides A1 and A2 than CONST. These findings are congruent with Marino's findings (1977) that

accelerating strides are shorter and choppier, with an increased percentage of single support time, thus the period of foot to ice contact would be proportionally less.

Due to the dampening characteristic of the skate blade and boot, or lack there of, it is reasonable to assume that there would be a substantial amount of soft tissue vibration due to the impact of skate on ice, similar though not necessarily as great in magnitude as has been shown in walking and running studies, causing shockwaves to travel through both the soft-tissues and skeletal components of the body. Exposure to impulse vibrations have been shown to have detrimental effects on the soft tissues including reductions in motor unit firing rates, muscle contraction force, and decreases in nerve conduction velocity and attenuated sensory perception (Wakeling et al. 2002, Nigg et al. 2001). Summed together, these effects would decrease muscle function and in turn impair performance. Therefore some of the muscle function of the lower leg is to likely control the vibration of the soft tissue package of the lower leg via tuning of the resonance frequency of the muscle and thereby reduce the uncomfortable performance hindering effects of this vibration. Similar to these findings in running, these muscle tuning strategies may be relevant to skating in particular during the acceleration phase. At constant velocity skating when foot contact has been described as less 'choppy' as during acceleration strides the magnitudes of the shockwaves are, perhaps, less pronounced than during the acceleration phase perhaps requiring less muscle activation to tune the soft tissues resonance frequency. This is congruent with the myoelectric activation at initial stride and provides a possible explanation for the co-activation of antagonist muscles in these elite skaters.

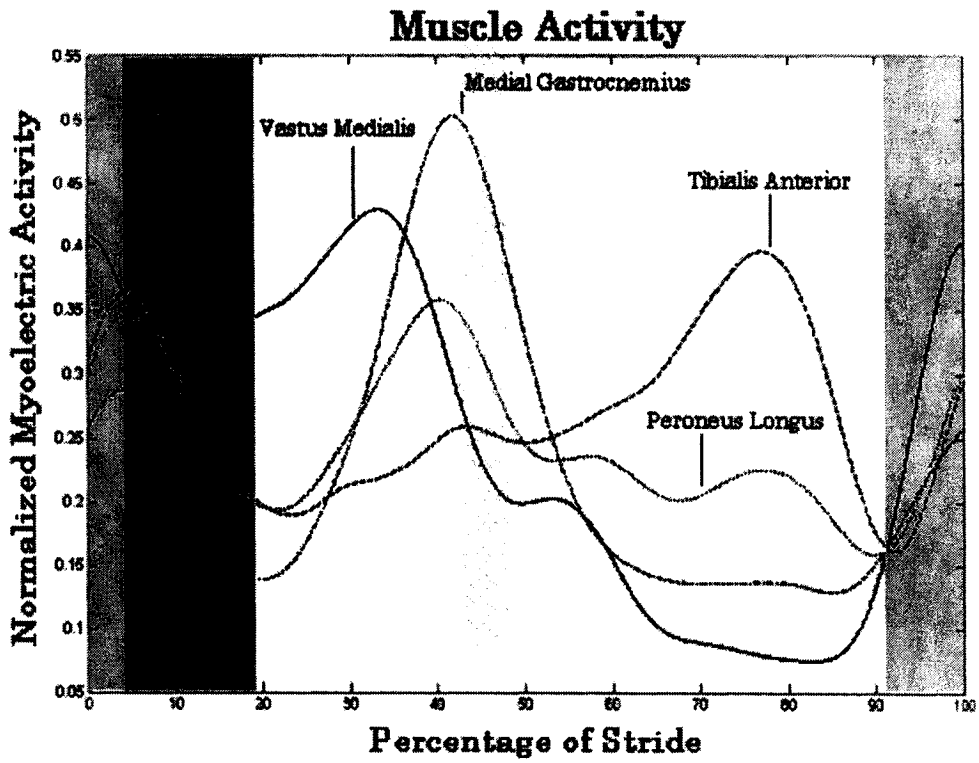

Figure 5.1.1 Muscle activation of the Vastus Medialis, Tibialis Anterior, Peroneus Longus, and Medial Gastrocnemius during constant velocity skating. Notice the increase in muscle activity for all muscles just prior to foot contact (0% of stride) and the cessation of activity shortly after foot contact. Initial muscle activation values are greater during the acceleration strides than constant velocity strides. Light grey region depict a general trend for increasing muscle activity. Dark grey region shows a significant decrease in muscle activity. The striped area represents the approximate time phase at which the blade left the ice surface.

An alternative or complementary explanation may be that the muscle activities function is to create resiliency at the ankle and knee joint. This resilience or joint 'stability' is inherent in maintaining postural balance and control, Latash and Zatsiorsky (1993). Perhaps the loading during acceleration in skating requires increased muscle tension in anticipation of foot contact to maintain a desired joint position for an optimal base of support for the lower leg. This could be due to an increased loading rate caused by greater vertical tibial accelerations causing the 'choppier' appearance noted by Marino (1979). Thus a muscle tuning strategy and/or joint stability theories provide possible

explanations for this trend in the myoelectric profiles. It is stressed that the two explanations are not necessarily mutually exclusive; however it is beyond the scope of this investigation to identify either of the two functions.

Another observation of the myoelectric profiles that begs inspection is the relatively early activation of the medial gastrocnemius compared to observed ankle plantar flexion. Peak medial gatrocnemius activity occurs well before ankle plantar flexion velocity, approximately 12 percent of stride or approximately 80-90 milliseconds, there is a large period of time when the gastrocnemius activity is increasing but no plantar flexion is occurring. An electromechanical delay (EMD) may account for some of this inconsistency; however the EMD, although it varies based on muscle properties, has been found to be approximately 50 milliseconds. A certain amount of musculo-tendinous tension would be expected in the medial gastrocnemius due to the dorsi-flexed position of the ankle, thus reducing or eliminating the EMD effect. Presumably the purpose of the medial gastrocnemius during skating stride is to perform eccentric work by resisting dorsi flexion and to generate a knee flexion moment to slow the knee extension angular velocity before full knee extension is approached. If the knee extension velocity in stride is not reduced, a significant amount of stress would be placed on the passive connective tissues of the knee, likely resulting damage to these structures over time. Through linked chain dynamics this activity may additionally cause the transfer of some of the knee extension moment into an ankle plantar flexion moment, as well as contributing to an anterior shift in the centre of pressure on the plantar surface of the foot (see figures 4.3.1 (A) (B), 4.3.5 (A) (B)). This knee extension, plantar flexion energy transfer was observed by van Ingen Schenau (1989) in jumping and in speed skating.

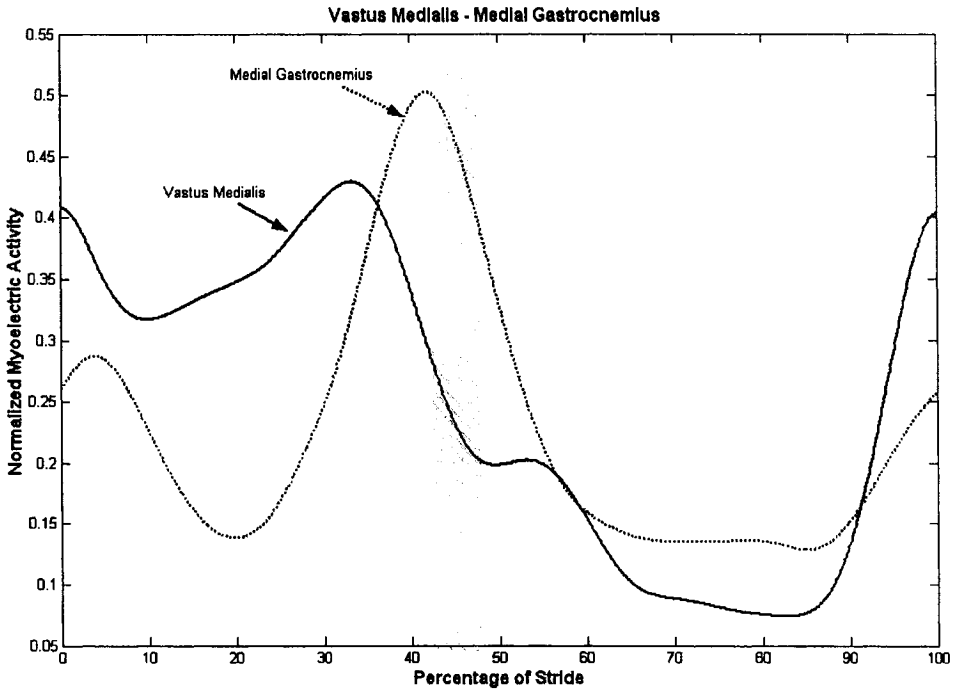

Figure 5.1.2 Muscle activation of the Vastus Medialis, and Medial Gastrocnemius during constant velocity skating. Notice the rapid decline in Vastus Medialis activation followed by the peak Medial Gastrocnemius muscle activity. This figure is congruent with the suggestion that the Gastrocnemius tension is contributing to a knee flexion moment. The striped area represents the approximate time phase at which the blade left the ice surface.

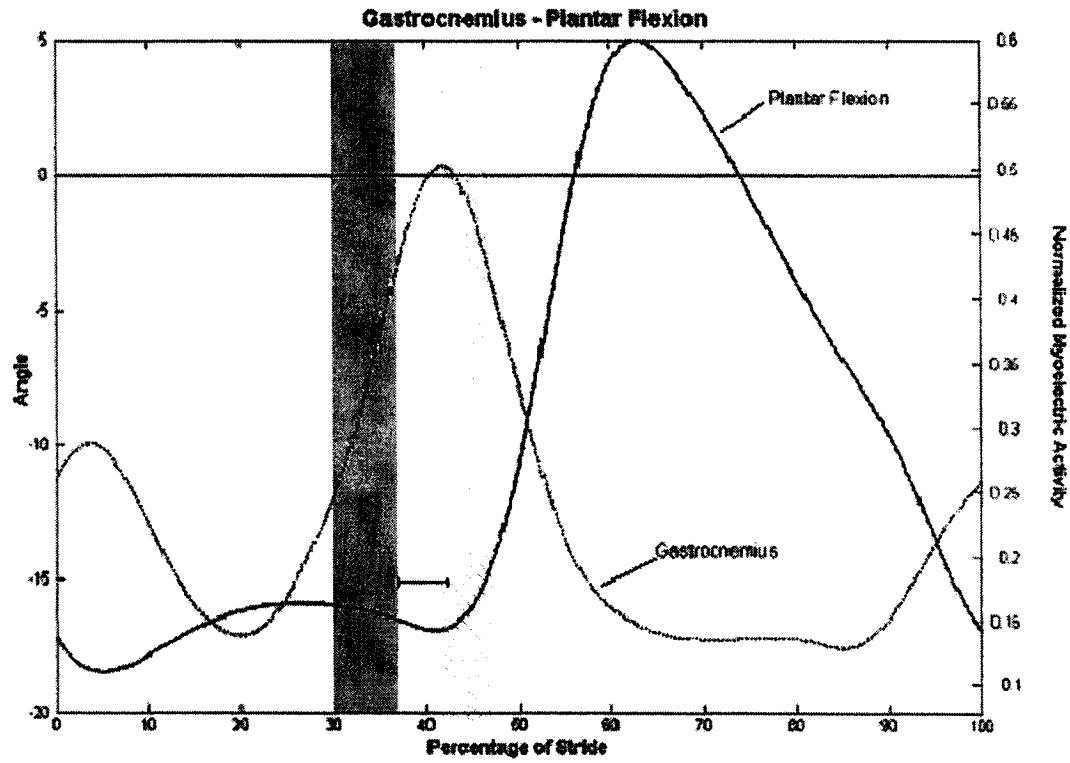

Figure 5.1.3 Muscle activation of the Medial Gastrocnemius on the same normalized time scale as ankle: plantar-dorsi flexion during constant velocity skating. Notice the temporal delay between muscle activation and plantar flexion prior to the electromechanical delay (EMD). In fact the Medial Gastrocnemius is working eccentrically due to the continued ankle dorsi-flexion after the EMD. The EMD is assumed to be approximately 50 milliseconds long and accounts for approximately 7.1% of stride; this area is represented by the grey band. The muscle activity threshold is set at 25% of the MDC value. The striped area represents the approximate time phase at which the blade left the ice surface.

Figure 4.2.4 shows some interesting differences in peroneus longus profiles throughout strides A1 – CONST. Interestingly the muscle profile of the peroneus longus mirrors that of the medial gastrocnemius at constant velocity. Since the peroneus longus acts as a plantar flexor as well as an evertor of the ankle and due to the similarities in curve profiles the author assumes that the purpose of the peroneus longus activation is mainly to create a plantar flexion moment at the ankle joint at push-off, however it is also likely acting to stop invesion collapse at blade contact. Figure 5.1.6 shows that the ankle is primarily everted during the stride and that there is no apparent relationship between

peroneus longus activation and eversion of the ankle. Therefore it is suggested that it is the location of stress concentrations in the skater relative to the ankle centre of rotation that is creating this ankle eversion, (see figure 5.1.5) in addition to the coupling of ankle dorsi-flexion and ankle eversion with the ankle dorsi flexed during most of the skating stride (see figure 4.1.7).

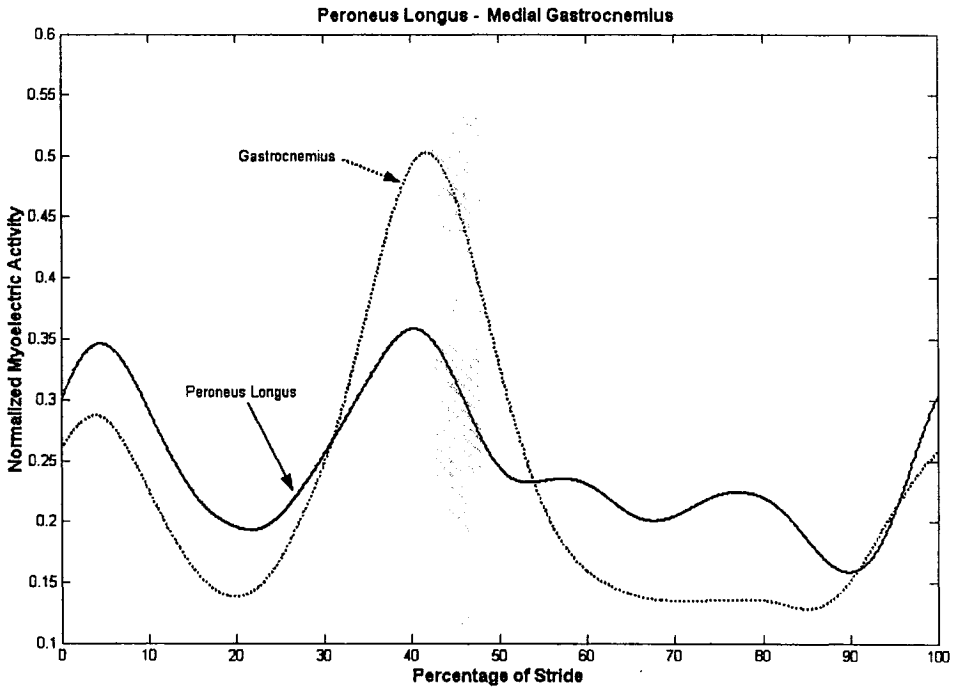

Figure 5.1.4 Shows the muscle activation of the Peroneus Longus, and Medial Gastrocnemius during constant velocity skating. Notice the similarities in curve profiles during the stride despite the differences in magnitudes. The striped area represents the approximate time phase at which the blade left the ice surface.

Figure 5.1.5 Diagram depicting the estimated direction and location of the forces transmitted through the skater's right leg and acting on the ice. The arrows indicate longitudinally oriented force vectors and their approximate locations. The dot indicates the centre of rotation, therefore explaining the eversion of the ankle during stance phase.

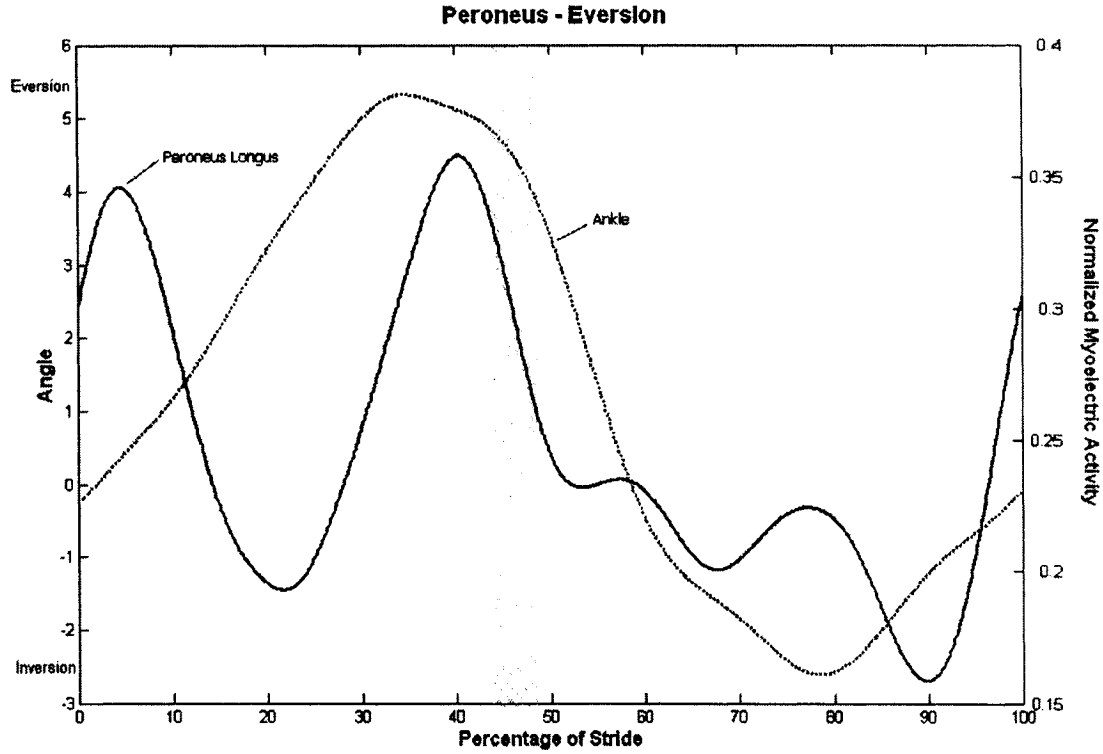

Figure 5.1.6 Activation of the Peroneus Longus in comparison to ankle: inversion - eversion during constant velocity skating. The curve profile suggests that the Peroneus Longus isn't the primary contributor much to ankle eversion during constant velocity skating. The striped area represents the approximate time phase at which the blade left the ice surface.

Peak tibialis anterior activity at constant velocity occurs during swing phase. Initial dorsi flexion of the ankle is seen at this peak. A similar peak is seen in the early phase of stance when the foot is in contact with the ice. The tibialis anterior activity is at its lowest level during medial gastrocnemius and peroneus longus excitation at push-off. The latter is a sensible strategy to reduce antagonistic muscle activations in the elite level skaters.

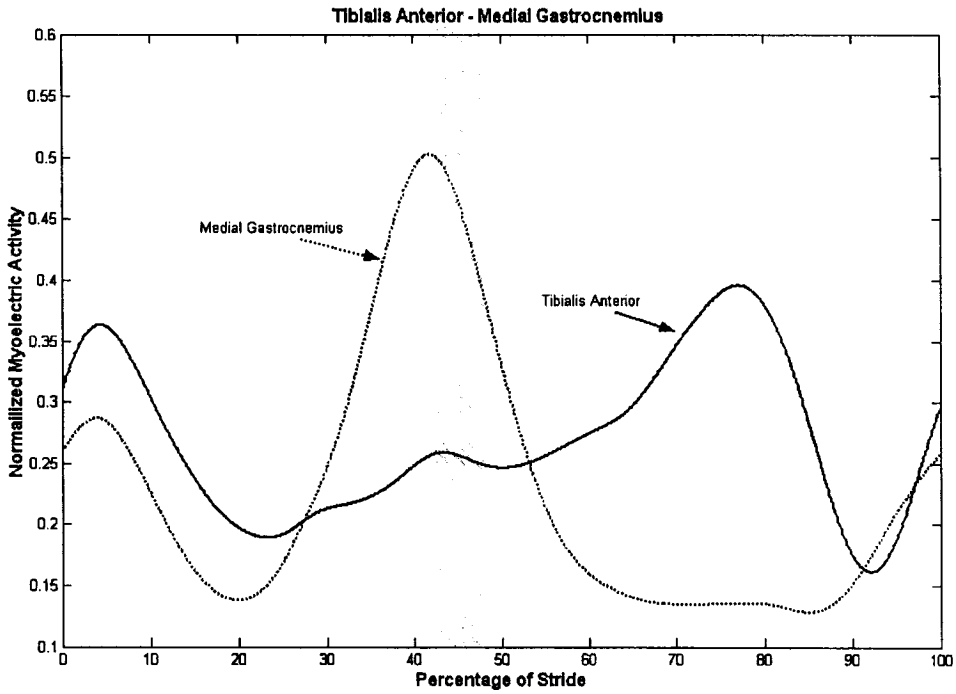

Figure 5.1.7 Muscle activation of the Tibialis Anterior, and Medial Gastrocnemius during constant velocity skating. Notice the biphasic increase in muscle activity for the two muscles. The striped area represents the approximate time phase at which the blade left the ice surface.

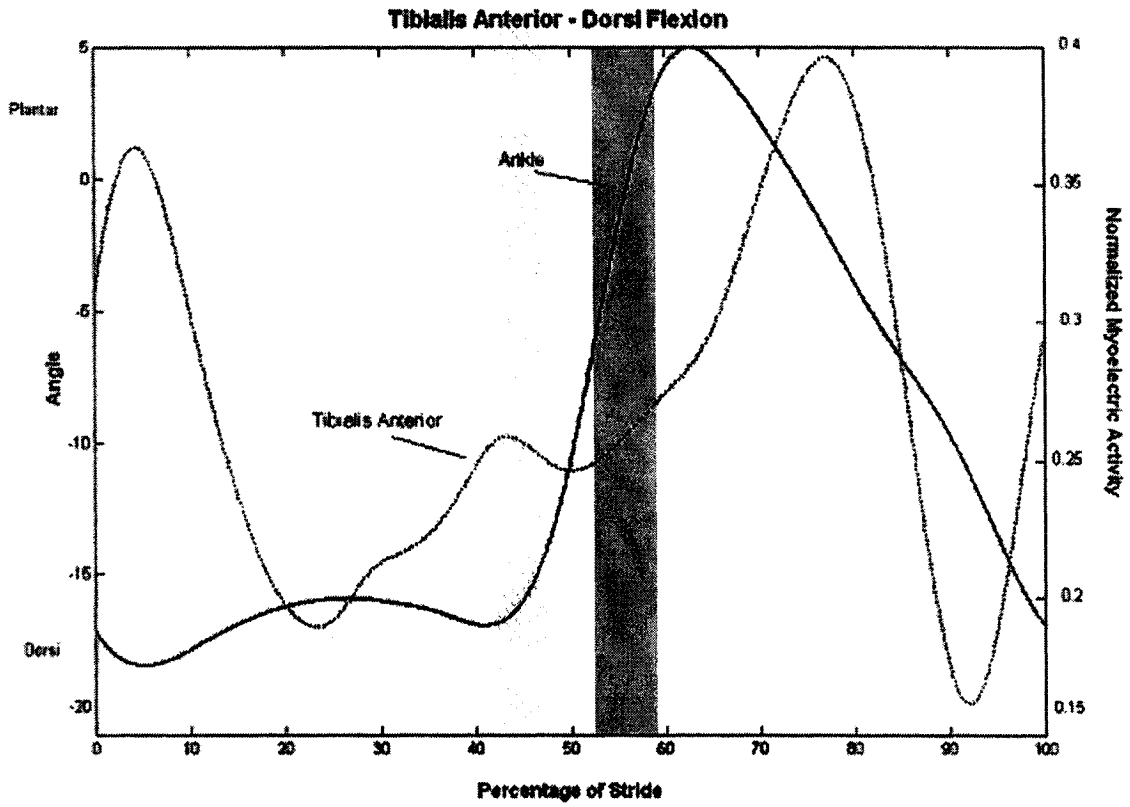

Figure 5.1.8 Muscle activation of the Tibialis Anterior on the same normalized time scale as ankle: plantar-dorsi flexion during constant velocity skating. Notice the increase in Tibialis Anterior activity as the ankle changes movement direction from plantar to dorsi in the latter part of stride. The grey zone depicts the Electromechanical Delay and is based on the same assumptions of figure 5.1.3. The striped area represents the approximate time phase at which the blade left the ice surface.

Vastus medialis activity was found to be significantly greater during acceleration strides A1 compared to constant velocity strides CONST ($p<0.05$.) The mean maximum myoelectric values for strides A2 and A3 are also greater than constant velocity values. A potential explanation for this finding is that the quadriceps in general provides a greater propulsive mechanism, via knee extension, in overcoming the skaters' inertia during the acceleration strides than at constant velocity.

Despite different criteria for identifying foot strike, the experimental EMG results in this study are show strong congruence with the results of Goudreault (2002) for each

of the four muscles. Using the criteria of Goudreault foot strike occurs approximately thirteen percent earlier than with the current criteria. Notable differences did exist between the magnitudes of normalized values however. The amplitudes during CONST in this study were significantly lower than those found by Goudreault et al. (2002) for each muscle throughout the entire skating stride. This difference is thought to be due to the application different normalization coefficients based on differing maximum dynamic contraction criteria. In the current study, the greatest myoelectric amplitudes were observed during the acceleration strides; hence using these values to normalize the amplitude of myoelectric signals during CONST would proportionally lower the MDC for the latter. One noticeable difference in EMG profiles between studies is that there is no initial peak, or a much less substantial one, in myoelectric activity in the medial gastrocnemius and the peroneus longus at touch down. The function of this initial peak is still unclear and is only speculatively stated above, but differences suggest a degree neuromuscular adaptation to the relatively novel skating treadmill stimuli (i.e. the test conditions for the Goudreault study). It is important to note that some of these differences may be accounted by inter-tester and intra-tester variability, or by the difference between treadmill skating and on ice skating at different intensities. Despite the above mentioned differences the congruence between the myoelectric profiles findings in the two conditions indicates that on ice skating and on treadmill skating are quite similar. This finding shouldn't be very surprising due to the visually observable similarities in skating kinematics. Given the advantages inherent in the use of the skating treadmill, i.e. reducing the required volume for calibration and the converse increase in measurement resolution for motion analysis and temperature control that allows a comfortable enough

environment for the use of skin based markers, and eliminates electronics concerns, further investigation is merited to investigate the specificity and applicability of treadmill skating on skating technique analysis, athlete rehabilitation and as a tool in the testing protocols for skate design modifications. It is likely that any findings will suggest a high degree of specificity or similarity between the two conditions.

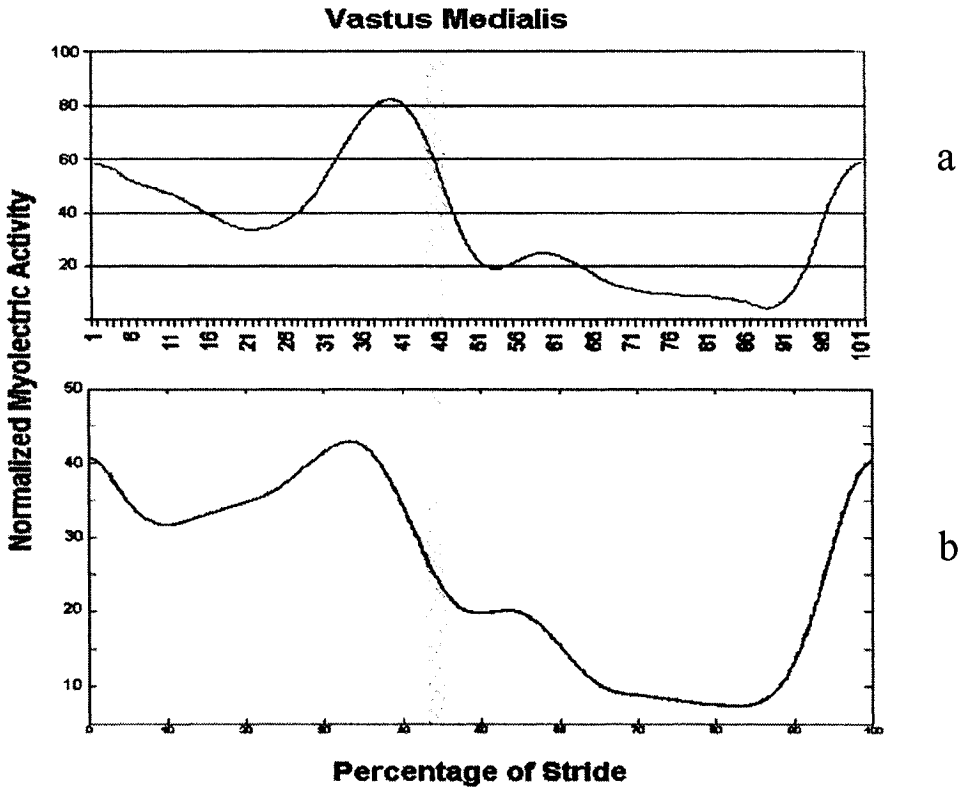

Figure 5.1.9 Muscle activation of the Vastus Medialis during Constant Velocity Skating on a skating treadmill (a) and on ice (b). Mean myoelectric profiles on treadmill have been adjusted to account for different stride parsing criteria. The striped area represents the approximate time phase at which the blade left the ice surface.

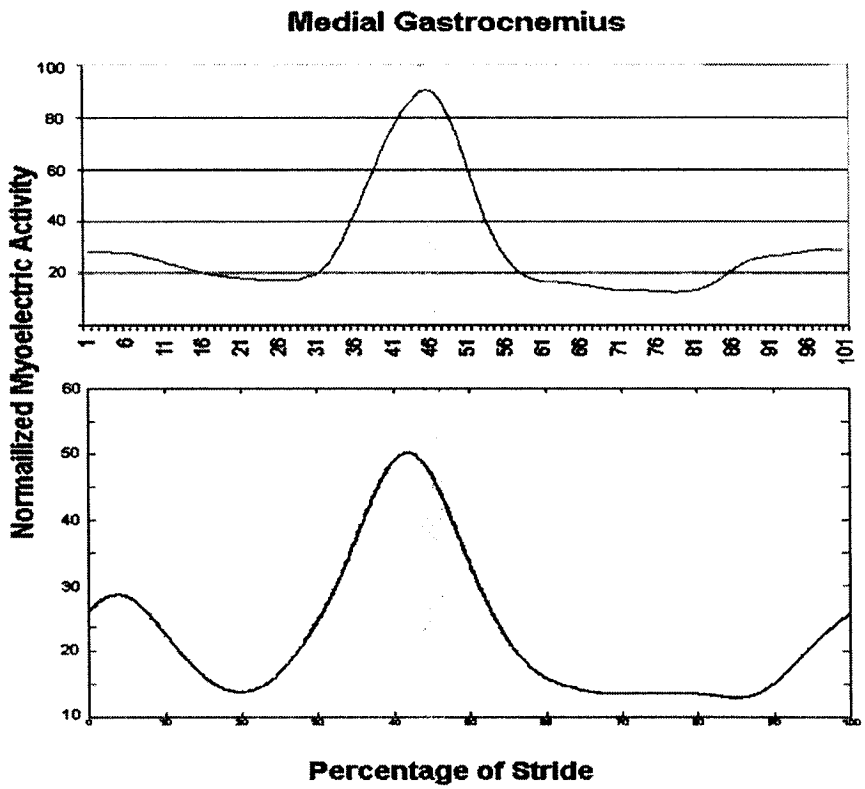

Figure 5.1.10 Muscle activation of the Medial Gastrocnemius during Constant Velocity Skating on a skating treadmill (a) and on ice (b). Mean myoelectric profiles on treadmill have been adjusted to account for different stride parsing criteria. The striped area represents the approximate time phase at which the blade left the ice surface.

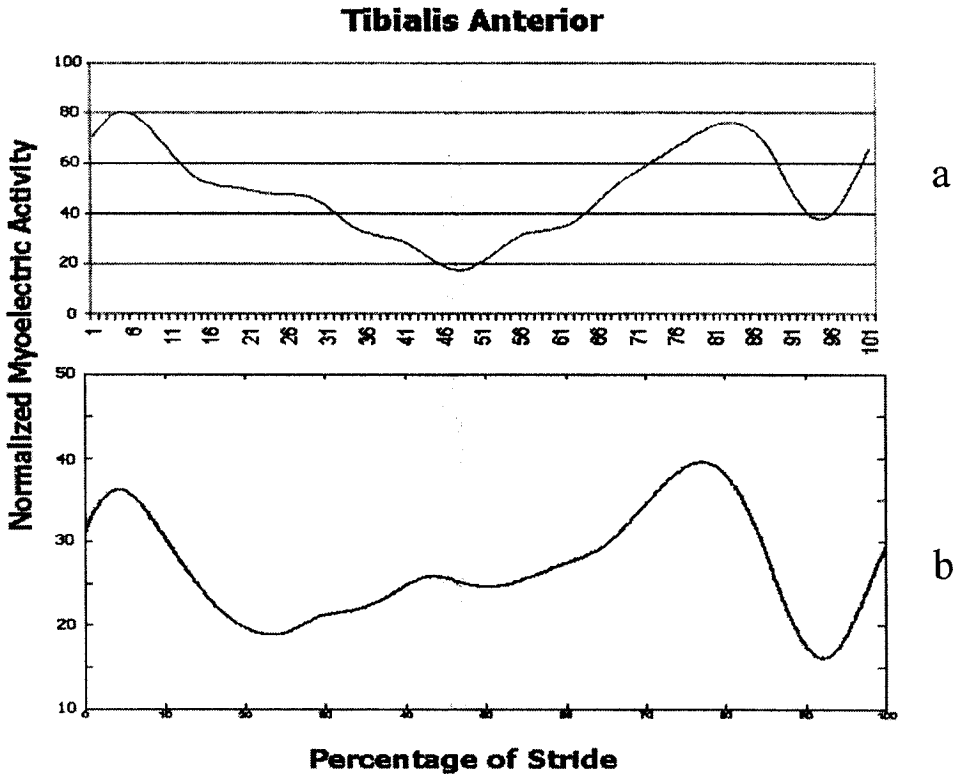

Figure 5.1.11 Muscle activation of the Tibialis Anterior during Constant Velocity Skating on a skating treadmill (a) and on ice (b). Mean myoelectric profiles on treadmill have been adjusted to account for different stride parsing criteria. The striped area represents the approximate time phase at which the blade left the ice surface.

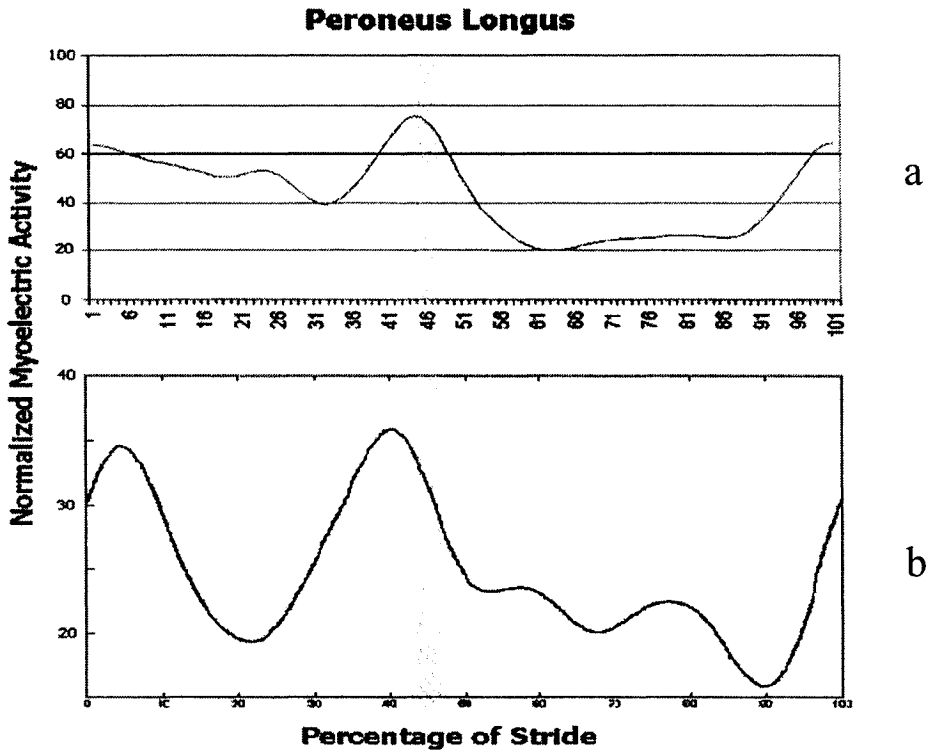

Figure 5.1.12 Muscle activation of the Peroneus Longus during Constant Velocity Skating on a skating treadmill (a) and on ice (b). Mean myoelectric profiles on treadmill have been adjusted to account for different stride parsing criteria. The striped area represents the approximate time phase at which the blade left the ice surface.

5.2 Kinematics

The movement measurement system used in this study, electrogoniometry, provided benefits but it also had some financial costs associated with it. The goniometers permitted high resolution kinematic data without requiring the calibration of a large volume of space. However, the goniometers are rather expensive and are relatively fragile. Over the course of this experiment three goniometers were damaged. The cause of the damage was assumed to be related to general overuse from past experiments. Prior to conducting the study there was the concern that the rigidity of the skate boot and the preference for some skaters to tightly lace their skates would alias the measurement signal; however, data collected during the experiment quelled these concerns. For

instance, one of the sixteen pressure sensors was placed on the calcaneal tuberosity directly underneath the placement of the distal block of the goniometer. The negligibly low pressure values at that location (see figure 4.3.23 (A), (B)) give evidence that there is not a significant interaction between the posterior compartment of the skate boot and the goniometer that would alias the kinematic signal.

Houdijk et al. (2001) gave a mechanical explanation for the occurrence of plantar flexion in speed skating based on magnitude and position of the ground reaction force relative to the skate blade. In a parallel comparison to ice hockey, it can be said that rotation of the skate (i.e. in the sagittal plane) occurs when the net ankle moment, mainly generated by the plantar flexor muscles exceeds the moment of the external forces that act on the foot. During the skating stride, these two moments are in balance to permit the skate blade to remain in gliding contact with the ice as well as to permit the rocking action from rear to front blade edge. The balance of both moments is maintained until the point of application of the ground reaction force shifts forward along the blade, which increases the moment arm of the external forces. This is the case until the centre of pressure of the ground reaction force reaches the point of curvature of the blade (i.e. progress of the blade corresponding to blade curve vertex.) Thereafter, the plantar flexor moment will exceed the external moment and the skate starts to rotate. In this instance the occurrence and angular velocity of plantar flexion during the skating stride is determined by the rate at which the centre of pressure between skate blade and ice moves anteriorly along the skate blade. The kinematic data of the ankle in the sagittal plane reveal that during most of stance phase the ankle is in a rather fixed position (i.e. dorsi-flexed). The ankle starts plantar flexion at approximately 42 percent of stride when the ankle in near

maximally dorsi-flexed. At which time there is a rapid increase in plantar flexion angular velocity (see figure 5.2.1). Due to the high angular velocity of the ankle plantar flexion and due to the force-velocity relationship of muscle it is reasoned that most of the ankle plantar flexion occurs after the foot contact phase and does not contribute substantially to the acceleration of the skaters' mass in the propulsive phase of the skating stride.

The ankle range of motion in the sagittal plane during forward ice hockey skating does not approach the anatomical range of motion data reported in the literature (i.e. 80° range of motion suggested by Levangie, and Norkin 2001). Plantar flexion of the ankle is limited in the ice hockey skate due primarily to the long and rigid achilles tendon guard of the skate and its effective arresting of angular displacement between the foot and tibia segments. Despite the limitation imposed by the Achilles tendon guard, it is not likely to be a performance hindrance since the limited amount of ankle plantar flexion occurred during the swing phase of stride. The trend of increasing plantar flexion values throughout strides A1 – A3, and CONST is likely the result of a greater amount of rotational energy in the more proximal segments of the thigh and leg being transferred to the foot and thereby placing more stress on the Achilles tendon guard barrier, thus creating more strain of the achilles tendon guard and finally allowing for greater plantar flexion of the ankle.

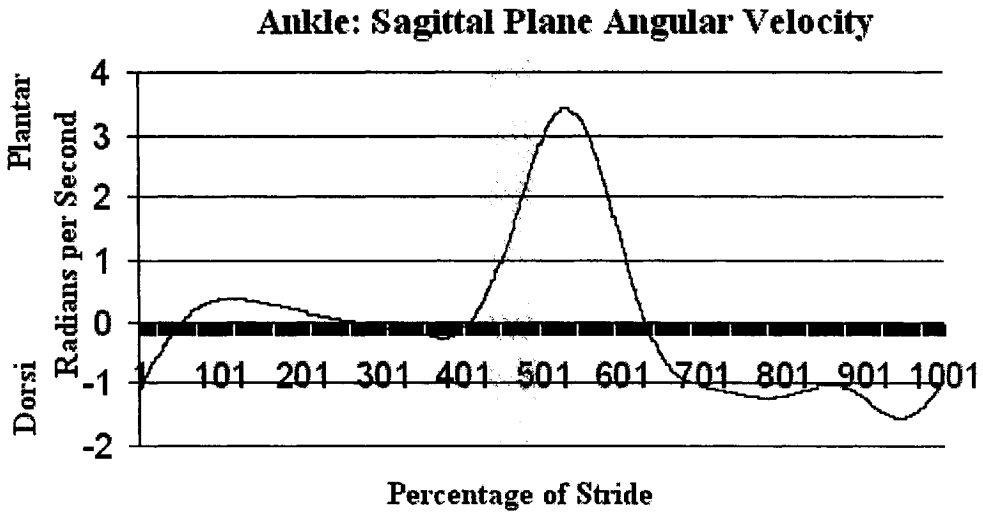

Figure 5.2.1 Angular velocity of the ankle in the sagittal plane. The striped area represents the approximate time phase at which the blade left the ice surface. X-axis is values represent 1000 points on a time normalized scale, where data point 1 = 0%, data point 501 = 50% and data point 1001 = 100%.

Frontal plane ankle kinematic data were similar to the sagittal plane data in that there were no extreme variations among strides. There was a trend for the ankle to invert more through strides A1 to CONST. The occurrence of peak ankle inversion was during the swing phase of stride and as such mirrored ankle plantar flexion. Due to the coupling between ankle plantar flexion and inversion it is likely that the increase in inversion of the ankle is due to the coupling with ankle plantar flexion.

The eversion results of the ankle showed no significant differences between strides and revealed that the ankle was near maximally everted at the time of push-off. These data are consistent with the results of Chang et al. (2002) and Hoshizaki et al. (1989). The measurement of ankle eversion is especially revealing in the ice hockey context due to the torsional rigidity of the foot bed of the ice hockey skate, the constant pressure seen at the entire plantar foot surface. For these reasons movement of the

forefoot and rearfoot may be assumed to be coupled. Furthermore, the movement of inversion/eversion of the calcaneus has been linked, respectively, anatomically to the external/internal rotation of the tibia; an additional determinant of tibial rotation is the height of plantar arch of the foot and the stiffness property of the arch. Therefore measurement of inversion/eversion and of the properties of the arch will provide an indicator of the amount of subject specific tibial rotation. Speculating even further it can be said that the amount of tibial rotation determines the amount of knee flexion/extension due to the functional requisite of maintaining the congruence the condylar surfaces of the tibia and femur. Thus the frontal plane kinematics of the calcaneus in ice hockey skating serves as an indicator of both proximal and distal skeletal movements.

5.3 Pressure

The use of piezo resistive pressure sensors in this study was rather telling of the local pressures acting at various locations of the global surface anatomy of the foot and ankle. There was significant inter-subject difference in pressures at certain regions. These pressure differences can be explained to some extent by geometric differences in the anatomy of the subjects. Standard subject variation can cause a point load effect that increases or decreases localized pressure. A second factor for inter-subject differences in pressure is the level of tension or tightness in the lacing of the skates. The subjects were instructed to lace their skates with the amount of tightness needed to provide the fit that they are accustomed to. Third, although no foot volume or any anthropometric measures of the foot and ankle were performed there almost certainly are differences in the foot volume: boot volume ratio and in the respective width, length and height of certain anatomical structures relative to features of the skate boot.

Despite the variations among subjects, a unique insight into the pressure patterns of the foot and ankle were revealed. Interpretation of these pressure patterns in relationship to the myoelectric and kinematic data are presented in the following text.

Prior to describing regional pressure measures it should be noted the force estimates cannot be literally extrapolated from these pressure measures. As observed by Hennig and Milani (2000), plantar foot pressure measurements are not good predictors of ground reaction force in running 'Low correlations were found for the relationships of plantar pressures to ground reaction force or shock related variables.' Hence in this study it was assumed that plantar foot pressures in ice hockey skating would not correlate well with ground reaction force and no assumptions on the amount of force are stated based on this data. Future studies should attempt to calculate force to permit the generation of mechanical model of skating, and a series of free body diagrams. Nonetheless, differences in pressure patterns reflect the dynamic interface between the foot and ankle as it applies leverage to the boot or vice versa.

5.3.1 Plantar Surface

Figure 4.3.5 (A) shows the plantar lateral pressures become successively lower the more distal (i.e. towards the forefoot) the sensor is located. The succession of peak pressures from proximal to distal is before and later respectively, for each sensor placement. This is indicative of a medially and anteriorly shifting centre of pressure. These results are congruent with Figure 5.3.1 which demonstrates a delay in the onset of peak pressure values closely corresponding to the movement of the centre of mass and centre of pressure anteriorly during the stance phase of the skating stride. The occurrence of peak plantar pressure on the forefoot, the most distal sensor on the foot preceded ankle

plantar flexion. This provides further evidence confirming the constraint of the rigid ice hockey blade on ankle plantar flexion.

There was a statistically significant difference in the maximum pressure under the head of the fifth metatarsal between the first and second acceleration stride, and between the second acceleration stride and constant velocity skating. In both instances the second acceleration stride had a significantly lower maximum pressure. This difference is difficult to reconcile due to the different angles of obliquity between the skate and the direction of travel; however the finding shows that different plantar foot loading pattern is being employed throughout the acceleration phase and constant velocity phase of ice hockey skating.

Figures 4.3.1 ('a' and 'b') shows the difference in peak medial-lateral pressures at the heel indicates a fundamental difference in the foot landing strategies between running and skating. In running, generally the heel bears greater load laterally than medially in the vast majority of runners (Hennig and Milani 2000), while in skating the opposite is evident. This may be produced by both (1) the greater medial-lateral whole body shift as the body progresses in a sinusoidal pattern within the transverse plane as well as (2) the oblique orientation of boot/blade to ice necessary to "catch an edge" for sufficient friction.

The pressure data collected from the plantar surface of the foot showed a constant or residual pressure exerted throughout the entire stride phase, including swing, these results are congruent with the finding of Loh (2003.)

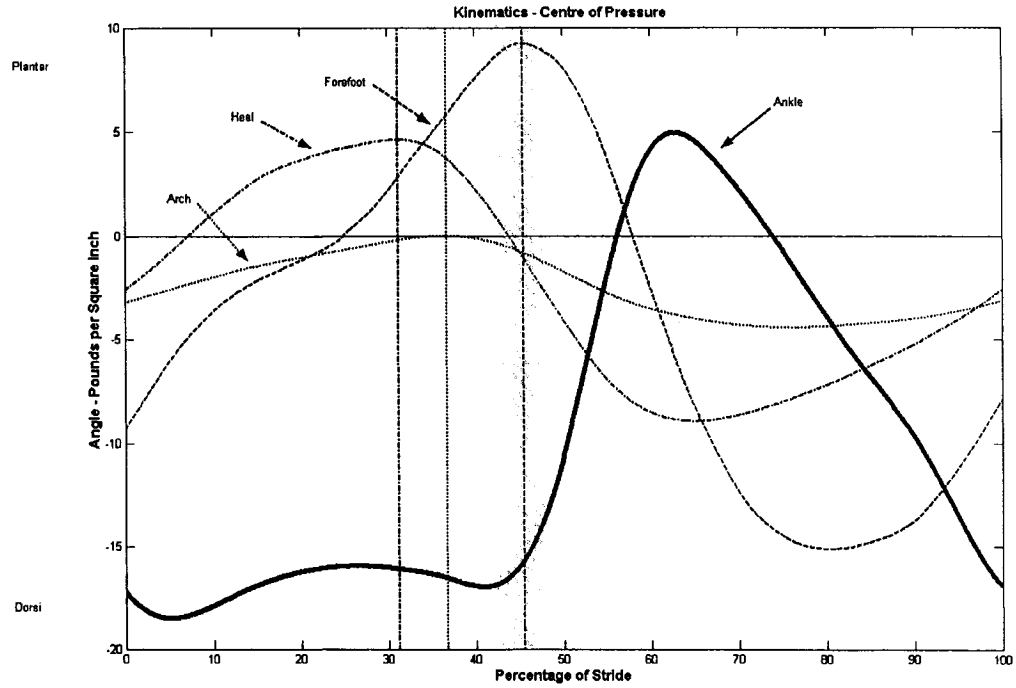

Figure 5.3.1 Shows the relationship between plantar flexion occurrence of peak pressures along the plantar surface of the foot. Plantar flexion occurs once the Centre of Pressure moves anteriorly along the skate blade. Notice the decreasing plantar pressures coinciding with ankle plantar flexion. The striped area represents the approximate time phase at which the blade left the ice surface.

5.3.2 Medial - Lateral Surface

Figures 4.1.4 & 4.3.12 (A) show an increasing pressure in the medial calcaneus that coincides with ankle eversion. Figures 4.14 & 4.3.16 (A) shows a tendency for the lateral malleolus pressure to increase as the ankle everts and then decrease as the foot inverts in swing phase. Conversely more distally at the lateral: fifth metatarsal base a decrease in pressure occurs during peak eversion of the calcaneus; peak pressure occurs at approximately the same time as peak inversion during the swing phase. Pressure at the medial calcaneus was rather minimal in comparison to other regions; the fluctuation in pressure was also quite small. A strong relationship was observed between medial malleolus pressure and lateral calcaneus pressure see figure 5.3.3. Both pressure profiles

demonstrated an increase in pressure during the early phase of stance followed by a substantial lowering in pressure during the middle of the stance phase.

To provide a possible mechanical explanation of the relationship between medial and lateral foot pressure a few assumptions from the skating stride taken from Stamm (1989), Loh (2003), and Chang (2003) are inferred. Kinematic data collected in this study are strictly local to the ankle. For a complete understanding of skating stride, in addition to local kinematics, global kinematics are required however; as stated earlier, such values are difficult to obtain with a high degree of resolution. However some speculation on global kinematics of the skating stride can be drawn from the remnants of the skating stride. The minute finite contact area between the skate blade and the ice supports the body weight of the skater. This high pressure dynamic creates an ice channel that is preserved after the skating stride. Stamm (1989) depicted the indentation left in the ice after a skating stride. Stamm stated the difference between, what was defined as proper forward skating technique and improper forward skating technique could be identified by examination of the ice channels of the skater. Differences between the two were based mostly on step width while the skate indentations left were quite similar and sinusoidal.

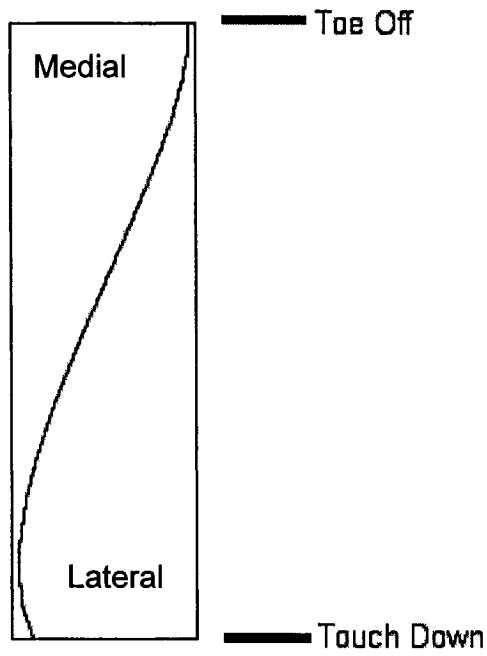

Figure 5.3.2 A depiction of the ice channel remnant of a skating stride for the right skate blade of an elite skater at a high constant velocity, based on the work of Stamm (1989).

During the initial part of stride right after touch down, the skater is on the outside or lateral edge of the skate blade. By continuing to skate on this edge with the body centre of mass shifted laterally towards the skate edge, the skater would veer laterally along a radius of curvature. Since the intention of the skater is to progress forward, this outcome is not desired. In an attempt to correct for this, the skate must decelerate the lateral progression of the centre of mass so that it remains medially. While the lateral centre of mass drift is arrested the penetrating edge of the skate rolls within the frontal plane from the outside or lateral edge to the inside or medial edge. It is necessary for the inside edge of the skate to be in contact with the ice so that the resultant ground reaction force traverse through the contact area of the edge of the skate. Coincident with the lateral to medial edge transition, is a reduction of the force exerted by the skater on the surface of the ice. This unweighting is seen in the experimental data reported by Loh et

al. (2003) who found a bimodal force profile with a definite decrease in force during midstance (see figure 5.3.5) at CONST. A similar phenomenon of unweighting was reported by Muller et al. (1998), this unweighting occurred prior to a change in the penetrating edge of the ski in the snow. It is suggested that this phenomenon occurs in ice hockey skating although much less pronounced. The inference in ice hockey skating is that the unweighting or reduction of the force exerted by the skater is in part an adaptation by the skater that eliminates a lateral 'skidding' of the blade into the ice that would occur as the blade orientation is in this transition phase. Interestingly the kinematic data at of the knee recorded by Chang et al. (2003) during treadmill skating at 24 km/hr shows a reduction in knee and hip extension velocity and a maintenance of knee joint angle during the early part of stance (see figures 5.3.6 & 5.3.7.) Caution should be taken in equating treadmill and on ice skating, especially in relation to the blade surface interface, however the results confirm this unweighting phenomenon. It is hypothesized by the author that the skater during this time applies force against the medial surface of the skate in attempt to change the blade orientation. The medial force applied is represented by the increase in pressure at the medial malleolus, this pressure causes a less pronounced counter pressure distally, at the lateral calcaneus (See figure 5.3.3). Once the skater has achieved the proper blade orientation the pressures at both regions decrease.

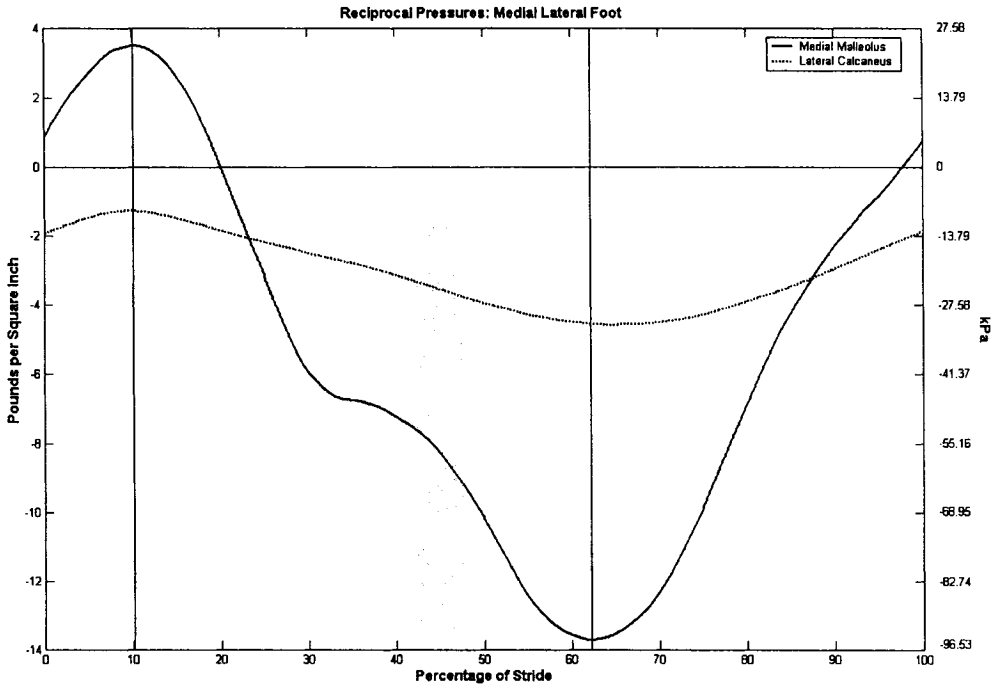

Figure 5.3.3 Shows a strong relationship between the occurrence of minimum and maximum pressure between the medial malleolus and the lateral calcaneus sites. The striped area represents the approximate time phase at which the blade left the ice surface.

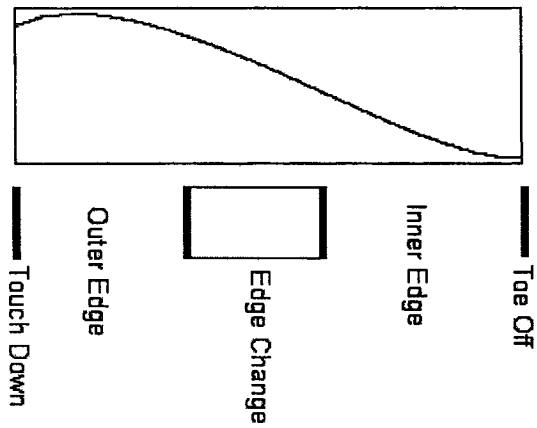

Figure 5.3.4 A depiction of the changes in blade orientation along the ice channel of a skating stride for the right skate blade, based on the work of Stamm (1989).

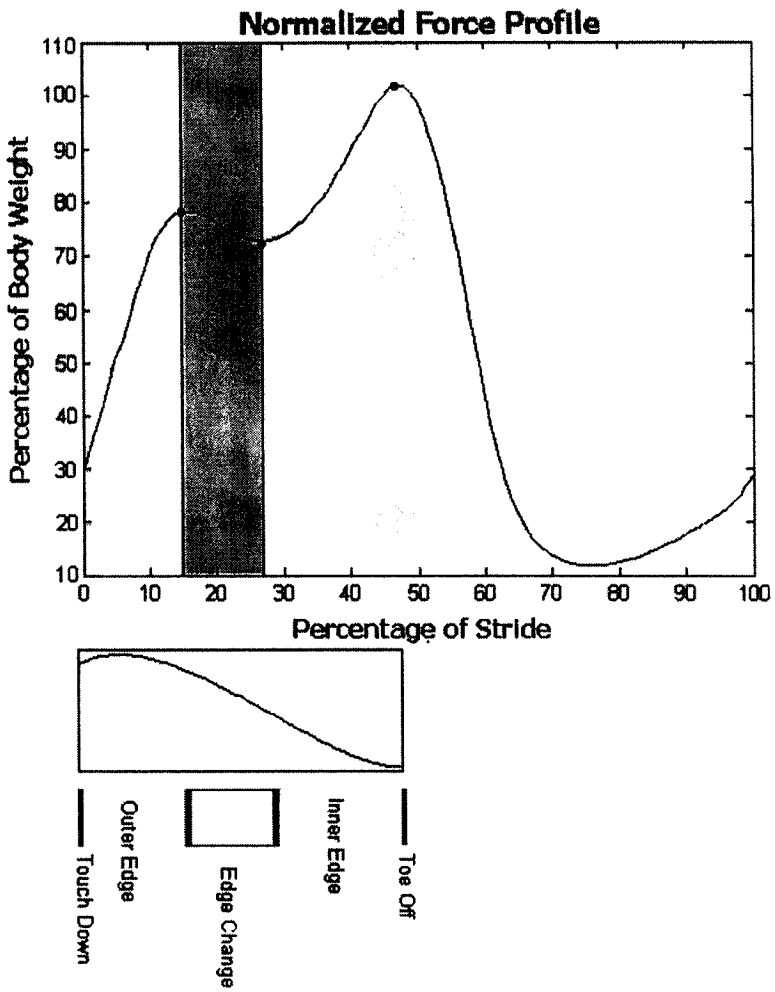

Figure 5.3.5 The grey region illustrates the occurrence of skater 'unweighting' coinciding with edge changing. The striped area represents the approximate time phase at which the blade left the ice surface (adapted from Loh et al. 2003.)

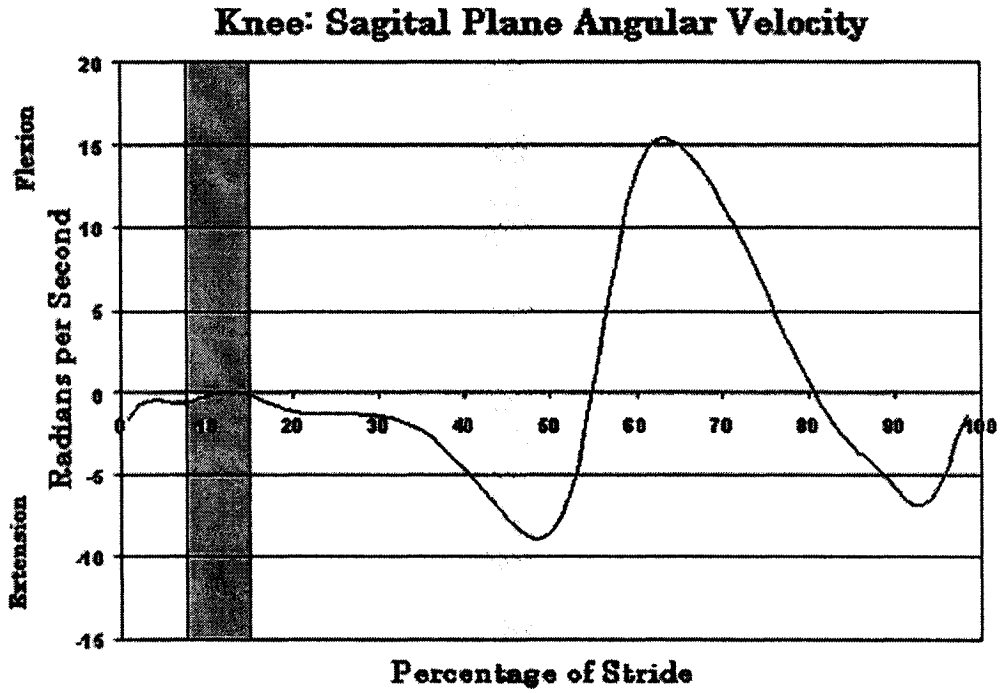

Figure 5.3.6 (A) The grey region is where an unweighting is expected to occur; this is coincident with the decrease in knee extension velocity. The striped area represents the approximate time phase at which the blade left the ice surface (adapted from Chang et al. 2003.)

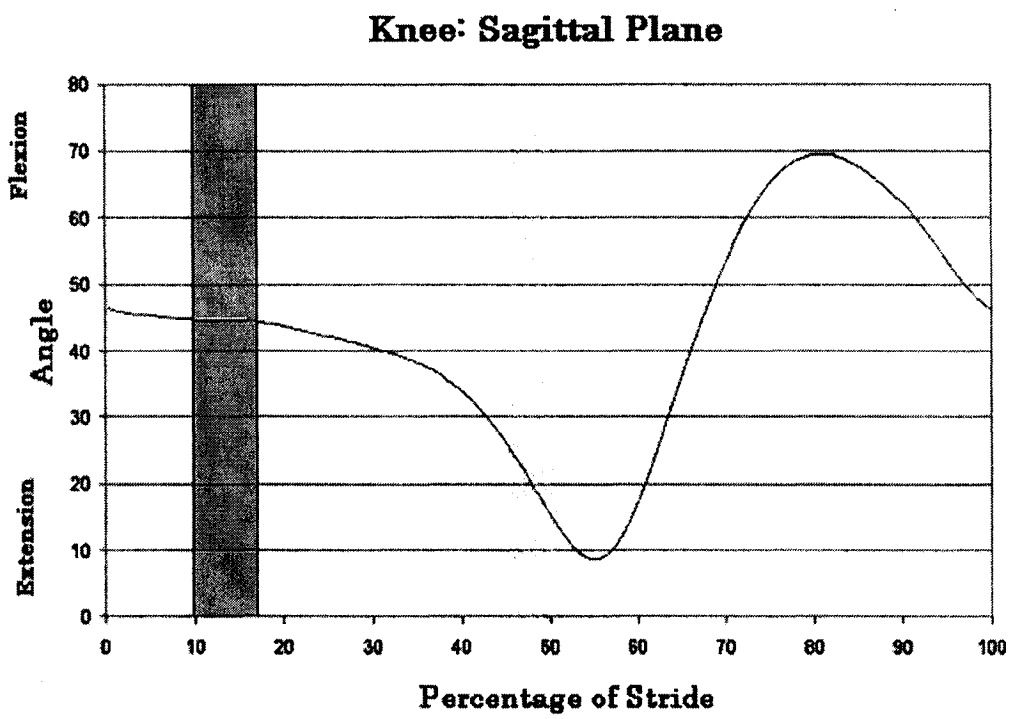

Figure 5.3.6 (B) The grey region is where an unweighting is expected to occur; this is confirmed by the maintenance in knee joint angle. The striped area represents the approximate time phase at which the blade left the ice surface (adapted from Chang et al. 2003.)

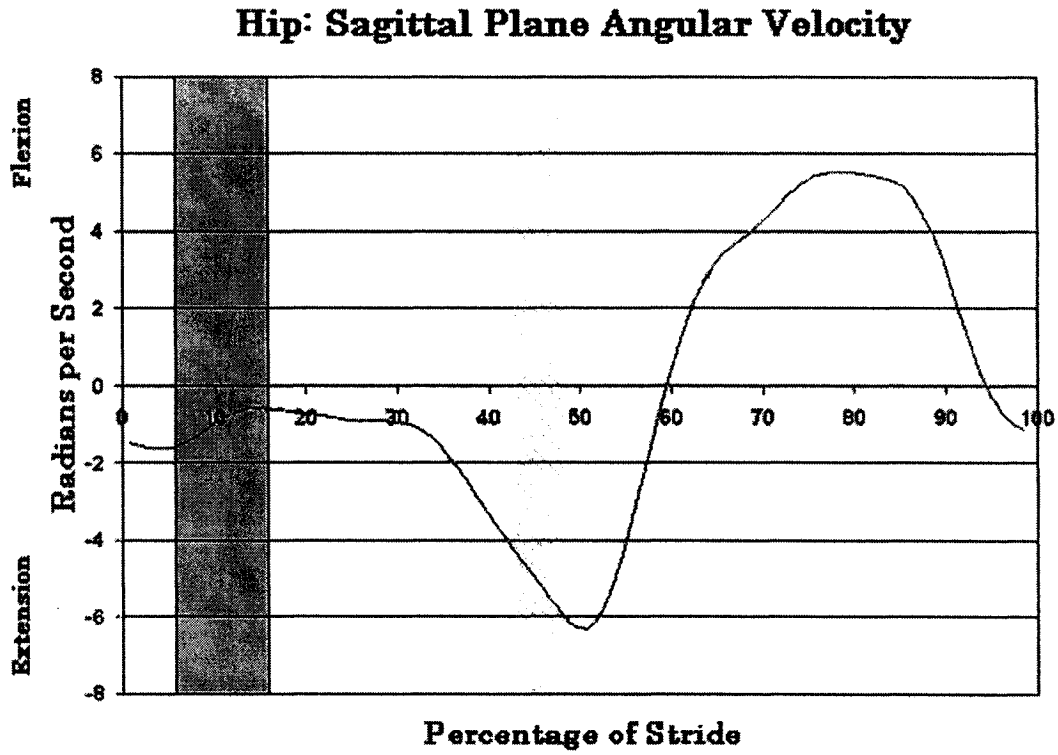

Figure 5.3.7a The grey region is where an unweighting is expected to occur; this is confirmed by the decrease in hip extension velocity. The striped area represents the approximate time phase at which the blade left the ice surface (adapted from Chang et al. 2003.)

The pressure profile of the medial: first metatarsal head reveals that pressure at the location is greatest as the centre of pressure on the plantar surface of the foot is most anterior. Just before the blade lifts off the ice the hip is near maximally abducted and the angle of penetration of the skate blade into the ice in reference to the horizontal plane is at its minimum. At this point in time the force vector generated through longitudinal axis of the skater is oriented rather horizontally and is not contributing much force to the normal surface of the ice. Therefore it is hypothesized that this increase in pressure in the medial, and anterior portion of the skate boot is an adaptation by the skater to generate force that is normal to the surface of the ice (see figure 5.3.7b). This normal force is

important in maintaining the friction between blade and ice that permits a propulsive force by the skater. This adaptation may attribute, in part to the near maximal ankle eversion during terminal push-off.

Figure 5.3.8 Depiction of the force vectors transmitted through the foot and ankle to the ice.

5.3.3 Dorsal Surface

Figures 4.1.1 & 4.3.20 (A) show peak dorsalis pedis site pressure occurring at the same time as maximum ankle dorsi flexion. As the ankle becomes more plantar flexed the dorsalis pedis site pressures decrease substantially. An explanation for this increase in pressure is that dorsi flexion of the ankle causes a compression of the dorsalis pedis region into the tongue and laces of the skate and this compression causes an elevation in

local pressure. An interesting phenomenon of the dorsalis pedis site pressure during skating is that it is constantly above the neutral weight bearing value. This may seem illogical based on the relationship between foot movement and ankle rotation; and due to the fact that both planar kinematic measures of the ankle movement intersected with their neutral value during the skating stride. It seems then that there are other factors that contribute to dorsalis pedis site pressure. Perhaps the pressure at the dorsalis pedis location is the resulting counter pressure from the 'residual' pressure that exists on the plantar surface of the skate even in swing. Conversely, perhaps the plantar surface residual pressure is the consequence of this dorsalis pedis site pressure and can be labelled a counter and concurrent pressure.

5.3.4 Posterior Surface

The pressure in the posterior region of the foot were not substantial; however the pressure curve profiles seemed to coincide quite strongly to movement of the ankle in the sagitttal plane. Figures 4.1.1 & 4.3.23 (A) show that the posterior calcaneus pressure decreases as the foot plantar flexes and increases as the ankle becomes more dorsi flexed.

The pressure profile of the achilles tendon mirrors that of ankle plantar flexion so closely (see figure 4.1.1 & 4.3.23 (A)) that, given its anatomical placement it is assumed the pressure is accountable mainly by the compressive deformation of the skin and a bending of the piezo resistive fabric of the pressure sensor and may be unique to the structural characteristics of the specific skate model and size used.

5.3.5 Implications to Fit

The results of this study have some implications for the assessment of fit comfort and the three dimensional distortion of foot shape. Intuitively, it would seem that for a

given fit an increase in pressure would necessitate a counter pressure increase in an opposing region surrounding the foot and ankle; and, due to the constant foot volume be reciprocated by deficit in pressure in another region. It was found that, in this study there was an increase in average pressure in the foot and ankle during the foot contact phase than during the swing phase. Furthermore it was found that the increase in pressure during foot contact occurred at all regions of the foot (see figure 5.3.9 – 5.3.13); however on the medial – lateral surfaces of the foot the average pressure during stride was less than the average pressure during the static weight bearing collection. The implications of these findings are that during the dynamic foot contact period or during the loading phase there is a general increase in pressure about the global surface of the foot and ankle, by inference this increase in pressure is due to a differing interaction between foot and footwear, and thus a different fit. Due to the relationship between fit and comfort, and the relationship between comfort and performance, these results highlight the inadequacy of the typical 'storeroom' static fit test that consumers use to evaluate not only skates but footwear in general. To best assess the fit of footwear consumers should be given a trial period or should have the opportunity to test the footwear in a manner that adequately mimics the real world dynamic conditions, that the footwear is designed for.

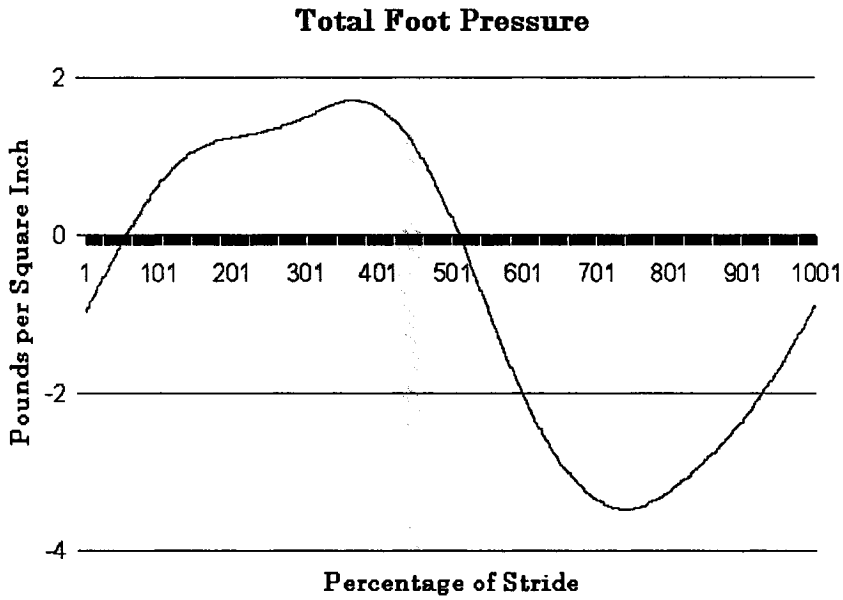

Figure 5.3.9 The average pressure value during forward ice hockey skating at the sixteen sites measured on the foot and ankle. The striped area represents the approximate time phase at which the blade left the ice surface. X-axis is values represent 1000 points on a time normalized scale, where data point 1 = 0%, data point 501 = 50% and data point 1001 = 100%.

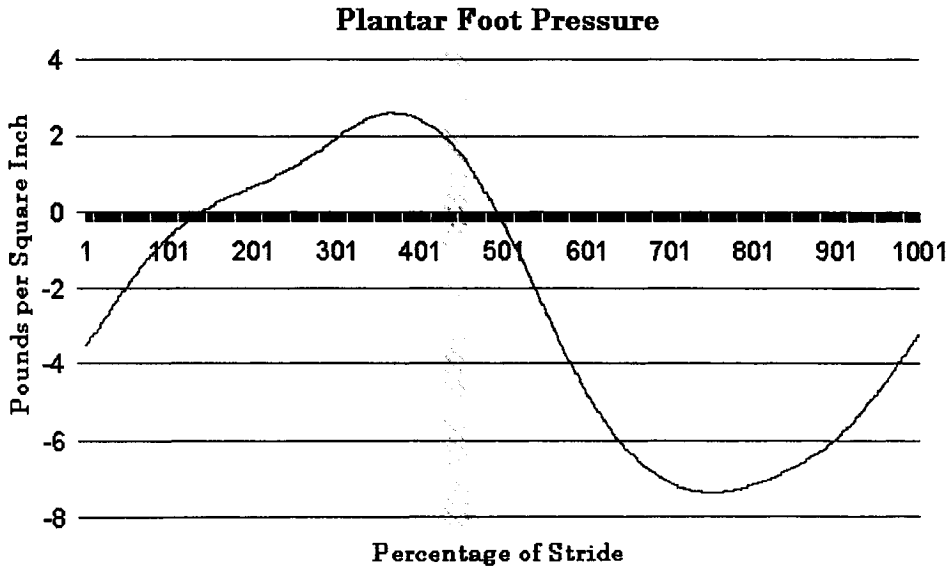

Figure 5.3.10 The average pressure value during forward ice hockey skating at the Medial and Lateral: Heel, Arch, and Forefoot sites. The striped area represents the approximate time phase at which the blade left the ice surface. X-axis is values represent 1000 points on a time normalized scale, where data point 1 = 0%, data point 501 = 50% and data point 1001 = 100%.

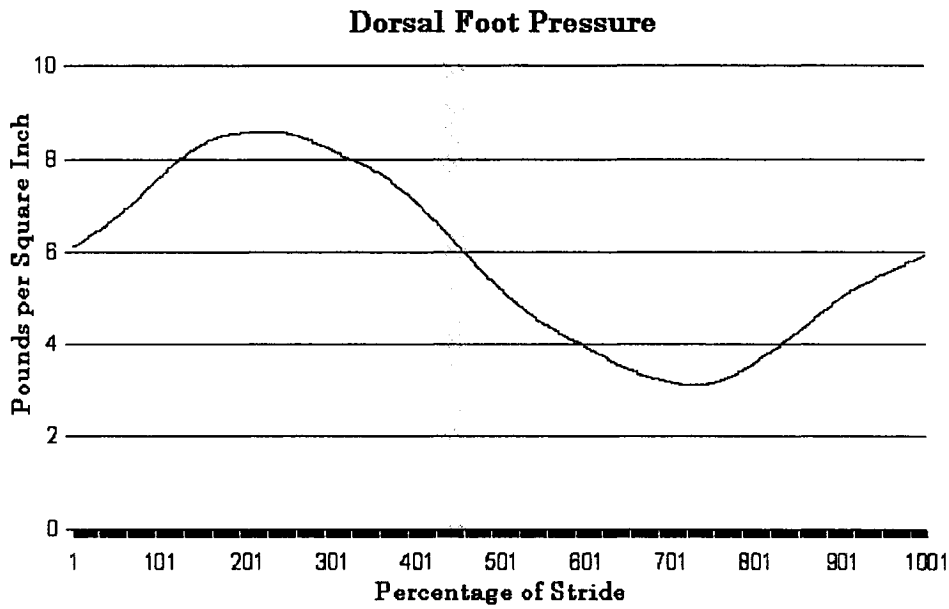

Figure 5.3.11 The average pressure value during forward ice hockey skating at the Dorsalis Pedis, and at the Dorsal: First Metatarsal base sites. The striped area represents the approximate time phase at which the blade left the ice surface. X-axis is values represent 1000 points on a time normalized scale, where data point 1 = 0%, data point 501 = 50% and data point 1001 = 100%.

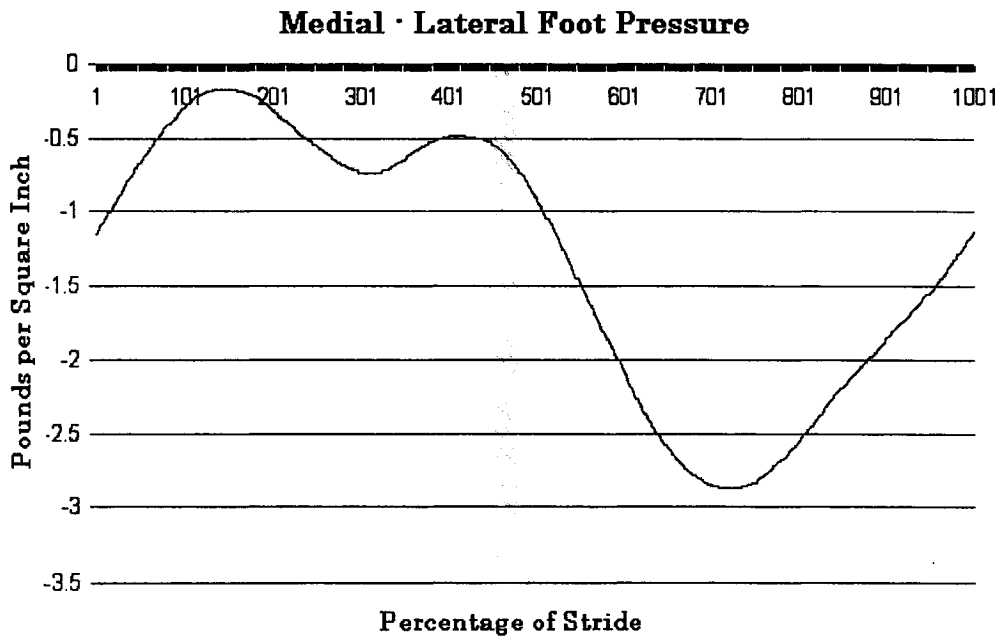

Figure 5.3.12 . The average pressure value during forward ice hockey skating at the Medial Malleolus, Medial Calcaneus, Medial: First Metatarsal head, Lateral Malleolus, Lateral Calcaneus, and Lateral: Fifth Metatarsal base sites. The striped area represents the approximate time phase at which the blade left the ice surface. X-axis is values represent 1000 points on a time normalized scale, where data point 1 = 0%, data point 501 = 50% and data point 1001 = 100%.

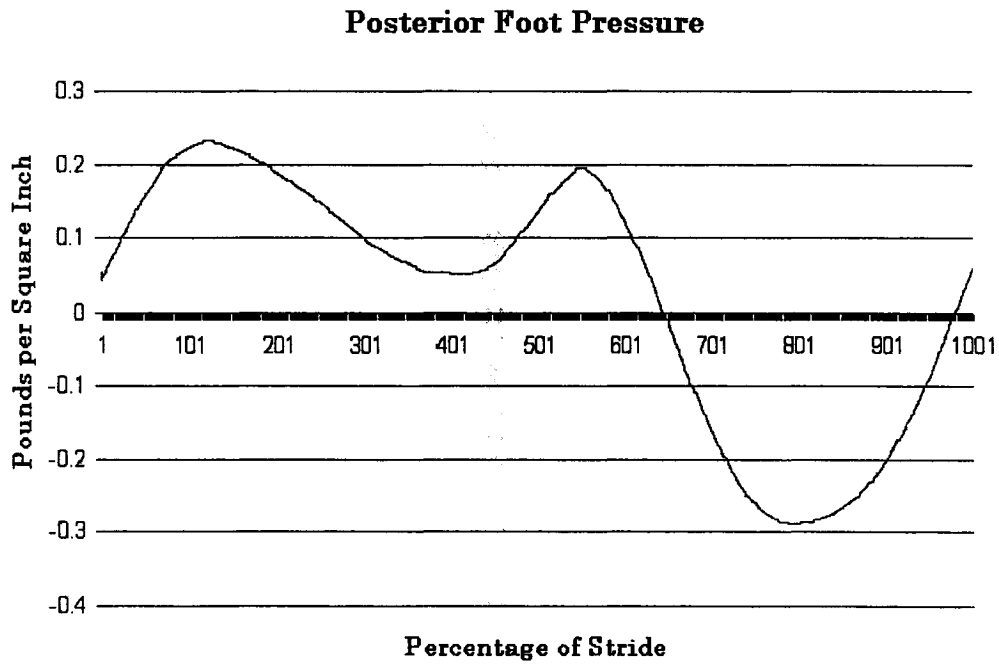

Figure 5.3.13 The average pressure value during forward ice hockey skating at the Achilles Tendon, and at the Posterior Calcaneal tuberosity sites. The striped area represents the approximate time phase at which the blade left the ice surface. X-axis is values represent 1000 points on a time normalized scale, where data point 1 = 0%, data point 501 = 50% and data point 1001 = 100%.

5.4 Future Directions

Numerous questions remain for researchers to address the underlying mechanics of skating. To this point in time, there is no consensus among skating coaches or biomechanists as to what is the optimal skating technique. Furthermore an optimization of skating technique based on individual anthropometric parameters is further on the research horizon. Calculating joint moments via the inverse dynamics model similar to the seminal work of Bresler and Frankel (1950) in ice hockey skating could be very insightful and may elucidate some sources of chronic or overuse injuries and to identify innovations in product design and performance. In order to designate the function of individual muscles during skating stride a measurement tool such as the Hill based

muscle model, with global 3D kinematic values, force measurements and surface EMG should be performed in ice hockey skating.

To this point most ice hockey research has been mostly empirically based, focusing on elite level male skaters. Future research should include comparative studies, with a large sample size, measuring the mechanical properties of different levels of skaters; different aged skaters i.e. children, to seniors; and should analyze females, the fastest growing group of hockey players in Canada. Biomechanical analysis in future should investigate the issue of symmetry in skating between right and left sides of the skater. This analysis should include skating tasks other than forward skating which has been most dominantly reported on in the literature. Other activities such as cross-over skating, backwards skating, tight turns, stopping, and pivoting should be analyzed with the intention of improving performance and reducing injury prevalence. A kinematic, kinetic and myoelectric validation of the skating treadmill based on ice skating results is also required.

At the foot-boot interface future research should analyze the shear component of force at the plantar surface in addition to the other surface of the foot and ankle. An understanding of the contribution of these forces to skating performance and to the aforementioned foot pathologies is required to guide future development of a better skate for the performance and health of the skater. Due to the properties i.e. flexible, thin fabric of the pressure sensors that are now commercially available, the potential for fit and comfort in footwear to be quantified in terms of pressure is looming. In hockey skates, pressure differences in static fit tests should analyze differences between new 'off the

shelf' skates with the equivalent 'broken in' skate, different skate models; and the effectiveness of heat moulding the skate on relieving local pressures and improving fit.

5.5 Conclusion

In conclusion, this experiment offers objective measurements to the kinematic, kinetic, and myoelectric parameters of ice hockey skating total of ice hockey skating. There were significant increases in stride duration and a trend to increase range of motion throughout the transition phase of forward skating. There was a trend of increased muscle activity at the initiation of stance the phase during the acceleration phase of skating, as compared to the constant velocity skating. Additionally there was a statistically significant increase in myoelectric activity of the vastus medialis during the acceleration phase compared to constant velocity. Pressure measurements around the global surface of the foot and ankle were measured. There was an average increase in pressure amongst each of the surfaces of the foot during the foot-ice contact phase of the skating stride. Some functional explanations for the shape of the pressure profiles were speculated on based on previous work in forward ice hockey skating.

References

Al Hadi, M. and Lamontagne, M. Motion of the Foot Inside a Hockey Skate: As Measured from Bone, Skin, and Boot Markers. In XIth Congress of the Canadian Society for Biomechanics Proceedings, 2000;139-139.

Areblad M, Nigg BM, Ekstrand J, Olsson KO, Ekstrom H. Three dimensional measurement of rearfoot motion during running. J Biomech 1990; 9: 933-940

Ball,P. and Johnson,G.R. Reliability of hindfoot goniometry when using a flexible electrogoniometer. Clinical Biomechanics; 1993, 8, 13-19.

Basmajian JV, DeLuca CJ. Muscles Alive: Their Function Revealed by Electromyography. Fifth Edition, Baltimore: Williams & Williams, 1985.

Boocock,M.G. and Jackson,J.A. Continuous measurement of lumber posture using flexible electrogoniometers. Ergonomics; 1994, 37, 175-185.

Bongiovanni LG, Hagbarth KE, Stjernberg L. Prolonged muscle vibration reducing motor unit output in maximal voluntary contractions in man. Journal of Physiology; 1990 *423*: 15–26.

Bresler E, Frankel, JB. SThe forces and moments in the leg during level walking. Journal of Applied Mechanics; 1950, 72, 27-36.

Chang R, Turcotte R, Lefebvre R, Montgomery D, Pearsall DJ. Lower limb kinematics of ice hockey forward skating. IV World Congress of Biomechanics, August 4-9, 2002, Calgary, Alberta, Canada

Chang R. Lower limb kinematics of ice hockey skating. MSc Thesis, McGill University, Montreal, Canada 2002.

Chapin M. Contemporary Canada, New York: Oxford University Press. 1959, 225-226.

Clarys JP. Application of EMG for the evaluation of performance in different sports. In, Marconnet, P. and Komi, P.V. (eds.), Muscular function in exercise and training, Basel, Karger, 1987, p. 200-223.

De Boer RW, Cabri J, Vaes W, Clarijs JP, Hollander AP, de Groot G, van Ingen Schenau GJ. Moments of Force, power, and muscle coordination in speed skating. International Journal of Sports Medicine; 1987a, 5: 371-378,.

De Boer RW, Ettema GJC, Faessen BGM, Krekels H, Hollander AP, De Groot G, Van Ingen Schenau GJ. Specific characteristics of speed skating: implications of summer training. Medicine and Science in Sports and Exercise; 1987b, 10:504-510.

De Boer RW, de Groot G, and van Ingen Schenau JG. Specificity of training in speed skating In Biomechanics X-B University park press: Baltimore; 1985, p. 685-689.

Delagi EF, Perotto A, Iazzetti J, Morrison D. Anatomic Guide for the Electromyographer. Second Edition, Charles C Thomas, Springfield, 1980.

DeLuca CJ. The use of surface electromyography in Biomechanics.. Journal of Applied Biomechanics; 1997, 13:135-163.

De Koning JJ, De Groot G, Van Ingen Shenau GJ. Coordination of leg muscles during speed skating. Journal of Biomechanics; 1991, 24(2):137-146.

De Koning JJ. Houdijk H. de Groot G. Bobbert MF. From biomechanical theory to application in top sports: the klapskate story. Journal of Biomechanics; 2000, 33(10):1225-9,.

Di Fabio, R P, M B Badke, A Mcevoy, and A Breunig. Influence of local sensory afference in the calibration of human balance responses. Experimental Brain Research ; 1990, 80: 591–599.

Dreger RW. Using the skate-treadmill to train hockey players for speed. Strength & Conditioning; 1997, 19(6):33-35.

Dreger RW, Quinney HA. Development of a hockey-specific, skate-treadmill VO2 max protocol. Canadian Journal of Applied Physiology; 1999, 24(6):559-69.

Edington CJ, Frederick EC, Cavanagh PR. Biomechanics of distance running. In: Cavanagh PR (ed). Chmapaign, IL. Human Kinetics Books; 1990: 135 – 164.

Forestier N, Teasdale N, Nougier V. Alteration of the position sense at the ankle induced by muscular fatigue in humans. Medicine & science in sport & exercise; 2002, 34 (1) 117–122.

Gilioli R, Tomasini M, Bulgheroni C, and Grieco A. Effects of vibrating tools on the peripheral vessels and the peripheral nervous system in workers of an iron foundry preventative suggestions. Man Under Vibration—Suffering and Protection, edited by Bianchi G, Frolvlov KV, and Oledzky A. Amsterdam: Elsevier; 1981, 97–129.

Goudreault R, Pearsall DJ, Turcotte R, Montgomery D, Lefebvre R. Forward ice hockey skating: comparison of EMG activation patterns at three velocities. IV World Congress of Biomechanics, August 4-9, 2002, Calgary, Alberta, Canada

Goudreault R. Forward skating in ice hockey: comparison of EMG activation patterns at three velocities using a skate treadmill. MA Thesis, McGill University, Montreal, Canada 2002.

Guyton & Hall. Textbook of Medical Physiology 9th Ed.,W.B. Saunders Company, 1996.

Hancock S, Lamontagne M, Stothart JP, Sviestrup H. The influence of three hockey skate boots on the range of motion, elastic moment and stiffness of the human ankle joint complex. http://www.health.uottawa.ca/biomech/lab/docs/isb17_sh.pdf

Hennig EM, Valiant GA, Liu Q. Biomechanical variables and the perception of cushioning for running in various types of footwear. Journal Applied Biomechanics; 1996, 12: 143-150.

Hennig EM, Milani TJ Pressure distribution measurements for evaluation of running shoe properties. Sportverletz Sportschaden; 2000, 14, 90-97.

Hicks JH. The mechanics of the foot. II. The plantar aponeurosis and the arch. Journal of Anatomy; 1954.

Hillmann A, Rosenbaum D, Winkelmann W. Plantar and dorsal foot loading measurements in patients after rotationplasty. Clinical Biomechanics; 2000, 15, 359-364.

Hinrichs J. EMG activity of ice skating and treadmill skating in hockey players. Thesis, St.Cloud State University (USA), 1994.

Hosein R, Lord M. A study of in-shoe plantar shear in normals. Clinical Biomechanics; 2000, 15, 46-53.

Hoshizaki, T. B., Kirchner, G. Hall, K. Kinematic analysis of the talocrural and subtalar joints during the hockey skating stride. In Safety in Hockey ASTM STP 1050. ed. Castaldi,C.R. and Hoerner,E.F.; 1989, 141-149.

Houdijk H, Wijker AJ, De Koning JJ, Bobbert MF, De Groot G. Ice friction in speed skating: can klapskates reduce ice frictional loss? Medicine & Science in Sports & Exercise; 2001 500-504.

Ishida, A, S Imai, and Y Fukuoka. Analysis of the posture control system under fixed and sway-referenced support conditions: male and female athletes. Journal Athletic Training; 199934:106–114.

Jobse,H., Schuurhof,R., Cserep,F., Schreurs,A.W. and de Koning,J.J. Measurement of push-off force and ice friction during speed skating. International Journal of Sport Biomechanics; 1990, 6, 92-100.

Lafontaine D et al. International Society Biomechanics Sports Proceedings; 1998, 1: 481-483.

Lamontagne M et al. Can Journal Applied Sport Science; 1983, 8(3):169-179.

Latash ML, Zatsiorsky VM. Joint Stiffness: Myth or Reality. Human Movement Science; 1993, 12, 653-692.

Levangie PK, Norkin CC. Joint Structure and Function: A Comprehensive Analysis Third Edition; F.A. Davis; 2001.

Loh JJ. Forward Ice Hockey Skating: Comparison of EMG activation Patterns at Three Velocities. MSc Thesis, McGill University, Montreal, Canada 2003.

Marino GW. Kinematics of ice skating at different velocities. Research Quarterly; 1977, 48(1):93-97.

Marino GW. Acceleration-time relationships in an ice skating start. Research Quarterly; 1979, 50:55-59.

Marino, G.W. Selected mechanical factors associated with acceleration in ice skating. Research Quarterly; 1983, 54: 234-238.

Marino GW, and Weese RG. A Kinematic analysis of the ice skating stride. In Science in Skiing Skating and Hockey.(Eds, J. Terauds, and H.J. Gros.), Academic Publishers: Del; 1979, Mar, p. 65-74,.

Milani TL, Hennig EM. Measurements of rearfoot motion during running. Sportverletz Sportschaden; 2000, 14, 115-120.

Miller DI. Ground reaction forces in distance running. In: Cavanagh PR (ed): Biomechanics of distance running. Champaign, Ilinois. Human Kinetics; 1990, 203-224.

Minkoff J, Varlotta GP, Simonson BG, Ice Hockey. In, Fu FH, Stone D, eds. Sports Injuries: Mechanisms, prevention and treatment. Baltimore: Williams & Williams; 1994, p. 397-444.

Montgomery DL In Exercise & Sport Science, Ed. WE Garrett Jr, DT Kirkendall, Williams & Wilkins; 1999, Ch 42.

Muller E, Bartlett R, Raschner C, Schwameder H, Benko-Bernwick U, Lindinger S. Comparison of the ski turn technique of experienced and intermediate skiers. Journal of Sports Sciences; 1998, 16, 545-559.

Naud et al. Canadian Journal of Applied Sport Science; 1979, 4 (1): 8.

Naud et al. Canadian Journal of Applied Sport Science; 1985, 5 (2): 94.

Nicol, A. C. A new flexible electrogoniometer with widespread applications. In International Series on Biomechanics, Biomechanics X-B ed. Jonsson,B Champaign: Human Kinetics Publishers; 1987, pp. 1029-1033.

Nicol,A.C. Measurement of joint motion. Clinical Rehabilitation; 1989, 3, 1-9.

Nigg BM. Herzog W. Biomechanics of the musculo-skeletal system. John Wiley & Sons 2nd ed, West Sussex; 1999, p. 349-375.

Nigg BM. The Role of Impact Forces and Foot Pronation: A New Paradigm. Clinical Journal of Sport Medicine, Lippincott Williams & Wilkins, Philadelphia, 2001, 2–9.

Nobes, K.J. A comparison of skating economy on-ice and on the skating treadmill, Thesis, McGill University (Montreal, Canada); 2001.

Pearsall DJ et al. 4th Symp Footwear Biomechanics. Alberta, Aug 5-7, 1999.

Pearsall DJ, Turcotte, RA, Murphy SD. Biomechanics of Ice Hockey. Exercise and Sport Science, Lippincott Williams & Wilkins, Philadelphia; 2000, 675-692.

Pearsall, D. J., Turcotte, R. A., Lefebvre, R., Bateni, H., Nicolau, M., Montgomery, D. L. and Chang, R. Kinematics of the foot and ankle in forward ice hockey skating. In XIX International Symposium on Biomechanics in Sport Proceedings, ed. Blackwell, J.R; 2001, 78-81.

Purvis, N. Prediction on acceleration in elite hockey players using peak anaerobic power. Ref Type: Audiovisual Material; 2001

Reinschmidt C, Nigg BM. Current Issues in the Design of Running and Court Shoes Sportverl Sportschad 2000; 14: 71-81.

Reinschmidt C, van den Bogert AJ, LundbergA, Nigg BM, Murphy N, Stacoff A, Stano A. Tibiofemoral and tibiocalcaneal motion during walking: external versus skeletal markers. Gait and Posture 1997; 6: 98-109

Reinschmidt C, van den Bogert AJ, Murphy N, Lundberg A, Nigg BM. Tiobiocalcaneal motion during running, measured with external and bone markers. Clinical Biomechanics; 1997, 12: 8-16

Renger, R. Identifying the task requirements essential to the success of a professional ice hockey player: a scout's perspective. Journal of Teaching in Physical Education; 1994, 13: 180-195.

Rowe,P.J., Nicol,A.C. and Kelly,I.G. Flexible goniometer computer system for the assessment of hip function. Clinical Biomechanics; 1989, 4: 68-72.

Roy B, Delisle G. Caracteristiques geometriques et dynamique des batons de hockey en regard de leur performance. Canadian Journal of Applied Sport Science; 1984, 4: 214-219,.

Rozzi, S L, S M Lephart, and F H Fu. Effects of muscular fatigue on knee joint laxity and neuromuscular characteristics of male and female athletes. J. Athletic Training; 1999, 34:106–114.

Schaff P, Hauser W. Dynamic measurement of pressure distribution with flexible measuring mats--an innovative measuring procedure in sports orthopedics and traumatology. Development--use--value. Sportverletzung Sportschaden; 1987, 1(4):185-222.

Sherif MH, Gregor RJ, Liu LM, Roy RR, Hager CL. Correlation of myoelectric activity and muscle force during selected cat treadmill locomotion. Journal of Biomechanics; 1983, 16:691–701.

Stacoff A. Skeletal lower extremity motions during running. Calgary, Canada. Doctoral dissertation; 1998.

Stamm L. Power Skating, 2nd ed. Champaign, IL: Human Kinetics; 1989.

Stegeman DF, Blok JH, Hermens HJ, Roeleveld. Surface EMG models and: Properties and applications. Journal of Electromyography and Kinesiology; 2000, 10:313-326.

Turcotte R, Pearsall DJ, Montgomery DL. Stiffness properties of ice hockey skates. Sports Engineering; 2001a, 4:43-48

Turcotte R, Pearsall D, Montgomery D, Lefetbvre R, Nicolaou M, Loh J Plantar pressure measures during forward skating in ice hockey. XIX Int Symp On Biomechanics In Sports, ISBS, San Francisco; 2001, June 20-26, 82-85

Turcotte R, Pearsall DJ, Montgomery DL, Lefevre R, Ofrir D, Loh JJ. Comparsion of ice versus treadmill training: plantar pressure distribution patterns. 4th Int Symp on Safety in Ice Hockey, May 5-6, 2002, Pittsburgh, PA, USA

Van Ingen Schenau GJ. From rotation to translation: Constraints on multi-joint movements and the unique action of bi-articular muscles. Human Movement Science; 1989, 8, 301-337.

Van Ingen Schenau GJ., de Boer RW, de Groot G. Biomechanics of speed skating. In, Biomechanics of Sport (Vaughn CL) CRC Press: Boca Raton; 1989, 121-167.

Vaughan G. http://www.birthplaceofhockey.com website © 2001.

Wakeling JM, Nigg BM, Rozitis AI. Muscle activity in the leg is tuned in response to ground reaction forces. Journal of Applied Physiology; 2002, 93, 1093-1103.

Winter, D. A. Overall Principle of Lower Limb Support during Stance Phase of Gait. Journal of Biomechanics; 1980, 923-927.

Winter, David A. Biomechanics and motor control of Human Movement, 2nd Ed. John Wiley & Sons Inc. USA; 1990.

Appendix A: Electrode Placement

The placements suggested by Delagi for the study were used in this experiment.

The electrodes were placed on the muscles of interest using the guidelines from Anatomical Guide for the Electromyographer (Delagi et al., 1980).

1. Vastus Medialis (distal fibres) four fingerbreadths proximal to superiomedial angle of the patella.
2. Gastrocnemius (medial head): one handbreadth below the popliteal crease on the medial mass of the calf.
3. Peroneus Longus: three fingerbreadths below the fibular head, directed towards the lateral aspect of the fibula.

Vastus Medialis Four fingerbreadths away from proximal to superiomedial angle of the patella *0.3 of length (22.1cm) from knee towards pubic tubercle*
Tibialis Anterior Four fingerbreadths below the tibial tuberosity and 1 fingerbreadth lateral to the tibial crest *0.2 of length (18.3cm) from external tibial tuerosity towards 1st cuneiform)*
Peroneus Longus Three fingerbreadths below the fibular head, directed towards the lateral aspect of the fibula *0.2 of length (16.4cm) from head of fibula towards lateral malleolus*
Gastrocnemius (medial) One handbreadth below the popliteal crease on the medial mass *0.3 of length (23.1cm) from medial to calcaneus*

4. Tibialis Anterior: four fingerbreadths below the tibial tuberosity and one fingerbreadth lateral to the tibial crest.

Table A1. The placements suggested by Delagi for the study were used in this experiment.